



IDENTIFICATION OF FEEDBACK CONTROL LAWS IN HUMAN  
STANDING AND WALKING

HUAWEI WANG

Master of Science in Control Engineering

Beihang University

June 2015

Bachelor of Science in Aviation Engineering

Civil Aviation University of China

June 2012

Proposal of Doctoral Candidacy Exam

Submitted in partial fulfillment of requirement for the degree

DOCTOR OF ENGINEERING IN MECHANICAL ENGINEERING

at

CLEVELAND STATE UNIVERSITY

AUGUST 2019

## ABSTRACT

Humanoid robots and powered prosthetic/orthotic(P/O) devices have been in development for many years. Although effective control algorithms have been developed, motion derived from them is not as natural as humans. This unnatural motion may cause inconvenience and problem. For instance, humanoid-robots which have inhuman-like motion is less-likely to be accepted by us to join our daily life; P/O devices which have inhuman-like motion can cause high energy expenses or even injuries of their users who have disabilities. We assume that human motion and control is a good reference for humanoid robots and P/O devices since they were designed with the goal to mimic human motion. Therefore, it is reasonable to believe that by using the identified control algorithms from human motion data, the a better performance of humanoid robots and P/O devices, for instance human-like motion and balance ability, can be achieved. To achieve this goal, in this dissertation study, we plan to identify control algorithms for two basic human motions: standing and walking.

For identification of the standing postural control, we designed and conducted an experiment to record healthy humans' responses in a standing balance task. Eight young adults were tested and their posture changes under a random perturbation were recorded. Based on the recorded data, we identified five types of feedback control laws, from simple to complex, to check these control laws' ability in explaining the experimental data. In addition, stochastic trajectory optimization was introduced to prevent finding unstable controllers. Results showed that non-linearity and time delay are needed in the standing balance controller to explain the experimental data precisely. Furthermore, eigenvalue analysis was applied on the identified stable controllers and suggested that most subjects tend to have similar feedback system characteristics in the standing balance task.

For identification of walking control laws, we first identified the step strategy control law on the walking data of nine able-bodied young adults, in which the experimental data was

recorded by Moore et al. (2015). The step strategy control law determines the foot location in coming step which is critical in walking balance. Identified results showed that control gains are similar among nine young adults. This is a positive evidence supporting that real step strategy control laws were identified. In addition, the identified gains are similar to those suggested by the capture theory which is widely used in humanoid robots. One significant difference is that the control gains identified from experimental data vary based on walking speeds, while the capture theory has constant gains for all walking speeds. Future work on the step strategy controller primarily include forward simulations of human walking. The purpose of these simulations is to compare the stable walking ability between identified control laws and the capture theory.

Another work in the identification of walking control laws is to identify joints' impedance parameters from perturbed walking data. Our hypothesis is that the close-loop identification method is more accurate than the curve fitting method (open-loop) in finding the real impedance parameters. A large difference is that full-body dynamics is involved in the close-loop identification method, while not in the open-loop method. This identification work will use the same framework that is used in the step strategy control law identification, but with different outcomes. After the identification, we will apply identified impedance control parameters on the Indego exoskeleton to check whether they are useful for P/O devices.

## TABLE OF CONTENTS

LIST OF TABLES . . . . .	ix
LIST OF FIGURES . . . . .	x
CHAPTER I. INTRODUCTION . . . . .	1
1.1 Humanoid Robot . . . . .	4
1.1.1 Zero Moment Point . . . . .	4
1.1.2 Step Strategy . . . . .	5
1.2 Prosthetic and Orthotic Devices . . . . .	7
1.2.1 Trajectory Tracking . . . . .	8
1.2.2 Impedance Control . . . . .	9
1.3 Human motion control . . . . .	9
1.3.1 Human Standing Control . . . . .	10
1.3.2 Human Walking Control . . . . .	11
1.4 Problem Statement . . . . .	12
1.5 Specific Aims . . . . .	13
1.6 Outline . . . . .	14
1.7 REFERENCES . . . . .	16
CHAPTER II. METHOD FOR CONTROL IDENTIFICATION . . . . .	26
2.1 Introduction . . . . .	27
2.2 Indirect Approach . . . . .	28
2.3 Trajectory Optimization . . . . .	29
2.4 Direct Collocation . . . . .	31
2.5 Nonlinear Programming . . . . .	33
2.6 REFERENCES . . . . .	34

PART I. CONTROL OF STANDING . . . . .	36
CHAPTER III. STANDING BALANCE EXPERIMENT WITH LONG DURATION RANDOM PERTURBATION . . . . .	37
3.1 Introduction . . . . .	38
3.2 Methods . . . . .	39
3.2.1 Participants . . . . .	39
3.2.2 Equipment . . . . .	40
3.2.3 Perturbation signal . . . . .	44
3.2.4 Protocol . . . . .	45
3.3 Experimental Data and Post Processing . . . . .	47
3.3.1 Raw Data . . . . .	47
3.3.2 Filling missing marker data . . . . .	48
3.3.3 Joint angle calculation . . . . .	48
3.3.4 Joint torque calculation . . . . .	53
3.3.5 Data Repository . . . . .	53
3.3.6 Analysis of joint motions . . . . .	53
3.4 Discussion . . . . .	57
3.5 Conclusion . . . . .	58
3.6 REFERENCES . . . . .	58
CHAPTER IV. IDENTIFICATION OF STABLE HUMAN POSTURAL CONTROL LAWS THROUGH STOCHASTIC TRAJECTORY OPTIMIZATION . . . . .	60
4.1 Introduction . . . . .	62
4.2 Methods . . . . .	63
4.2.1 Experiments . . . . .	64
4.2.2 Controller Structures . . . . .	65
4.2.3 Controller Identification in Deterministic Environment	67

4.2.4	Controller Identification in Stochastic Environment . . . . .	67
4.2.5	Stability evaluation . . . . .	69
4.3	Results . . . . .	70
4.4	Discussion . . . . .	70
4.5	Conclusion . . . . .	73
4.6	REFERENCES . . . . .	73
IV.7	Appendix . . . . .	75
<b>CHAPTER V. IDENTIFICATION OF CONTROL LAWS IN HUMAN STANDING BALANCE.</b>		76
5.1	Introduction . . . . .	77
5.2	Methods . . . . .	79
5.2.1	Indirect Approach . . . . .	79
5.2.2	Human Body Dynamics . . . . .	81
5.2.3	Controller Structures . . . . .	81
5.2.4	Avoid Unstable Controllers . . . . .	84
5.2.5	Summary of the Identification . . . . .	84
5.3	Results . . . . .	84
5.4	Discussion . . . . .	91
5.5	Conclusion . . . . .	92
5.6	REFERENCES . . . . .	92
<b>PART II. CONTROL OF WALKING.</b>		95
<b>CHAPTER VI. IDENTIFICATION OF THE STEP STRATEGY IN HUMAN WALKING</b>		96
6.1	Introduction . . . . .	97
6.2	Methods . . . . .	100
6.2.1	Experimental Data . . . . .	100
6.2.2	Human Body Dynamic Model . . . . .	102

6.2.3	Human Walking Control System . . . . .	103
6.2.4	Identification Problem Define . . . . .	109
6.2.5	Solution Method . . . . .	110
6.3	Results . . . . .	111
6.4	Discussion . . . . .	115
6.5	Conclusion . . . . .	119
6.6	REFERENCES . . . . .	119
PART III.	SUMMARY AND PROPOSED WORK . . . . .	123
CHAPTER VII.	SUMMARY AND PROPOSED WORK . . . . .	124
7.1	Completed Work . . . . .	124
7.2	Future Work . . . . .	126
7.3	REFERENCES . . . . .	130

## LIST OF TABLES

Table	Page
I. Participants' information in standing experiment . . . . .	41
II. Descriptions of 27 subject markers and 5 treadmill markers . . . . .	43
III. Descriptions of nine Electromyography sensors (EMGs) . . . . .	44
IV. Quality of recorded raw data . . . . .	49
V. Participants' information in walking experiment . . . . .	101
VI. Coefficient of determination ( $R^2$ ) of step strategy identification fit . . . . .	111
VII. Number of similar best results in each identification problem . . . . .	113
VIII. Standard deviation of the pelvis position gain in the similar best results . .	113
IX. Standard deviation of the pelvis velocity gain in the similar best results . .	113
X. Results of a pilot study in impedance identification . . . . .	128
XI. Time-line and Milestones . . . . .	130

## LIST OF FIGURES

Figure	Page
1. Three famous humanoid robots . . . . .	2
2. Three famous P/O devices . . . . .	3
3. Direct and indirect identification approaches . . . . .	28
4. Diagram plot of trajectory optimization . . . . .	29
5. The double pendulum model of human standing balance system . . . . .	31
6. Settings of human standing balance experiment . . . . .	42
7. D-Flow modules used in the standing balance experiment . . . . .	42
8. Perturbation signal in the standing balance experiment . . . . .	45
9. Example of the effect in filling marker gaps . . . . .	50
10. Diagram of the human standing balance model . . . . .	51
11. One example of calculated joint motion . . . . .	52
12. Joint angle analysis in subject 3 . . . . .	54
13. Joint angle analysis in subject 4 . . . . .	54
14. Joint angle analysis in subject 5 . . . . .	55
15. Joint angle analysis in subject 6 . . . . .	55
16. Joint angle analysis in subject 7 . . . . .	56
17. Joint angle analysis in subject 8 . . . . .	56
18. Diagram of the indirect approach in standing postural control law identification . . . . .	64
19. Stability results of the stochastic and deterministic optimizations . . . . .	71
20. Diagram of the indirect approach in engineering applicable standing balance controller identification . . . . .	80
21. Structure of the neural network controller . . . . .	83
22. $R^2$ comparison of optimized trajectory with different controller types . . . . .	86

23.	One example of ankle motion fit with different controller types . . . . .	87
24.	One example of hip motion fit with different controller types . . . . .	88
25.	Gains of identified PD controllers . . . . .	89
26.	Eigenvalues of identified PD controllers . . . . .	89
27.	Gains of identified FPD controllers . . . . .	90
28.	Eigenvalues of identified FPD controllers . . . . .	90
29.	Diagram of the indirect approach used in step strategy identification . . .	100
30.	Structure of the locomotion control system . . . . .	104
31.	Experimental data of the swing path . . . . .	106
32.	Optimization results of the normalized polynomial function . . . . .	107
33.	One example of joint trajectory fit in the step strategy control law identifi- cation . . . . .	112
34.	Control gains of the identified step strategies . . . . .	114
35.	One example of the swing leg motion with the estimated foot placement under identified step strategy . . . . .	115
36.	Results of the consistency check for the identified step strategies . . . . .	118
37.	One example of joint trajectory fit of the identified impedance parameters .	128

## CHAPTER I

### INTRODUCTION

Humanoid robots are robots with their body shape built to resemble the human body. In general, humanoid robots have a head, two arms, a torso, and two legs. Three well known and advanced humanoid robot platforms are ASIMO (Honda), Valkyrie (NASA), and ATLAS(Boston Dynamics), shown in Figure 1 [1–4]. The advantage of humanoid robots compared to wheeled robots is that they can function in human working and living environments. However, this requires human-like motion [1–3, 5, 6], which is difficult to achieve. Controlling humanoid robots’ legs to generate the human locomotion is one of the main concerns. On one hand, in a controlled and predictable environment, it is easy to make humanoid robots reproduce the general joints’ trajectories in human locomotion [7–9]. On the other hand, humanoid robots have not demonstrate the same balance and locomotion ability as humans in uncontrolled and unpredictable environments [2, 5]. The bipedal locomotion performance is challenged by many unexpected instances, for instance external perturbations, uneven terrains, and slippery ground. Therefore, in this work, we propose an approach to find human-inspired control strategies that can improve the locomotion ability of humanoid robots.

Powered prosthetics and orthotics/exoskeletons (P/O) are wearable robotic devices that are designed to restore locomotion functions for disabled patients [10]. Unlike passive P/O de-



Figure 1: Three most famous humanoid robot hardware platforms in the world. From left to right, they are: ASIMO, designed by Honda Motor Company; Valkyrie, designed by NASA; Atlas, designed by Boston Dynamics.



Figure 2: Three most famous prosthetics, orthotics, and exoskeleton devices in the word. From left to right, they are: Exosuit, designed by ReWalk; Indego, designed by Parker Hannifin; C-leg, designed by Ottobock.

vices, powered P/O devices have the ability to offer more assistance, especially at higher-levels of patient activities [11–14]. For example, it has been established that powered prostheses can reduced the metabolic cost of amputees [15]. Several well known advanced power P/O devices are Exosuit (Rewalk), Indego (Parker Hannifin), and C-leg (Ottobock), shown in Figure 2. Impedance control strategies are mostly used in current powered P/O devices. Even though the application of impedance control strategy has improved the wearing experience, its parameters are usually turned manually [14, 16]. In this work, we will design human-inspired controllers to improve the performance of powered P/O devices.

Taking together, the approach we propose will be used to directly identify the control laws of human locomotion from human experiments. Since both humanoid robots and P/O devices have a similar body structure as humans, the identified controller can be easily applied. Furthermore, we predict that the identified control laws improve the performance

of humanoid robots and P/O devices as they contain the information on how humans control their legs under perturbed environment. Before describing the details of control law identification, we will first briefly review the main developments of control algorithms in humanoid robot and P/O devices. In addition, we will also review the studies in human locomotion control.

## 1.1 Humanoid Robot

Here, we focus on control algorithms used in humanoid robots which contributed to achieve dynamic locomotion, which means the control algorithms can control humanoid robots walking stably in uncontrolled environments, such as under external perturbation. There are two commonly used control strategies in achieving dynamic locomotion: zero moment point and step strategy.

### 1.1.1 Zero Moment Point

Zero moment point (ZMP) is the first widely used concept that been proposed that can enable humanoid robot to achieve stable locomotion. The ZMP is a point where the ground reaction force has no moments but only forces. In biomechanics, the ZMP is also known as the center of pressures (CoP). Vukobratović et al. (1972) proposed the concept of Zero Moment Point (ZMP), in which he concluded that ZMP trajectory is essential for human walking balance [17]. Path control of ZMP was quickly applied to the humanoid/bipedal robots to achieve normal walking stability. Yamaguchi et al. (1993) applied ZMP trajectory control into humanoid robot to keep walking balance, which improved the balance walking speed [7]. After Yamaguchi's study, several studies were done to develop his idea into more complex applications. For example, robustness was introduced which defined as the distance from ZMP to the edge of the support area. Nishiwaki and Kagami (2010) worked on modifying the reference ZMP trajectory online based on the walking status change, including small changes in local ZMP and large changes which caused changes in step

placement [8]. Sugihara (2010) used ZMP as an input for central pattern generator control algorithm which generated stable walking in simulation [18]. Dasgupta et al. (1999) used motion capture data of human walking as reference to control humanoid robot motion, in which he used a feedback controller to control robot's ankle joints to tracking the target ZMP trajectory from human walking data [9]. Although some levels of stable walking can be achieved in humanoid robots, one limitation of ZMP control algorithm is that it is too conservative to keep the ZMP inside the support area. In general, stable walking using ZMP strategy requires static stability and the ASIMO robot is well known as an example of ZMP strategy applications [2]. One example of the ZMP limitation is that ZMP itself cannot be applied in fast walking motions which feet roll from heel to toe in stance phase, since the support area for ZMP has a rapid change. Besides ZMP strategy, human can also 'catch' themselves by foot placement when ZMP went outside the support area [19]. The foot placement strategy is also named as step strategy.

### 1.1.2 Step Strategy

Step strategy has been proposed to overcome the limitations of the ZMP concept. Townsend et al. (1985) pointed out that human walking balance was mainly achieved by placing the swing foot at the right place, which is called step strategy [20]. Based on a simple model, he suggest that the foot placement should be related to the position and velocity of Center of Mass (CoM). Pai et al. (1997) analyzed the stability of an inverted pendulum model with fixed foot-point, calculated the region of stability in respect to the positon and velocity of CoM with the constraints of contact force, foot region and muscle forces. This was an early attempt to use invert pendulum model in analyzing human stability [21]. Maki et al. (1999) investigated how swing leg dynamics, especially swing time, affect stability in stepping strategy. He proposed the stability margin with respect to the swing time. In his paper, human experiments have suggested that healthy human chose their swing time between minimum and maximum velocity stability margin [22]. Dasgupta et al(2003) used

ZMP regulator and three dimensional linear inverted pendulum (3D-LIP) model reference to control humanoid robot in simulation. Simulation results showed that the 3D-LIP model is valid in controlling humanoid robot to achieve stable walking [23]. Komura et al. (2005) introduced angular momentum in addition to 3D-LIP model to better control humanoid robot. Angular momentum was usually caused by external force that applied on the body segments of the humanoid robot or human. Two strategies are used to compensate the introduced momentum: 1). modify the landing position of the swing leg; 2). opposite rotational momentum will be generated by control trunk flexion and extension in the double support phase [24].

Pratt et al. (2006) first introduced the concepts of capture point and capture region. Capture theory answered the question when and where to land the swing foot. 3D-LIP with a flywheel model was used to predict the capture point, in which the flywheel is to generate the angular momentum. Simulation showed that capture point theory works well on a biped robot [25]. Hyon et al. (2007) proposed three dimensional full body robot control using passivity-based contact force control with gravity-compensation. This control strategy was mentioned to have the ability of reject external perturbation [26]. Benjamin Stephens (2007) used an invert pendulum model to load ankle, hip, and step strategies, achieved locomotion balance of a humanoid in simulation environment. [27]. Wight et al. (2008) invented a Foot Placement Estimator (FPE) to achieve balance walking of humanoid robot [28]. The FPE is based on a double leg invert pendulum model and three stability regions were proposed. Hof (2008) defined extrapolated center of mass (XCoM), which is the same formula with capture point, biped robot can keep balance by stepping to the line connected CoP and XCoM. An inverted pendulum model with foot was used to do the simulation. Sagittal and lateral stepping controllers were defined. His simulation model can keep stable walking with external perturbation [29]. Koolen et al. (2012) systematically described capture theory. He started with 3D-LIP, then went to more complex model by

adding foot, trunk rotation. The key idea of capture theory is to step towards falling direction, the length of step is based CoM, velocity of CoM, and swing time [30]. Pratt (2012) applied capture theory onto a biped robot M2V2. This paper described the platform and structure of stance and swing controllers. A standing controller is used to control standing leg to generate appropriate ZMP trajectories. A swing controller is used to calculate capture point and control swing leg reach the capture point [31]. Capture theory has became a successful control method in step strategy and has been tested on several robotics (Atlas, NASA), which improved their balance ability.

## 1.2 Prosthetic and Orthotic Devices

Powered P/O devices are becoming widely used than passive P/O devices due to their potential to dramatically improve the mobility for impairment people [13, 32]. Powered prosthetic legs are developed to provide locomotion support for disabled people. Prosthetic legs include blow knee and above knee prostheses [10]. In rehabilitation, orthotic devices help patients with mobility disorders to improve their musculoskeletal strength, motor control, and gait stability. In locomotion assistance, exoskeleton devices are commonly used for helping paralytic patients who have lost motor and sensor function in their lower limbs to regain locomotion abilities [33]. Despite the difference of powered P/O devices, their control systems are similar, which is to produce full or part of human locomotion ability. Comparing to the hardware design, our interests are in the control algorithms that can achieve this.

In following several paragraphs, currently used control algorithms will be reviewed. The control systems of powered P/O devices usually are hierarchical structure, in which three levels exist. The high level controller needs to perceive the user's locomotive intent, which also can be called motion intention estimation. The middle level controller translates the user's motion intentions from the high level control to desired device states for the low

level controller to track. Finally, the low level controller tracks the target motions or forces using feedback control techniques [10].

Here, we are interested the middle and low level controller: how human transfers the locomotion intent into segment motions. Trajectory tracking and impedance control are mainly used as the middle and low level controller in powered P/O devices. Studies in these two control strategies will be reviewed here.

### **1.2.1 Trajectory Tracking**

Trajectory tracking was the first common used control technique in P/O devices. Classical control theory has developed for a long time in tracking problems with external disturbance, which makes this control strategy easy to achieve. Also, trajectory tracking is valuable for the locomotion assistant function, which helping paralyzed patients which lost the full control of muscles. Since they cannot contribute to locomotion with their own muscles at all, strong following forces are needed to make the gait possible [34]. A lot of researches and companies are using trajectory tracking for their exoskeletons to achieve locomotion assistance [35]. The ReWalk exoskeleton, which was developed to help thoracic-level complete SCI patients to walk independently, is controlled by a predefined trajectory. The Vanderbilt exoskeleton [12], the Robotic Upper Extremity Repetitive Trainer (RUPERT) exoskeleton [36], and a joint-coupled orthosis [37] have also adopted similar control strategies [38]. However, literature has suggested that P/O devices which controlled by trajectory tracking may decrease the patient's effort and participation in the training, in which resulted ineffective in motor training and learning [39]. To date, trajectory tracking control is primarily used in the P/O devices which helps paralytic patients to regain walking ability or for early stage rehabilitation when patients have weak muscle strength [40, 41].

### 1.2.2 Impedance Control

Impedance control is another control strategy which used in P/O devices to provide the smooth force assistant to users. The basic idea of impedance control is to regulate the dynamic relation between the assisting device and the users by relating the position error (e.g., joint angles) to the interaction force/torque through a mechanical impedance [33, 42]. This mechanical impedance is the output impedance of the exoskeleton, which is usually modelled as a mass-damper-spring system. Impedance control generate the virtual elastic and damping properties to represent the human-like joints' functions. With this technology, several good devices have been built, for instance C-leg (ottobockus), Indego (Parker Hannifin), ReWalk Rehabilitation, and BiOM foot (MIT)[12, 13, 43]. The C-leg prosthesis uses a hydraulic cylinder to generate damping property at its knee joint. A small valve is controlled to adjust the oil flow speed between upper and lower chambers to achieve the designed damping parameters. Exoskeletons and prostheses in Goldfarb's lab are controlled by electrical motors. Control strategy inside is controlling the stiffness and damping properties of the joints. BiOM foot is also using impedance control by simulating the muscle impedance.

In addition, changing impedance parameters can achieve additional features. High output impedance will increase the assistance from the exoskeleton to guide the patient's limb onto the reference trajectory. If a patient shows greater effort in the training, the desired output impedance of the exoskeleton will similarly be low to allow the patient to deviate more from the reference trajectory [44–47].

## 1.3 Human motion control

Besides the above studies in designing control laws for humanoid robots and P/O devices, many studies have been done trying to understand how human beings control their motion. Since the approach of identify control laws from human locomotion data is similar to some

of the studies in human locomotion control, we will review their results in this section.

Standing and walking are two the main activates in human daily life, and also two main directions of human motion control studies. In this section, the review work will divided into two parts: human standing control and human walking control.

### 1.3.1 Human Standing Control

It has been accepted that humans use feedback control to control their regular motions, such as, standing and walking [48]. CoM and CoP are the most important information when trying to extract standing balance information from human recover data under perturbation. In order to keep standing balance, studies suggested that CoP needs to stay inside the support area (area defined by the out curves of two feet) [49, 50]. However, how human keep balance when the CoP is inside support area is still unclear. To understand how humans use feedback control to maintain standing balance, several studies has been done trying to identify control structure and parameters from experiment data. In experiments, subjects were either perturbed with external forces, or the standing platform has unpredictable accelerations. Indirect approach is always used, since open-loop identification will introduce error [51]. Park et al. (2004) identified stable full state proportional-derivative (PD) controller parameters for different amplitudes of perturbation. They concluded that the controller gains are changing with the ramp perturbation amplitude [52]. Welch et al. (2008,2009) used ramp perturbations to identify muscle activation [53, 54]. Kiemel et al. (2011) identified a non-parametric neural feedback model for the standing balance under mechanical perturbation. The identified results suggested that humans tend to maintain stability rather than minimize sway [55]. Peterka and van der Kooij (2002, 2007, 2011) identified non-parametric motor-sensor control information from experimental data in frequency domain. Continuous perturbations and a linear controller structure were used in their studies [56–58]. Goodworth et al. (2018) tested the identification method on simu-

lated data in frequency domain, but have not yet reported results on human experiment data [59].

### 1.3.2 Human Walking Control

Researchers have studied different aspects of the human walking control algorithms from experiment data. Ehtemam et al. (2018) studied the neural control of speed in human walking. In his study, joint input and output method was used to identify the reactions of muscles with respect to mechanical (belt speed) perturbation [60]. Logan et al. (2017) using a similar approach, studied how the neural system (muscle activation) responds to vision perturbation [61]. Mombaur et al. (2010, 2013) identified the underlying optimality criteria of biological motions, for instance walking [62, 63]. However, it is the high criteria which generating the walking pattern, instead of the motion control of walking. Lee et al. (2012) identified the time-varying ankle impedance during walking using an ankle robot [64]. Their results suggested that most subjects increased ankle impedance just before heel strike in both degrees of freedom. Rouse et al. (2013, 2014) identified impedance parameters (stiffness and damping) for ankle using the perturbed data of the stance phase in walking [65, 66]. Their results suggested an increasing stiffness of ankle joint from early stance to terminal stance phase. In addition, they got similar ankle impedance results as the well known 'quasi-stiffness'. Mrachacz-Kersting and Sinkjaer (2003) studied knee joint stiffness with respect to the relative contributions of the knee extensor stretch reflex [67]. They found a positive linear relationship between basic and tonic EMG stretch responses and background torques. Wang et al. (2014) attempted to extract control laws of swing foot location from the variation of normal walking gait cycles [68].

## 1.4 Problem Statement

Although the control performance of humanoid robots and P/O devices has been improved in past decades, their motion is still not as natural as in humans. The ZMP strategy, capture theory, and impedance control are three main control algorithms that are used in controlling standing and walking of humanoid robots and P/O devices. The idea of ZMP strategy is to keep ZMP inside the base of support region [7, 17], which is from the stability analysis of a inverted pendulum model. This control algorithm is useful for slow walking control, in which double stance phase exists. However, in fast walking situation, this criteria is not valid anymore [19]. In addition, the ZMP strategy only provide a high level requirement. What joint motions are needed to keep the ZMP inside the based of support is not given. The capture theory provided a more detailed control algorithm, in which the foot placement in next step is estimated [25, 30, 31]. It can produce dynamic walking motions since there is no ZMP requirement. However, several hypotheses are made in the capture theory, which limited the ability of generating human-like behaviors. For instance, it is assumed that the horizontal velocity of CoM will reduced to zero at mid-stance, while humans tend to keep a constant horizontal speed. In addition, the swing leg dynamics and landing energy lost (impact) were not considered [69, 70]. The impedance control is promising since it can model human joint properties and provide a soft interaction between human and P/O devices [16, 42, 71]. However, parameters of impedance controllers are mostly manually tuned in real applications to get a good walking pattern that is close to healthy humans. The manual tuning process is time consuming for both users and therapists and may not get the optimal controller.

The idea of directly identifying control laws from human motion data has not drawn much attention. Although the feedback controller identification in human standing balance has been attempted, their results are mostly not engineering applicable. For example, the control parameters identified from experimental data with ramp perturbation are functions of

perturbation amplitudes. This is not suitable for humanoid robots and P/O devices, because it is not possible to predict the amplitude of the perturbation before choosing the control gains [52–54]. Other identification studies found more generalized control information from random perturbation experimental data. However, the identified results are non-parametric [56–58]. In human walking studies, Wang et al. (2014) attempted to extract control laws of step strategy from human walking data [68]. Yet, the extracted step strategies were from the variation between normal gait cycles that may not explain the step strategy under larger perturbations. In addition, since there is no plant model involved in the analysis process, it is not guaranteed that the extracted control algorithms will work for humanoid robots. Studies have shown that the direct identification approach can introduce the bias because of the lack of plant, while indirect identification approach can prevent it [51].

Therefore, our main propose is to identify generalized control laws from experimental data of human standing and walking using the indirect identification approach. Our central hypothesis is that engineering applicable feedback control laws can be directly identified from human motion that responded to random perturbations. Here we propose three aims.

## 1.5 Specific Aims

**Aim 1: To identify control laws for standing balance.** In this aim, we first conduct an experiment to collect data of healthy humans' responses to random displacement perturbations; Then we identify several types of feedback control laws, including linear and nonlinear types, from the experimental data.

**Aim 2: To identify control laws for step strategy during walking.** In this aim, we identify the step strategy (foot placement) control laws from human walking data with random perturbations. Step strategy control determines where humans place their swing foot under

the perturbation environment. We will also test the identified control laws by doing forward simulation of the close-loop human walking.

**Aim 3: To identify impedance control parameters for leg joints during walking.** In this aim, we will identify ankle, knee, and hip impedance parameters from human walking data with random perturbations. Our intention is to understand how humans control their joints to achieve smooth joint trajectories under perturbations. The identified impedance parameters can also provide good references for the impedance controllers in P/O devices. We will test the identified control parameters by applying them on the Indego exoskeleton.

## 1.6 Outline

This dissertation study is divided into two main parts:

Before the main parts, *chapter I* discussed the past related researches and background. *chapter II* mentioned the solution methods and concepts that are used throughout this dissertation study.

**Part I** addresses **Aim 1** of this dissertation study, which is completed:

- *Chapter III:* We design human standing balance experiment to obtain the data on how healthy human control their ankle, knee, and hip joints under random perturbation.
- *Chapter IV:* We develop a stochastic optimization method to avoid identifying unstable controllers from the experimental data.
- *Chapter V:* We identify linear and nonlinear controllers from long duration standing balance experimental data.

**Part II** concerns **Aim 2** and **Aim 3** of this dissertation to identify control laws from walking data, which we are working on:

- *Chapter VI:* We identify step strategy control laws from nine subjects' data at three walking speeds.
- *Chapter VII:* We compare the stable walking abilities between identified control laws and the capture theory by doing forward simulations.
- *Chapter VIII:* We identify impedance control parameters from multiple gaits walking data.
- *Chapter IX:* We evaluate the identified impedance control parameters by applying them on Indego exoskeleton.

## 1.7 REFERENCES

- [1] Hirai Kazuo, Hirose Masoto, Yuji Haikawa, and Toru Takenaka. The Development of Honda Humanoid Robot. In *IEEE International Conference on Robotics & Automation*, pages 1321–1326, Leuven, Belgium, 1998.
- [2] Joel Chestnutt, Manfred Lau, German Cheung, James Kuffner, Jessica Hodgins, and Takeo Kanade. Footstep planning for the honda asimo humanoid. In *Robotics and Automation, 2005. ICRA 2005. Proceedings of the 2005 IEEE International Conference on*, pages 629–634. IEEE, 2005.
- [3] Nicolaus A Radford, Philip Strawser, Kimberly Hambuchen, Joshua S Mehling, William K Verdeyen, Stuart Donnan, James Holley, Jairo Sanchez, Vienny Nguyen, Lyndon Bridgwater, Reginald Berka, Robert Ambrose, Christopher Mcquin, John D Yamokoski, Stephen Hart, Raymond Guo, Adam Parsons, Brian Wightman, Paul Dinh, Barrett Ames, Charles Blakely, Courtney Edmonson, Brett Sommers, Rochelle Rea, Chad Tobler, Heather Bibby, Brice Howard, Lei Nui, Andrew Lee, Michael Conover, Lily Truong, Jacobs Engineering, David Chesney, Robert Platt, Gwendolyn Johnson, Chien-Liang Fok, Nicholas Paine, Luis Sentis, Eric Cousineau, Ryan Sinnet, Jordan Lack, Matthew Powell, Benjamin Morris, and Aaron Ames. Valkyrie: NASA’s First Bipedal Humanoid Robot. Technical report.
- [4] General information of atlas. <https://www.bostondynamics.com/atlas>. Accessed: 2019-02-13.
- [5] Masato Hirose and Kenichi Ogawa. Honda humanoid robots development. *Philosophical Transactions of the Royal Society A: Mathematical, Physical and Engineering Sciences*, 2007. ISSN 1364503X. doi: 10.1098/rsta.2006.1917.
- [6] Yoshiaki Sakagami, Ryujin Watanabe, Chiaki Aoyama, Shinichi Matsunaga, Nobuo Higaki, and Kikuo Fujimura. The intelligent asimo: System overview and integra-

- tion. In *Intelligent Robots and Systems, 2002. IEEE/RSJ International Conference on*, volume 3, pages 2478–2483. IEEE, 2002.
- [7] Jin-ichi Yamaguchi, Atsuo Takanishi, and Ichiro Kato. Development of a biped walking robot compensating for three-axis moment by trunk motion. *Journal of the Robotics Society of Japan*, 11(4):581–586, 1993.
  - [8] Koichi Nishiwaki and Satoshi Kagami. Strategies for adjusting the zmp reference trajectory for maintaining balance in humanoid walking. In *2010 IEEE International Conference on Robotics and Automation*, pages 4230–4236. IEEE, 2010.
  - [9] Anirvan Dasgupta and Yoshihiko Nakamura. Making feasible walking motion of humanoid robots from human motion capture data. In *Proceedings 1999 IEEE International Conference on Robotics and Automation (Cat. No. 99CH36288C)*, volume 2, pages 1044–1049. IEEE, 1999.
  - [10] Michael R Tucker, Jeremy Olivier, Anna Pagel, Hannes Bleuler, Mohamed Bouri, Olivier Lambercy, José del R Millán, Robert Riener, Heike Vallery, and Roger Gassert. Control strategies for active lower extremity prosthetics and orthotics: a review. *Journal of neuroengineering and rehabilitation*, 12(1):1, 2015.
  - [11] Andrew Chu. *Design of the Berkeley lower extremity exoskeleton (BLEEX)*. University of California at Berkeley, 2005.
  - [12] Hugo A Quintero, Ryan J Farris, and Michael Goldfarb. A method for the autonomous control of lower limb exoskeletons for persons with paraplegia. *Journal of medical devices*, 6(4):041003, 2012.
  - [13] Alberto Esquenazi, Mukul Talaty, Andrew Packel, and Michael Saulino. The rewalk powered exoskeleton to restore ambulatory function to individuals with thoracic-level motor-complete spinal cord injury. *American journal of physical medicine & rehabilitation*, 91(11):911–921, 2012.

- [14] Amanda H Shultz, Brian E Lawson, and Michael Goldfarb. Running with a powered knee and ankle prosthesis. *IEEE transactions on neural systems and rehabilitation engineering*, 23(3):403–412, 2015.
- [15] Samuel K Au, Jeff Weber, and Hugh Herr. Powered ankle–foot prosthesis improves walking metabolic economy. *IEEE Transactions on Robotics*, 25(1):51–66, 2009.
- [16] Frank Sup, Amit Bohara, and Michael Goldfarb. Design and control of a powered transfemoral prosthesis. *The International journal of robotics research*, 27(2):263–273, 2008.
- [17] Miomir Vukobratović and J Stepanenko. On the stability of anthropomorphic systems. *Mathematical biosciences*, 15(1-2):1–37, 1972.
- [18] Tomomichi Sugihara. Consistent biped step control with com-zmp oscillation based on successive phase estimation in dynamics morphing. In *2010 ieee international conference on robotics and automation*, pages 4224–4229. IEEE, 2010.
- [19] Jerry E Pratt and Russ Tedrake. Velocity-based stability margins for fast bipedal walking. In *Fast Motions in Biomechanics and Robotics*, pages 299–324. Springer, 2006.
- [20] Miles A Townsend. Biped gait stabilization via foot placement. *Journal of biomechanics*, 18(1):21–38, 1985.
- [21] Yi-Chung Pai and James Patton. Center of mass velocity-position predictions for balance control. *Journal of biomechanics*, 30(4):347–354, 1997.
- [22] Brian E Maki and WE McIlroy. The control of foot placement during compensatory stepping reactions: does speed of response take precedence over stability? *IEEE Transactions on Rehabilitation Engineering*, 7(1):80–90, 1999.

- [23] Shuuji Kajita, Fumio Kanehiro, Kenji Kaneko, Kiyoshi Fujiwara, Kensuke Harada, Kazuhito Yokoi, and Hirohisa Hirukawa. Biped walking pattern generation by using preview control of zero-moment point. In *ICRA*, volume 3, pages 1620–1626, 2003.
- [24] Taku Komura, Howard Leung, Shunsuke Kudoh, and James Kuffner. A feedback controller for biped humanoids that can counteract large perturbations during gait. In *Robotics and Automation, 2005. ICRA 2005. Proceedings of the 2005 IEEE International Conference on*, pages 1989–1995. IEEE, 2005.
- [25] Jerry Pratt, John Carff, Sergey Drakunov, and Ambarish Goswami. Capture point: A step toward humanoid push recovery. In *Humanoid Robots, 2006 6th IEEE-RAS International Conference on*, pages 200–207. IEEE, 2006.
- [26] Sang-Ho Hyon, Joshua G Hale, Gordon Cheng, et al. Full-body compliant human-humanoid interaction: Balancing in the presence of unknown external forces. *IEEE Trans. Robotics*, 23(5):884–898, 2007.
- [27] Benjamin Stephens. Humanoid push recovery. In *Humanoid Robots, 2007 7th IEEE-RAS International Conference on*, pages 589–595. IEEE, 2007.
- [28] Derek L Wight, Eric G Kubica, and David W Wang. Introduction of the foot placement estimator: A dynamic measure of balance for bipedal robotics. *Journal of computational and nonlinear dynamics*, 3(1):011009, 2008.
- [29] At L Hof. The ‘extrapolated center of mass’ concept suggests a simple control of balance in walking. *Human movement science*, 27(1):112–125, 2008.
- [30] Twan Koolen, Tomas De Boer, John Rebula, Ambarish Goswami, and Jerry Pratt. Capturability-based analysis and control of legged locomotion, part 1: Theory and application to three simple gait models. *The International Journal of Robotics Research*, 31(9):1094–1113, 2012.

- [31] Jerry Pratt, Twan Koolen, Tomas De Boer, John Rebula, Sebastien Cotton, John Carff, Matthew Johnson, and Peter Neuhaus. Capturability-based analysis and control of legged locomotion, part 2: Application to m2v2, a lower-body humanoid. *The International Journal of Robotics Research*, 31(10):1117–1133, 2012.
- [32] Atsushi Tsukahara, Ryota Kawanishi, Yasuhisa Hasegawa, and Yoshiyuki Sankai. Sit-to-stand and stand-to-sit transfer support for complete paraplegic patients with robot suit hal. *Advanced robotics*, 24(11):1615–1638, 2010.
- [33] Bing Chen, Hao Ma, Lai-Yin Qin, Fei Gao, Kai-Ming Chan, Sheung-Wai Law, Ling Qin, and Wei-Hsin Liao. Recent developments and challenges of lower extremity exoskeletons. *Journal of Orthopaedic Translation*, 5:26–37, 2016.
- [34] Shahid Hussain, Sheng Q Xie, and Prashant K Jamwal. Control of a robotic orthosis for gait rehabilitation. *Robotics and Autonomous Systems*, 61(9):911–919, 2013.
- [35] Timothy Alan Swift. *Control and trajectory generation of a wearable mobility exoskeleton for spinal cord injury patients*. PhD thesis, UC Berkeley, 2011.
- [36] Hang Zhang, Sivakumar Balasubramanian, Ruihua Wei, Hiroko Austin, Sharon Buchanan, Richard Herman, and Jiping He. Rupert closed loop control design. In *2010 Annual International Conference of the IEEE Engineering in Medicine and Biology*, pages 3686–3689. IEEE, 2010.
- [37] Ryan J Farris, Hugo A Quintero, Thomas J Withrow, and Michael Goldfarb. Design of a joint-coupled orthosis for fes-aided gait. In *2009 IEEE International Conference on Rehabilitation Robotics*, pages 246–252. IEEE, 2009.
- [38] Donald Lee Grimes. *An active multi-mode above knee prosthesis controller*. PhD thesis, Massachusetts Institute of Technology, 1979.

- [39] Jan F Veneman, Ralf Ekkelenkamp, Rik Kruidhof, Frans CT van der Helm, and Herman van der Kooij. A series elastic-and bowden-cable-based actuation system for use as torque actuator in exoskeleton-type robots. *The international journal of robotics research*, 25(3):261–281, 2006.
- [40] Gery Colombo, Matthias Joerg, Reinhard Schreier, Volker Dietz, et al. Treadmill training of paraplegic patients using a robotic orthosis. *Journal of rehabilitation research and development*, 37(6):693–700, 2000.
- [41] Kenta Suzuki, Gouji Mito, Hiroaki Kawamoto, Yasuhisa Hasegawa, and Yoshiyuki Sankai. Intention-based walking support for paraplegia patients with robot suit hal. *Advanced Robotics*, 21(12):1441–1469, 2007.
- [42] Neville Hogan. Impedance control: An approach to manipulation: Part ii—implementation. *Journal of dynamic systems, measurement, and control*, 107(1):8–16, 1985.
- [43] Siegmar Blumentritt, Thomas Schmalz, and Rolf Jarasch. The safety of c-leg: biomechanical tests. *JPO: Journal of Prosthetics and Orthotics*, 21(1):2–15, 2009.
- [44] Shahid Hussain, Sheng Q Xie, and Prashant K Jamwal. Adaptive impedance control of a robotic orthosis for gait rehabilitation. *IEEE transactions on cybernetics*, 43(3):1025–1034, 2013.
- [45] Ann M Simon, Kimberly A Ingraham, Nicholas P Fey, Suzanne B Finucane, Robert D Lipschutz, Aaron J Young, and Levi J Hargrove. Configuring a powered knee and ankle prosthesis for transfemoral amputees within five specific ambulation modes. *PloS one*, 9(6):e99387, 2014.
- [46] Navid Aghasadeghi, Huihua Zhao, Levi J Hargrove, Aaron D Ames, Eric J Perreault, and Timothy Bretl. Learning impedance controller parameters for lower-limb prosthe-

- ses. In *2013 IEEE/RSJ International Conference on Intelligent Robots and Systems*, pages 4268–4274. IEEE, 2013.
- [47] Ding Wang, Ming Liu, Fan Zhang, and He Huang. Design of an expert system to automatically calibrate impedance control for powered knee prostheses. In *2013 IEEE 13th International Conference on Rehabilitation Robotics (ICORR)*, pages 1–5. IEEE, 2013.
- [48] Arthur D Kuo. An optimal control model for analyzing human postural balance. *IEEE transactions on biomedical engineering*, 42(1):87–101, 1995.
- [49] David A Winter. Human balance and posture control during standing and walking. *Gait & posture*, 3(4):193–214, 1995.
- [50] At L Hof. The equations of motion for a standing human reveal three mechanisms for balance. *Journal of biomechanics*, 40(2):451–457, 2007.
- [51] Herman van der Kooij, Edwin van Asseldonk, and Frans CT van der Helm. Comparison of different methods to identify and quantify balance control. *Journal of neuroscience methods*, 145(1-2):175–203, 2005.
- [52] Sukyung Park, Fay B Horak, and Arthur D Kuo. Postural feedback responses scale with biomechanical constraints in human standing. *Experimental brain research*, 154(4):417–427, 2004.
- [53] Torrence DJ Welch and Lena H Ting. A feedback model predicts muscle activity during human postural responses to support surface translations. *Journal of neurophysiology*, 2008.
- [54] Torrence DJ Welch and Lena H Ting. A feedback model explains the differential scaling of human postural responses to perturbation acceleration and velocity. *Journal of Neurophysiology*, 2009.

- [55] Tim Kiemel, Yuanfen Zhang, and John J Jeka. Identification of neural feedback for upright stance in humans: stabilization rather than sway minimization. *Journal of Neuroscience*, 31(42):15144–15153, 2011.
- [56] RJ Peterka. Sensorimotor integration in human postural control. *Journal of neurophysiology*, 88(3):1097–1118, 2002.
- [57] Herman Van Der Kooij and Erwin De Vlugt. Postural responses evoked by platform perturbations are dominated by continuous feedback. *Journal of neurophysiology*, 2007.
- [58] Herman Van Der Kooij and Robert J Peterka. Non-linear stimulus-response behavior of the human stance control system is predicted by optimization of a system with sensory and motor noise. *Journal of computational neuroscience*, 30(3):759–778, 2011.
- [59] Adam D Goodworth and Robert J Peterka. Identifying mechanisms of stance control: a single stimulus multiple output model-fit approach. *Journal of neuroscience methods*, 296:44–56, 2018.
- [60] Farzad Ehtemam. *Neural Control of Speed in Human Walking*. PhD thesis, 2018.
- [61] David Logan, Tim Kiemel, and John J Jeka. Using a system identification approach to investigate subtask control during human locomotion. *Frontiers in computational neuroscience*, 10:146, 2017.
- [62] Katja Mombaur, Anh Truong, and Jean-Paul Laumond. From human to humanoid locomotion—an inverse optimal control approach. *Autonomous robots*, 28(3):369–383, 2010.
- [63] Martin L Felis, Katja Mombaur, Hideki Kadone, and Alain Berthoz. Modeling and

identification of emotional aspects of locomotion. *Journal of Computational Science*, 4(4):255–261, 2013.

- [64] Hyunglae Lee, Hermano Igo Krebs, and Neville Hogan. Linear time-varying identification of ankle mechanical impedance during human walking. In *ASME 2012 5th Annual Dynamic Systems and Control Conference joint with the JSME 2012 11th Motion and Vibration Conference*, pages 753–758. American Society of Mechanical Engineers, 2012.
- [65] Elliott J Rouse, Robert D Gregg, Levi J Hargrove, and Jonathon W Sensinger. The difference between stiffness and quasi-stiffness in the context of biomechanical modeling. *IEEE Transactions on Biomedical Engineering*, 60(2):562–568, 2013.
- [66] Elliott J Rouse, Levi J Hargrove, Eric J Perreault, and Todd A Kuiken. Estimation of human ankle impedance during the stance phase of walking. *IEEE Transactions on Neural Systems and Rehabilitation Engineering*, 22(4):870–878, 2014.
- [67] Natalie Mrachacz-Kersting and Thomas Sinkjær. Reflex and non-reflex torque responses to stretch of the human knee extensors. *Experimental brain research*, 151(1):72–81, 2003.
- [68] Yang Wang and Manoj Srinivasan. Stepping in the direction of the fall: the next foot placement can be predicted from current upper body state in steady-state walking. *Biology letters*, 10(9):20140405, 2014.
- [69] Lei Zhang and Chenglong Fu. Predicting foot placement for balance through a simple model with swing leg dynamics. *Journal of biomechanics*, 77:155–162, 2018.
- [70] Arthur D Kuo, J Maxwell Donelan, and Andy Ruina. Energetic consequences of walking like an inverted pendulum: step-to-step transitions. *Exercise and sport sciences reviews*, 33(2):88–97, 2005.

- [71] Frank Sup, Amit Bohara, and Michael Goldfarb. Design and control of a powered knee and ankle prosthesis. In *Proceedings 2007 IEEE International Conference on Robotics and Automation*, pages 4134–4139. IEEE, 2007.

**CHAPTER II**  
**METHOD FOR CONTROL IDENTIFICATION**

## ABSTRACT

*This chapter introduces several concepts that are used throughout this dissertation study. The overall goal of this study is to identify feedback control laws from human motion data. Therefore, this chapter discussed the indirect identification approach in section 2.2. This is followed by an overview of the trajectory optimization in section 2.3. Trajectory optimization provides a way to solve the indirect control law identification problem. Then, section 2.4 introduced the direct collocation method which discrete the trajectory optimization problem into nonlinear programming problem. The final section mentioned the interior point optimizer (IPOPT), a gradient based method, for solving the nonlinear programming problem. A method of preventing local optimum was also included in the final section.*

### 2.1 Introduction

In this chapter, basic concepts inside the controller identification problem are introduced. These concepts include indirect approach, trajectory optimization, direct collocation, and nonlinear programming. In order to describe these concepts closely with our research topic, the posture control laws identification in standing balance is used as an example here. The posture control law identification problem is to identify control laws from human standing balance experimental data. In this study, indirect approach is used to identify the control laws based on a close-loop simulation model. Because of using indirect approach, the identification problem is also a trajectory optimization problem. In the trajectory optimization, direct collocation is used to convert into a nonlinear optimization problem which is suitable for several nonlinear optimization solvers. Here we use interior point optimizer (IPOPT), a gradient based optimizer, to solve the nonlinear optimization problem. Besides, in order to prevent the local optimum issues, we run multiple optimizations with random initial guesses and select the best result as final result.

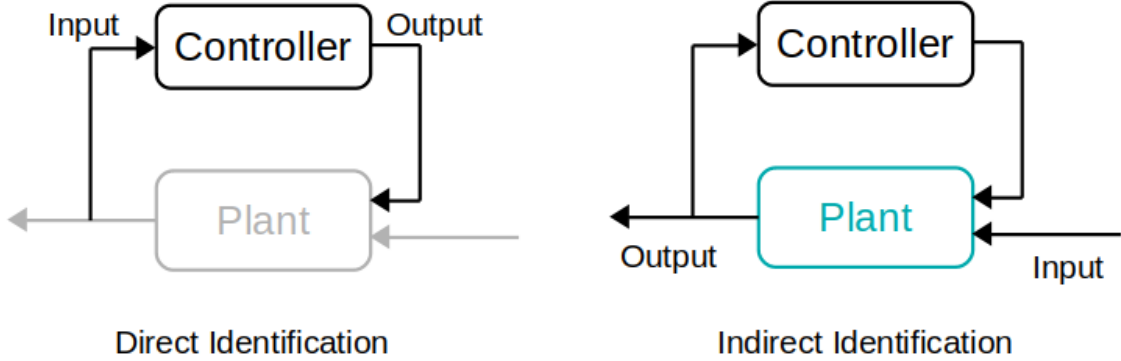


Figure 3: Direct and indirect identification approaches.

## 2.2 Indirect Approach

The indirect approach is widely used in controller identification problems, since it can prevent the bias issue in the direct approach [1, 2]. In the direct approach, only controller input and output are used to identify the control parameters, which ignored the close-loop connection between controller and plant. Thus, the identified results of direct approach could also be the inverse of plant dynamics, instead of the controller parameters. In the indirect approach, a close-loop system is needed to represent the identifying system. In general, a feedback controller and a plant model are included in the close-loop system. Normally, the plant model is pre-calculated and known. Then, the input and output of the entire system are used to identify the feedback controller which is the only unknown in the close-loop system. The diagram plots of the direct and indirect approaches are shown in Figure 3.

The indirect approach in controller identification is also an optimization problem. The general structure of indirect identification approach is shown in Figure 4. In general, there are two main components inside the indirect identification. One component is experiment, which experimental data is recorded under specific experimental conditions. In standing balance controller identification, the recorded experimental data is participants' postural responses, including ankle, knee, and hip joint trajectories. The experimental condition is the

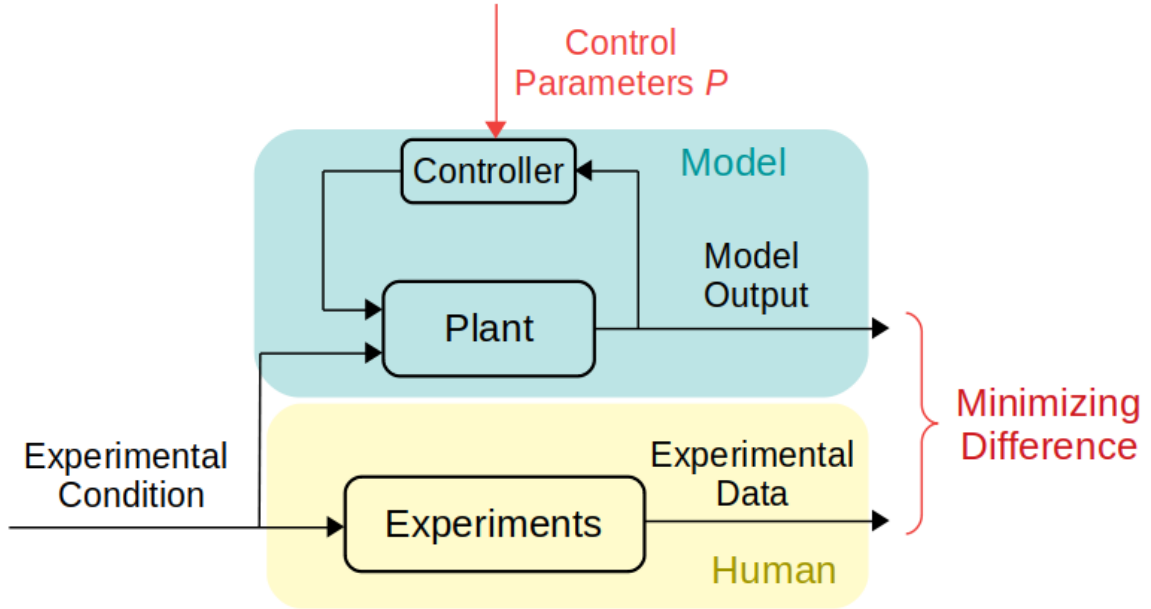


Figure 4: Diagram plot of trajectory optimization.

standing balance task which participants keep standing balance under random perturbation. The second component inside the indirect identification approach is the simulation model of the close-loop system that mentioned above. If a controller can be found that enable the close-loop simulation model to generate the same or close output with the recorded experimental data, we assume this controller is the controller that controlled the real participants in the experiment. This controller can be found using optimization method. Optimization can get the optimized feedback controller by minimizing the difference between simulation model output and experimental data. More specifically, this optimization problem is a trajectory optimization problem, since the the model output of the simulation model needs to optimize also. In posture control law identification, the output of the simulation model is the joint trajectories.

### 2.3 Trajectory Optimization

Trajectory optimization is to find the best feasible trajectories (optimal trajectory) for specific aims. In the posture control law identification of standing balance, the aim is to make

the trajectory output of simulation model has the best fit with recorded experimental data. Feasible trajectories mean that the trajectories must satisfy a variety of limits and constraints. In the posture control law identification of standing balance, feasible trajectories need to satisfy human body dynamics, boundary constraints, and bounds on state and control. The definition of trajectory optimization in posture control law identification is shown in Equation 2.1. There are no path constraints and boundary constraints inside the control law identification in our studies.

Optimize trajectory  $x(t)$  and control parameters  $P$

$$\text{Minimize the objective function } F = \int_0^T \|\theta_m(t) - \theta(t)\|^2 * dt$$

Subject to: human system dynamics:  $f(x(t), \dot{x}(t), P, a) = 0$  (2.1)

bounds on state:  $x_{low} \leq x(t) \leq x_{upp}$

bounds on control parameters:  $P_{low} \leq P \leq P_{upp}$

where,  $x(t)$  is the state of the human standing balance system, consisting of joint angles  $\theta$  and angular velocities  $\dot{\theta}$ ;  $P$  represent the unknown parameters of the identified controller;  $T$  is the total time period of optimized trajectory.  $\theta_m(t)$  is the measured joint angle variables inside the system state;  $\theta(t)$  is the optimized joint angle variables inside the system state.  $a$  is the acceleration of the applied perturbation.  $x_{low}$  and  $x_{upp}$  are the lower and upper bounds of the states.

For example, in posture control law identification of standing balance task, the human dynamic model is simplified as a two-link pendulum model shown in Figure 5. The dynamics equation of the human standing model has the format of  $M(\theta) * \ddot{\theta} + C(\theta, \dot{\theta}) * \dot{\theta} + G(\theta) + F(\theta, a) = \tau$ . In which,  $F(\theta, a)$  is the force component that caused by random perturbation. Combine the state feedback control law  $\tau = Con(\theta, \dot{\theta}, P)$ , the generalized human standing

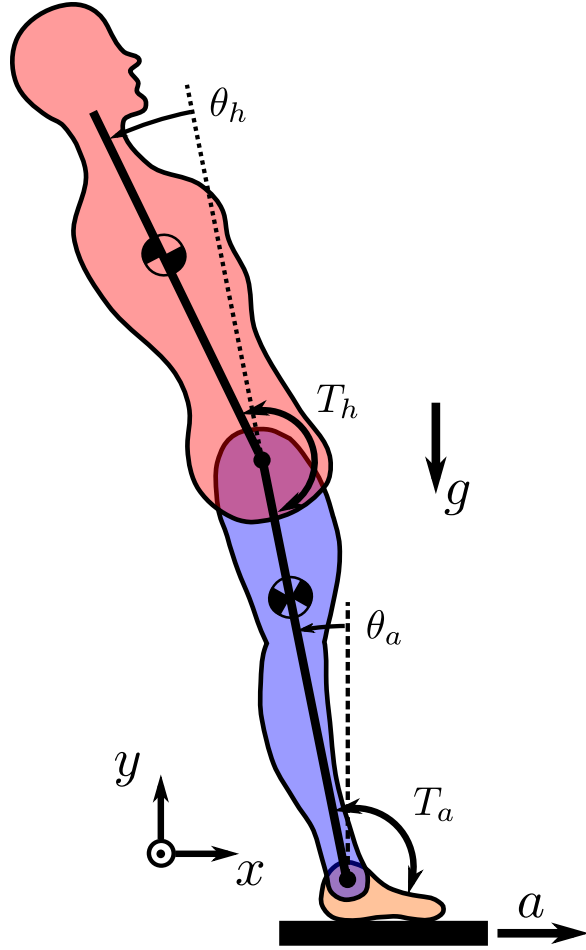


Figure 5: The double pendulum model of human standing balance system

balance system model is  $f(\theta, \dot{\theta}, \ddot{\theta}, P, a) = 0$ . By setting the system state  $x = [\theta, \dot{\theta}]$ , the dynamic function of the human standing system is  $f(x, \dot{x}, P, a) = 0$ .

## 2.4 Direct Collocation

Direct collocation has been mentioned has better efficiency than shooting method in trajectory optimization, especially for unstable systems [3]. Direct collocation discretizes the trajectory optimization problem into nonlinear programming problem. The constraints of system dynamics are applied on each collocation node. A linear polynomial is used to represent the connections between the nearby two or several collocation nodes. In direct collocation, higher density of collocation nodes and higher degree of polynomials give

more accurate results. In the posture control law identification, 50 collocation nodes per second were chosen and one degree of polynomial (linear) is used to connect the nearby two collocation nodes. The standing balance controller identification in direct collocation format is shown in Equation 2.2. The discrete trajectory optimization problem is also called nonlinear programming problem.

Optimize trajectory on collocation nodes  $x(t_1, \dots, t_N)$  and control parameters  $P$

$$\text{Minimize the objective function } F = \sum_1^N \|\theta_m(t_k) - \theta(t_k)\|^2$$

Subject to: approximate differentiation: 
$$\left\{ \begin{array}{l} \dot{x}_2 = (x_2 - x_1)/h \\ \dots \\ \dot{x}_k = (x_k - x_{k-1})/h \\ \dots \\ \dot{x}_N = (x_N - x_{N-1})/h \end{array} \right\} \quad (2.2)$$

human system dynamics: 
$$\left\{ \begin{array}{l} f(x(t_1), \dot{x}(t_1), P, a) = 0 \\ \dots \\ f(x(t_k), \dot{x}(t_k), P, a) = 0 \\ \dots \\ f(x(t_N), \dot{x}(t_N), P, a) = 0 \end{array} \right\}$$

bounds on state:  $x_{low} \leq x_{1,\dots,N} \leq x_{upp}$

bounds on control parameters:  $P_{low} \leq P \leq P_{upp}$

where,  $t_i$  is the time point of  $i^{th}$  direct collocation node;  $N$  is the total number of direct collocation nodes;  $h$  is the time interval between direct collocation nodes;

## 2.5 Nonlinear Programming

Nonlinear programming problem is defined as optimization problem which contains nonlinear constraints. In posture control law identification study, the nonlinear constraints are from the nonlinear dynamic equations of the human standing system. The above controller optimization problem can be write as nonlinear programming format, which is shown in equation 2.3.

$$\text{For } Y = (x_1, x_2, \dots, x_N, P)$$

$$\begin{aligned} & \text{Minimize } F(Y) \\ & \text{Subject to: } h(Y) = 0 \\ & Y_{low} \leq Y \leq Y_{upp} \end{aligned} \tag{2.3}$$

where,  $Y$  is the optimizing variables, including state trajectories  $x_1, \dots, x_N$  and controller parameters;  $P$ .  $F(Y)$  is the objective function;  $h(Y)$  is the nonlinear equality constrains.

There are many method to solve a nonlinear programming problem [4, 5]. Here, we choose the interior point optimizer (IPOPT) [6], an open source software package for large-scale nonlinear optimization, to solve the programming problem. It is a gradient based optimization method, which needs the gradient of objective function and Jacobin of the constrain functions. In our controller identification studies, objective is usually defined as quadratic function. Therefore, the gradient of it will be a vector contains linear functions, which is easy to get. Jacobin of nonlinear constraints is usually not easy to get, since the dynamic equations are quiet complicated, especially for high DOF system. In our controller identification studies, Jacobin of the nonlinear constraints are got using symbolic dynamic software, such as, Autolev (MotionGenesis), Sympy, and PyDy [7–9].

Gradient based optimization sometimes gives out local optimum results. This is mainly because the initial guesses for the optimization is not good. This could be unsolvable when you don't know the good initial guesses or the problem is too complex. One way to prevent this is to run multiple optimizations with different random initial guesses and choose the best result among these optimizations. More specifically, when several best optimizations give out similar result, there is a large possibility that the best results are global optimum. We will ran multiple optimizations with random initial guesses to prevent local optimum in our controller identification studies.

## 2.6 REFERENCES

- [1] Herman van der Kooij, Edwin van Asseldonk, and Frans CT van der Helm. Comparison of different methods to identify and quantify balance control. *Journal of neuroscience methods*, 145(1-2):175–203, 2005.
- [2] Sukyung Park, Fay B Horak, and Arthur D Kuo. Postural feedback responses scale with biomechanical constraints in human standing. *Experimental brain research*, 154(4):417–427, 2004.
- [3] Matthew Kelly. An introduction to trajectory optimization: how to do your own direct collocation. *SIAM Review*, 59(4):849–904, 2017.
- [4] Daniel Solow. Linear and nonlinear programming. *Wiley Encyclopedia of Computer Science and Engineering*, 2007.
- [5] John T Betts. *Practical methods for optimal control and estimation using nonlinear programming*, volume 19. Siam, 2010.
- [6] A. Wächter”. On the implementation of a primal-dual interior point filter line search algorithm for large-scale nonlinear programming.

- [7] Motiongenesis. <http://www.motiongenesis.com/index.html>. Accessed: 2019-04-22.
- [8] Pydy: Multibody dynamics with python. <http://www.pydy.org/>. Accessed: 2019-04-22.
- [9] Aaron Meurer, Christopher P. Smith, Mateusz Paprocki, Ondřej Čertík, Sergey B. Kirpichev, Matthew Rocklin, AMiT Kumar, Sergiu Ivanov, Jason K. Moore, Sartaj Singh, Thilina Rathnayake, Sean Vig, Brian E. Granger, Richard P. Muller, Francesco Bonazzi, Harsh Gupta, Shivam Vats, Fredrik Johansson, Fabian Pedregosa, Matthew J. Curry, Andy R. Terrel, Štěpán Roučka, Ashutosh Saboo, Isuru Fernando, Sumith Kulal, Robert Cimrman, and Anthony Scopatz. Sympy: symbolic computing in python. *PeerJ Computer Science*, 3:e103, January 2017. ISSN 2376-5992. doi: 10.7717/peerj-cs.103. URL <https://doi.org/10.7717/peerj-cs.103>.

**PART I.**

**CONTROL OF STANDING**

CHAPTER III  
STANDING BALANCE EXPERIMENT WITH LONG DURATION  
RANDOM PERTURBATION

**Conference Abstract:**

1. RAMP PERTURBATION TESTS ARE TOO SIMPLE TO IDENTIFY A REALISTIC CONTROLLER IN HUMAN STANDING BALANCE, BMES 2017.

## ABSTRACT

*Collecting standing balance experimental data of able-body subjects is a fundamental work for controller identification, since the generalized feedback controller will be identified from long duration balance data under random perturbations. Here we describe our standing balance experiment, in which a standing balance data-set collected from eight subjects. Each subject performed four experiment trials, including two quiet standing and two perturbed trials. Each trial lasted five minutes. A total of 80 minutes quiet standing and 80 minutes perturbed standing data are included in the data-set. Recorded information including three dimensional trajectories of twenty-seven markers (on subjects' trunk and legs), six dimensional ground reaction forces, and nine Electrocardiograph signals (EMGs, on subjects' right leg). In addition, joint angles and torques were calculated using a human body model and inverse dynamics. Basic descriptive analysis of the data is also included.*

### 3.1 Introduction

Studying human standing balance from experiment data has became a common approach. In order to obtain sufficient information about the feedback control system, perturbation is usually used in the experiment. Perturbation can trigger human standing balance system at more comprehensive situations than quiet standing. In most standing balance experiments, perturbation were usually applied on the standing plate, which has been accepted as a good protocol. There are two main types of perturbation signals: short ramp and long random. Several controller identification studies were done with these two kinds of perturbations. Park et al. identified full states proportional-derivative (PD) control parameters on the experiment data with different amplitudes of ramp perturbations. They concluded that feedback gains of the identified controllers are related with the ramp perturbation amplitude [1]. Welch et al. identified muscle activation also using ramp perturbation experiment data [2, 3]. Kiemel et al. studied the non-parametric neural responses on the standing

balance data under random mechanical perturbation. Their results suggested that human tends to keep stability rather than minimize sway [4]. Perterka and van der Kooij identified non-parametric motor-sensor control information from experiment data in frequency domain. Continually random perturbation and linear structure for controller were used in their study. [5–7]. Although the identified controllers of ramp reactions explained the experimental data, these controllers cannot be applied to humanoid robots and P/O devices. The main reason is that these controllers are perturbation amplitude depended, and it is impossible to predict perturbation amplitude in advance. Human balance data under random perturbation is more suitable to identify engineering applicable controllers. However, these data sets are not publicly accessible. In my study, an experiment with long duration random perturbation was done to support the standing balance controller identification, as well as provide a public accessible data set.

In this chapter, the experimental procedures for identification of human standing balance experiment is described. In section 2, experiment settings, participant exclusion criteria, and experiment protocol are described in detail. Recorded raw data, its quality, post-processing, and basic analysis are described in section 3. Discussion and conclusion of the standing balance experiment are in section 4 and 5, respectively.

## 3.2 Methods

In this section, we describe our experimental design beginning with descriptions of the participants and equipment. Then we show the protocol details. Finally, we talk about specifics on the perturbation design.

### 3.2.1 Participants

Eight able bodied subjects including one female and seven males with an average age of  $27 \pm 5.3$  years, height of  $1.71 \pm 0.08$  m, mass of  $65.3 \pm 9.2$  kg participated in the study.

This study was approved by the Institutional Review Board of Cleveland State University (# IRB-FY2018-40). Also, written informed consent was obtained from all participants. Participation exclusion criteria is showing below. All five conditions need to be satisfied.

- No any past extremity injuries on legs or feet and still affect movement and balance functions now.
- Haven't been diagnosed with any neuron-muscle disease.
- Body Mass Index (BMI: body weight/body height) below  $30 \text{ lbs}/\text{ft}^2$ .
- No neurological or other impairments that affects movements and balance.
- No pain or discomfort that could affect your movements.

Recorded data were anonymized with respect to the participants' identities. A unique identification number was assigned to each subject. A selection of the meta data collected for each participant is shown in Table I. The subjects were divided into those that were used for the protocol pilot trials, i.e., the first two (grey background), and those used for the final protocol. The final four columns provide the trial numbers associated with each experiment trials, Q means quiet standing trials; P means perturbed trials. The measured mass is computed from the mean of total vertical ground reaction force at quiet standing trial, if possible. Additional trial found in the data set with a trial number 0 is the unloaded trials that can be used for inertial compensation purposes, and are not shown in the table.

### 3.2.2 Equipment

Experiment was conducted in the Human Motion and Control lab at Cleveland State University. In the experiment, ten Osprey motion capture cameras (Motion Analysis) were used to tracking participants' motions during experiment. A computer software Cortex (version 5.0.1.1497) was used to control the recording process of these cameras. Motion

Table I: Information about the 8 study participants in the order of collection date.

Id	Gender	Age (yr)	Height (m)	Mass (kg)	Q1	P1	P2	Q2
1	female	22	1.60	$74.29 \pm 0.26$	1	2	3	4
2	male	–	–	$48.37 \pm 0.21$	5	6	7	8
3	male	18	1.80	$79.12 \pm 0.20$	9	10	11	12
4	male	27	1.78	$63.10 \pm 0.16$	13	14	15	16
5	male	32	1.79	$70.56 \pm 0.19$	17	18	19	20
6	male	35	1.65	$58.24 \pm 0.27$	21	22	23	24
7	male	28	1.75	$68.75 \pm 0.17$	25	26	27	28
8	male	27	1.63	$60.33 \pm 0.19$	29	30	31	32

was recorded at 100 Hz rate in the capture system. A four degree of freedom (DOF) V-Gait (Motek Medical) was used as standing plate and to apply perturbation. Six DOF force sensors were built in the V-Gait and used to detect ground reaction forces during experiment. Nine EMG sensors (Delsys Inc.) were used to record participants' muscle activation. EMG data was recorded at 1000Hz rate. Similar equipment used in the perturbed walking experiment done by Moore et al. [8]. Experiment setting is shown in Figure 6. In the experiment, D-Flow (version 3.26.0) software is used as an integral control tool to control all the equipment as well as to save collected data. The D-Flow application designed for the standing experiment is showing in Figure 7. In which, MoCap module controls the motion capture system and record EMG and 27 markers' data. V-Gait module controls the motion of V-Gait. XSens module connects with two accelerometers on V-Gait. Record Data module records V-Gait motion and XSens accelerometers' data.

In the experiment, twenty-seven markers were used to track the participants' movements. Five extra markers were placed on the standing platform to record its movement during experiment. Table II describes the landmarks of these 32 markers. Nine Electromyography (EMG) sensors were used in the experiment to record nine muscle activations in the right leg. The EMG sensors were placed according to ABC of EMG (SENIAM) [9]. The EMG sensor number, corresponding analogy channel number, and recorded muscles are shown in Table III.

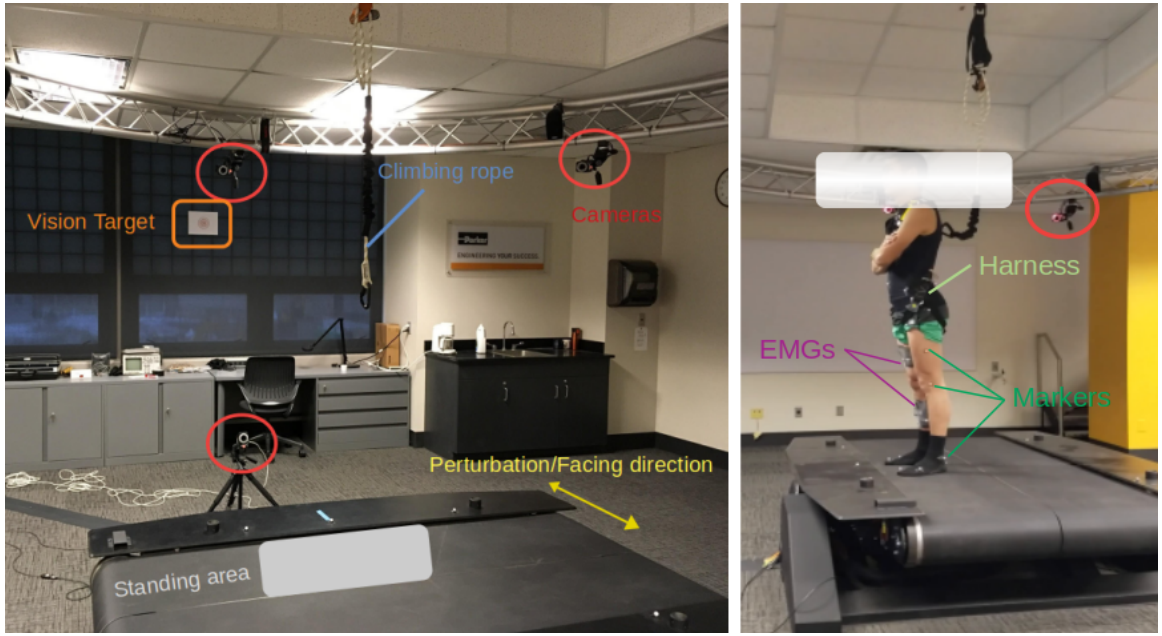


Figure 6: Standing balance experiment setting. Perturbation was applied in anterior and posterior direction using the sway motion of V-Gait. EMG sensors were placed on the right leg. Twenty-seven markers were put on participant's body to tracking motion.

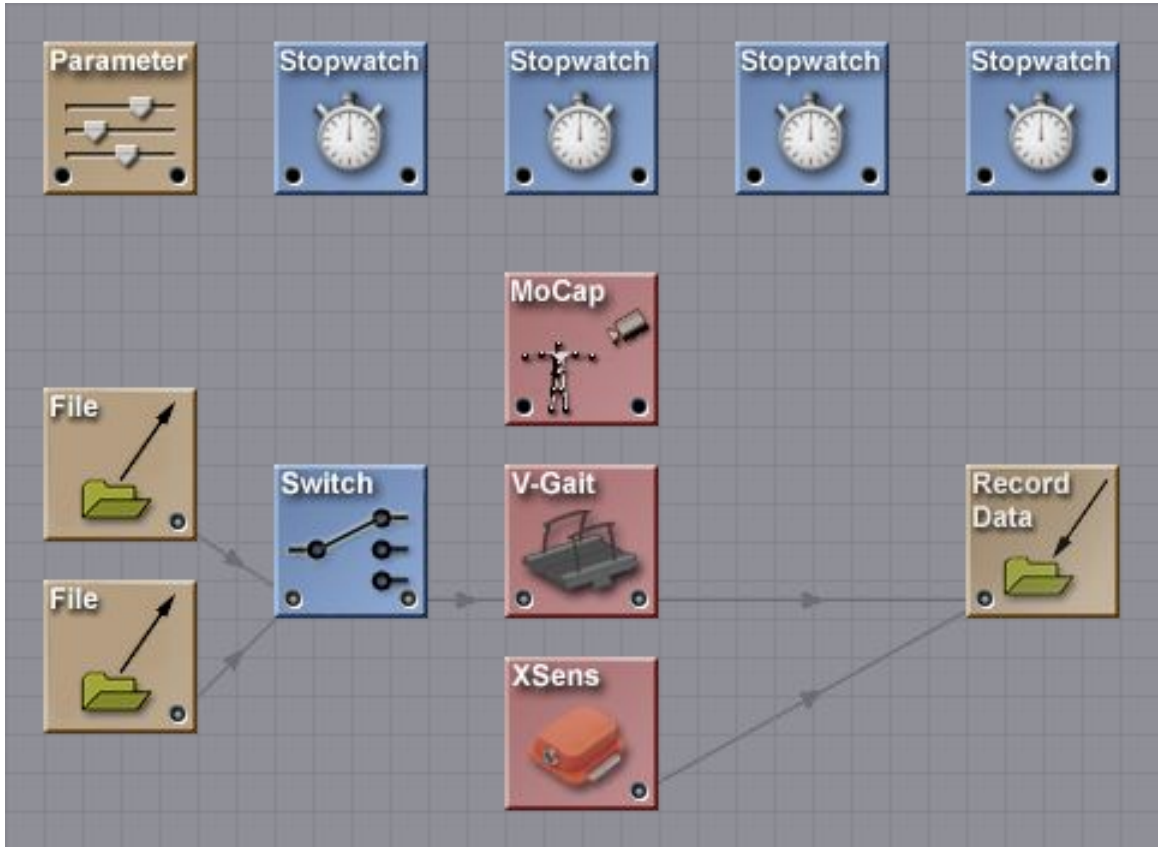


Figure 7: D-Flow application in standing balance experiment.

**Table II: Descriptions of the 27 subject markers and 5 treadmill markers used in this study.**  
The label column matches the column headers in the mocap-xxx.txt files. Location of these markers on human body are in the last column.

Label	Name	Description
T10	T10	On the 10th thoracic vertebrae
SACR	Sacrum bone	On the sacral bone
NAVE	Navel	On the navel
XYPH	Xiphoid process	Xiphoid process of the sternum
STRN	Sternum	On the jugular notch of the sternum
LASIS	Pelvis bone left front	Left anterior superior iliac spine
RASIS	Pelvic bone right front	Right anterior superior iliac spine
LPSIS	Pelvic bone left back	Left posterior superior iliac spine
RPSIS	Pelvic bone right back	Right posterior superior iliac spine
LGTRO	Left greater trochanter of the femur	On the center of the left greater trochanter
FLTHI	Left thigh	At 1/3 of the line between the LGTRO and LLEK
LLEK	Left lateral epicondyle of the knee	On the lateral side of the joint axis
LATI	Left anterior of the tibia	On 2/3 on the line between the LLEK and LLM
LLM	Left lateral malleoulus of the ankle	The center of the heel at the same height as the toe
LHEE	Left heel	Center of the heel at the same height as the toe
LTOE	Left toe	Tip of the big toe
LMT5	Left 5th metatarsal	Caput of the 5th metatarsal bone, on joint line midfoot/toes
RGTR	Right greater trochanter of the femur	On the center of the right greater trochanter
FRTHI	Right thigh	At 1/3 of the line between the RGTR and RLEK
RLEK	Right lateral epicondyle of the knee	On the lateral side of the joint axis
RATI	Right anterior of the tibia	At 2/3 of the line between the RLEK and RLM
RLM	Right lateral malleoulus of the ankle	The center of the heel at the same height as the toe
RHEE	Right heel	Center of the heel at the same height as the toe
RTOE	Right toe	Tip of the big toe
RMT5	Right 5th metatarsal	Caput of the 5th metatarsal bone, on joint line midfoot/toes
RACR	Right shoulder	Right acromion
LACR	Left shoulder	Left acromion
T1	Treadmill maker 1	On the left rear corner of the treadmill
T2	Treadmill maker 2	At 1/2 of the line between T1 and T2
T3	Treadmill maker 3	On the left front corner of the treadmill
T4	Treadmill maker 4	On the right front corner of the treadmill
T5	Treadmill maker 5	On the right rear corner of the treadmill

Table III: **Descriptions of nine EMGs used in this study.** # means the EMG numbers in Delsys system. EMG 6 was not used due to a wireless connection issue. Analog channel column listed the corresponding analog column number in the recorded analog files.

#	Analog Channel	Muscle Names	Muscle Locations
EMG 1	13	Tibialis anterior	In the upper two-thirds of the lateral (outside) surface of the tibia
EMG 2	17	Soleus	In the back part of the lower leg (the calf)
EMG 3	21	Medial gastrocnemius	On the medial back portion of the lower leg
EMG 4	25	Lateral gastrocnemius	On the lateral back portion of the lower leg
EMG 5	29	Vastus medialis	In the anterior and medial compartment of thigh
EMG 7	37	Vastus lateralis	In the anterior and lateral compartment of thigh
EMG 8	41	Rectus femoris	Situated in the middle of the front of the thigh
EMG 9	45	Biceps femoris	Begins in the thigh area and extends to the head of the fibula near the knee
EMG 10	49	Gluteus maximus	Located in the buttocks

### 3.2.3 Perturbation signal

In our standing balance experiment, perturbation was designed as random square wave signal, instead of a Gaussian random signal as used in van den Kooij's research [6]. The main reason is to avoid damaging the treadmill. The total mass of the V-Gait is about 800 lbs. In the experiment, the whole V-Gait will move laterally according to the perturbation signal, showing in Figure 6. The high frequency direction changes in Gaussian random signal will damage the motor. In order to have a random signal as well as not damage the treadmill, random square wave perturbation was designed.

Parameters that determined random square wave signal are amplitudes and stage duration. The principle of designing the signal is to let participants feel the greatest perturbation without taking a step as response. After several tests on lab members, a suitable perturbation signal was designed using square pulse with five amplitudes [-5, -2.5, 0, 2.5, 5] cm,

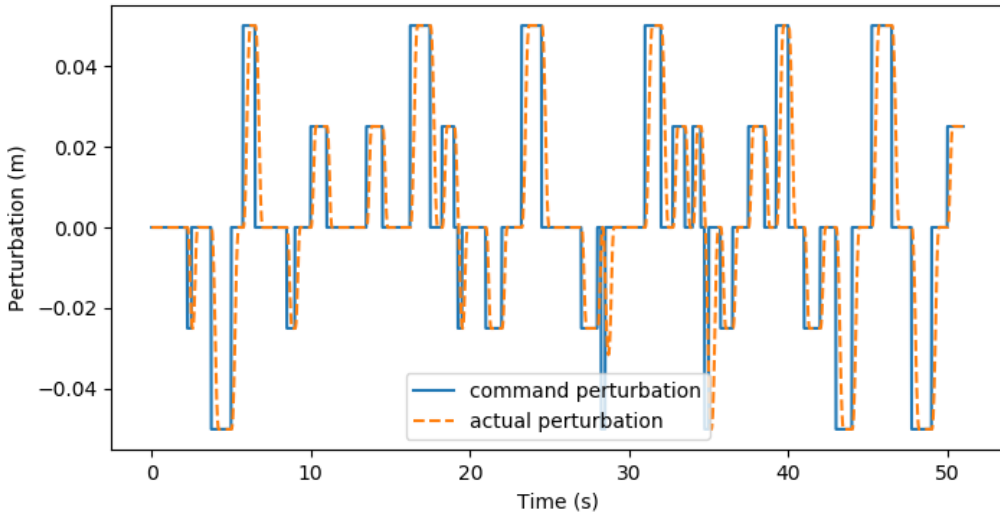


Figure 8: Comparison between the designed and actual standing balance perturbation. Designed perturbation has no dynamics and actual perturbation has a slow transient because of dynamics. Only the first 50 seconds is shown here.

and six stage duration [0.25, 0.5, 0.75, 1.0, 1.25, 1.5] seconds. Amplitudes and duration series were randomly generated to obtain a 300 second perturbation signal. All perturbed trials of eight participants used the same perturbation signal to check whether they have the similar responses.

The actual lateral motion of the V-Gait was calculated by averaging the motion of the five motion capture markers that were placed on the treadmill frame. The comparison between designed perturbation command and recorded Vgait movement is shown in Fig 8. The difference between actual and designed perturbation signal is mainly caused by the dynamics of treadmill. Generally, the actual perturbation reproduced the designed signal.

### 3.2.4 Protocol

The experimental protocol consisted of both static measurements and experimental recordings. Experimental recordings including standing on the treadmill for five minutes under unperturbed and perturbed conditions. Before a set of trials on the same day, the motion

capture system was calibrated using the manufacturer's recommended procedure. Prior testing, participants were asked to change into athletic shoes, shorts, a sports bra (for female). All twenty-seven markers were applied directly to the skin except for the heel, toe, and hip markers, which were placed on the respective article of clothing. Then age, gender, height, and mass were documented. Finally, their knee and ankle widths were measured by the experimentalist. After obtaining informed consent and a briefing by the experimentalist on the trial protocol, the experimental protocol for a participant was as follows:

1. The participant stepped onto the treadmill and markers were identified with Cortex.
2. A safety rope was attached loosely to the rock climbing harness such that no forces were acting on the subject during experiment. But the harness would prevent a full fall.
3. The participant started by stepping on sides of treadmill so that feet did not touch the force plates and the force plate signals were zeroed. Then participants were asked to step back to the treadmill.
4. A verbal countdown to the first quiet standing trial (Trial 1) was given by the experimentalist. Participants were asked to look at a target at roughly same height as their eyes. The quiet standing trial was five minutes long.
5. After the quiet standing trial, participant was asked to continue the first perturbation trial (Trial 2), in which 5 minutes anterior and posterior perturbation was applied on the treadmill . In the perturbation trial, participants were asked to keep balance without taking a step. However, he/she is free to adjust his/her pose by actively control his/her joints.
6. The participant was instructed to step off the force plate after the second trial to have a rest for five minutes.
7. The participant was asked to repeat the perturbation trial after rest (Trial 3).

8. The participant was asked to have another five minutes quiet standing trial (Trial 4) after the repeated perturbation trial.

For participants 3-8, specific instructions were given. Participants were instructed to keep their vision on the horizontal target, having the feet width similar to the width of shoulder, and feel free to bend the trunk to keep balance. The first participant had a wider stance, and the second participant used a strange (freezing) strategy to keep balance, instead of the normal relaxed strategy. The remaining six participants followed the regulations in the experiment. The identification work will use the last six participants' data.

### **3.3 Experimental Data and Post Processing**

In this section, we describe the recorded raw data; its quality, the filling process of the missing marker data. Then the post-processing and basic analysis will be described.

#### **3.3.1 Raw Data**

Each participants performed four trials. Each trial produced three raw data files. The first file is mocap file consisting of marker data recorded by the motion capture system and ground reaction force data recorded from the instrumented treadmill. The mocap data was recorded at 100 Hz rate. Another consisting of EMG analog data in 1000 Hz rate. Data columns of the EMG sensors can be found in Table III and the high recording rate is to satisfy the bandwidth of EMG analysis [10]. The last file is the V-Gait movement position and acceleration data recorded by D-Flow recording module. Acceleration data of V-Gait can be used in the inertia compensation process[11]. The sampling rate of D-Flow recording module is roughly 300 Hz. Time stamps in the mocap file and D-Flow recorded file are available to synchronize the data. In total, there are twelve raw data files recorded from each participant.

In the experiment, marker data was missing in some frames when a marker was obscured

or not recognized by the Cortex system. The quality of the marker data of all eight participants was assessed by determining the largest duration of missing frames and the overall percentage of missing frames, as shown in Table IV. Most trials had only a small time period of marker data missing. However, trial 3 in subject 2 had one large (2 seconds) period of missing data. The overall percentages of all trials are less than 0.1%, except the third trial of the second subject.

### 3.3.2 Filling missing marker data

Gaps (missing) of the marker data were filled using interpolation function in *MATLAB*. The filling process contains the following three steps:

1. Find out the index of marker data with value zero. D-Flow writes zero values on the file when a marker is not recognized. We assume that the position of marker will never be exactly zero if the marker was not missing.
2. Generate recorded marker data and corresponding time vector after removing the missing marker data and corresponding time stamps.
3. Generate the estimated value of missing marker data using *interp1* function in *MATLAB* with generated marker data in the above step.

Piece-wise Cubic Hermite Interpolating Polynomial (PCHIP) option was used in the 'interp1' function in **Matlab**. Good filling results were achieved even with large data gap period. One example of the gap filling is shown in Figure 9.

### 3.3.3 Joint angle calculation

Joint angles were calculated based on human body geometry. First, segment angles were calculated using the proximal and distal marker coordinates. Then, joint angles were calculated as the relative angles between segments. The same method was used in the "GaitAnalysisToolKit" developed by Moore et al in the perturbed walking paper [8]. In this

Table IV: Maximum numbers of continual missing frames and overall percentage of missing frames of all participants.

Participant No.	Trial	Max. gap (frames)	Missing data (%)
Participant 1	1	0	0
	2	0	0
	3	0	0
	4	0	0
Participant 2	1	2	0.05
	2	8	0.22
	3	194	0.015
	4	9	0
Participant 3	1	0	0
	2	0	0
	3	6	0.07
	4	0	0
Participant 4	1	0	0
	2	0	0
	3	0	0
	4	0	0
Participant 5	1	0	0
	2	1	0.005
	3	11	0.078
	4	0	0
Participant 6	1	0	0
	2	0	0
	3	10	0.0032
	4	0	0
Participant 7	1	0	0
	2	0	0
	3	10	0.0032
	4	0	0
Participant 8	1	0	0
	2	10	0.016
	3	0	0
	4	0	0

calculation, joint angles were averaged between left and right side leg based on a assumption that the participant movements were symmetric. Equation 3.1 shows the calculation of segment orientations, in which arc-tan function was used. Equation 3.2 shows the calculation of joint angles. The definition of joint angles in human standing model and their signs

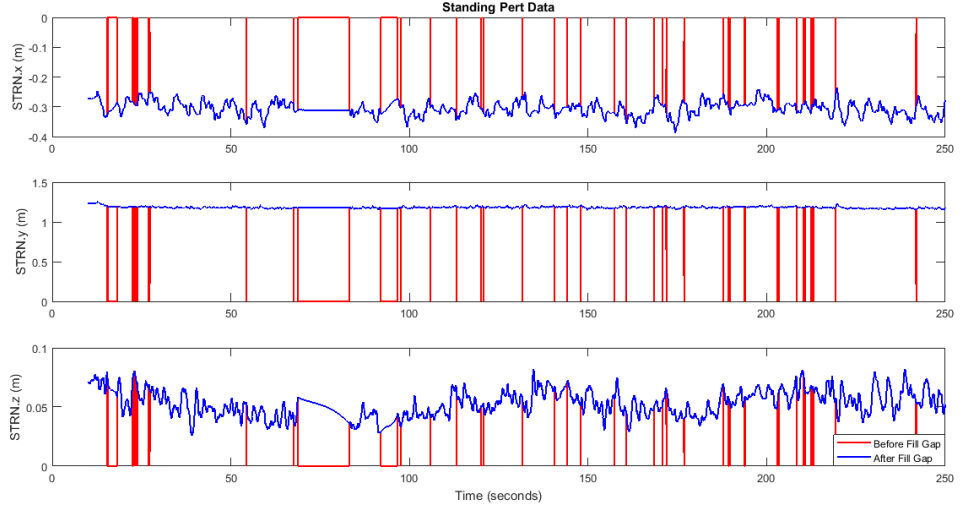


Figure 9: Gap filling result in experiment trial three of participant two. Red lines are original recorded data, which several frames' data were zero due to marker missing. Blue lines are filled marker data, which all the gaps were filled with reasonable data.

are defined in figure 10.

$$\begin{aligned}
 \theta_{Ltrunk} &= \arctan 2(y_{LACR} - y_{LGTRO}, x_{LACR} - x_{RGTR}) \\
 \theta_{Rtrunk} &= \arctan 2(y_{RACR} - y_{RGTR}, x_{RACR} - x_{RGTR}) \\
 \theta_{Lthigh} &= \arctan 2(y_{LGTRO} - y_{LLEK}, x_{LGTRO} - x_{LLEK}) \\
 \theta_{Rthigh} &= \arctan 2(y_{RGTR} - y_{RLEK}, x_{RGTR} - x_{RLEK}) \\
 \theta_{Lshank} &= \arctan 2(y_{LLEK} - y_{LLM}, x_{LLEK} - x_{LLM}) \\
 \theta_{Rshank} &= \arctan 2(y_{RLEK} - y_{RLM}, x_{RLEK} - x_{RLM}) \\
 \theta_{Lfoot} &= \arctan 2(y_{LTOE} - y_{LHEE}, x_{LTOE} - x_{LHEE}) \\
 \theta_{Rfoot} &= \arctan 2(y_{RTOE} - y_{RHEE}, x_{RTOE} - x_{RHEE})
 \end{aligned} \tag{3.1}$$

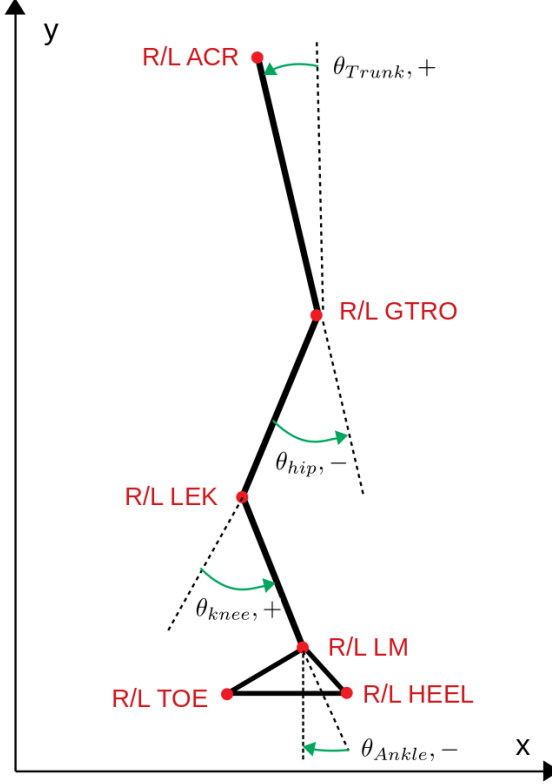


Figure 10: Human body diagram in standing balance task. The markers used for joint angles calculation is named in red color. The definition of joint angles is shown in the plot. Positive joint angles are defined with counterclockwise rotation. Joint torques have the same sign as joint angles.

$$\theta_{Trunk} = (\theta_{Ltrunk} + \theta_{Rtrunk})/2$$

$$\theta_{Hip} = \theta_{Trunk} - (\theta_{Lthigh} + \theta_{Rthigh})/2 \quad (3.2)$$

$$\theta_{Knee} = (\theta_{Lthigh} + \theta_{Rthigh})/2 - (\theta_{Lshank} + \theta_{Rshank})/2$$

$$\theta_{Ankle} = (\theta_{Lshank} + \theta_{Rshank})/2 - (\theta_{Lfoot} + \theta_{Rfoot})/2 + pi/2$$

A period of calculated joint angles of a participant is shown in Figure 11. The plot includes ankle, knee, and hip motions during a 100 second time period.

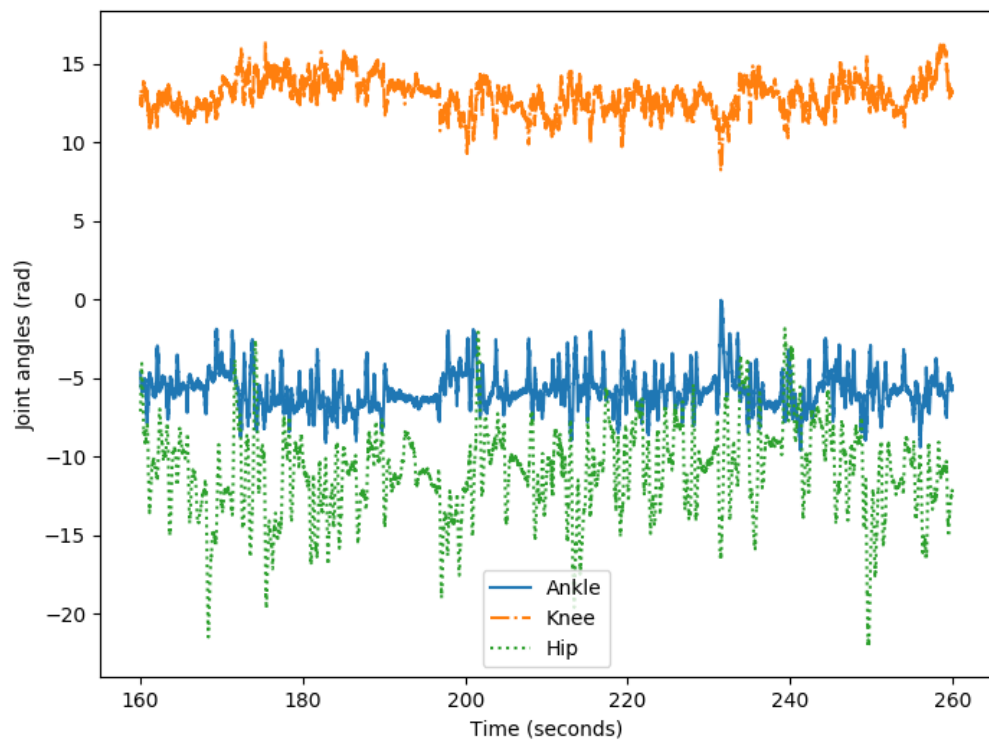


Figure 11: Calculated joints' angles of trail three of participant five. Hip, Knee, and Ankle joint angle data in 100 seconds range is showing in the plot.

### **3.3.4 Joint torque calculation**

Joint torques were calculated using "GaitAnalysisToolKit" [8], in which inverse dynamics was used. Before doing inverse dynamics, inertial compensation [12] was done using the ground reaction force and V-Gait motion from the unloaded trial. Inverse dynamics use the joint angles and ground reaction forces as inputs calculating joint torques based the human dynamic model. Since almost all reactions to perturbation were in sagittal plane, a two dimensional seven-link human body model was used [10]. Joint torques were average between left and right legs based on the assumption that movements of left and right legs in standing balance experiments were symmetric. The sign convention for joint torques are the same as joint angles.

### **3.3.5 Data Repository**

The gap-filled marker data, joint angles/torques are saved into text files and accessible for other possible users. They are saved to two files for each subject and each experiment trial. One file includes gap-filled marker data. Another file includes calculated joint angles and joint torques. Both two files are in 100 Hz sampling rate.

### **3.3.6 Analysis of joint motions**

Here we calculated the means and standard deviations of joint angles for six participants. These statistical information are shown in Figure 12 - 17. Here, joint angles include three joints: ankle, knee, and hip. The first and fourth experiment trials are quiet standing trials. The second and third trials are perturbed trials. The two quiet standing trials have similar variation of joint motion. However, there is a small difference in the variation of joint motion between two perturbed trials. Repeated perturbed trials tend to have a relative smaller joint motion variation than the first perturbation trial for almost all participants. In addition, variations of joint motion in perturbed trials are much larger than quiet standing trials.

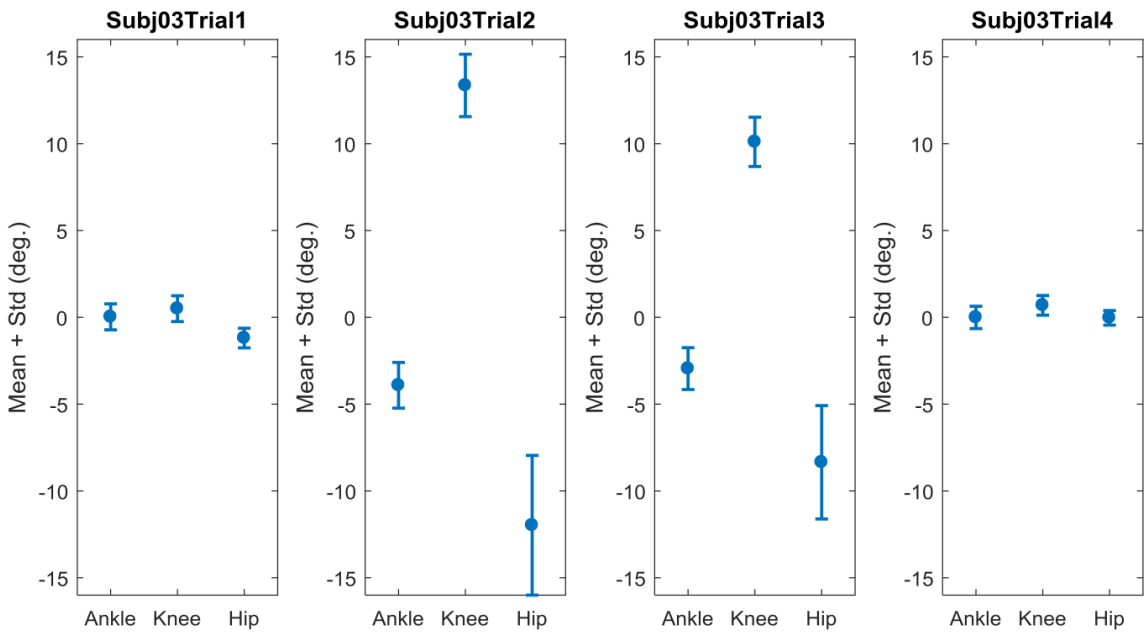


Figure 12: Joint angle analysis of subject 3. Analysis includes the mean and standard deviation of the ankle, knee, and hip joint motions.

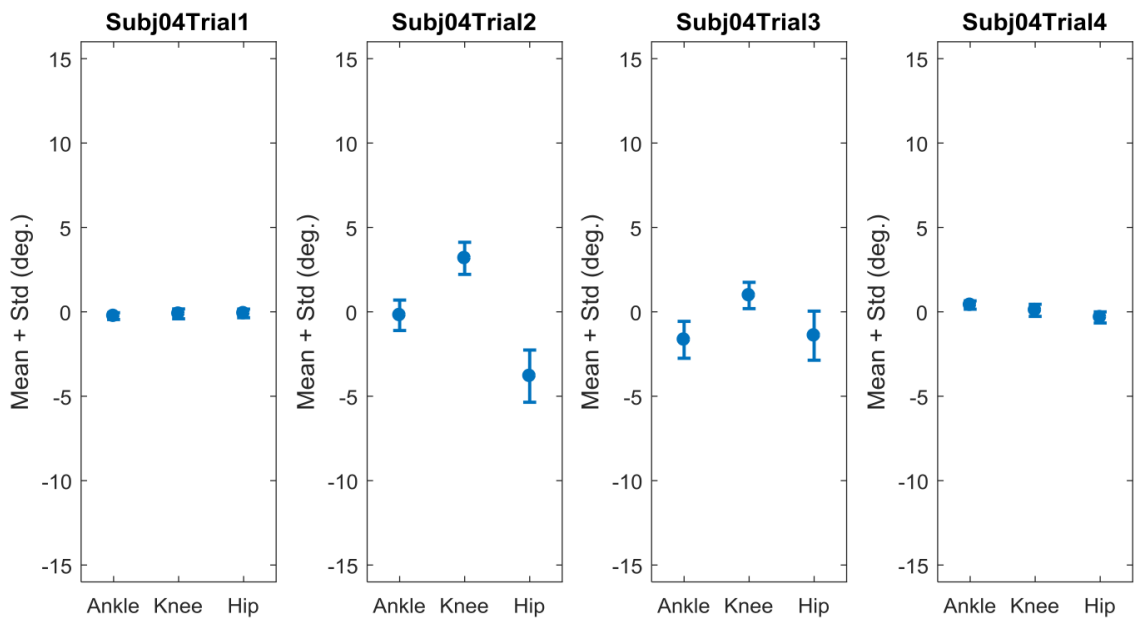


Figure 13: Joint angle analysis of subject 4. Analysis includes the mean and standard deviation of the ankle, knee, and hip joint motions.

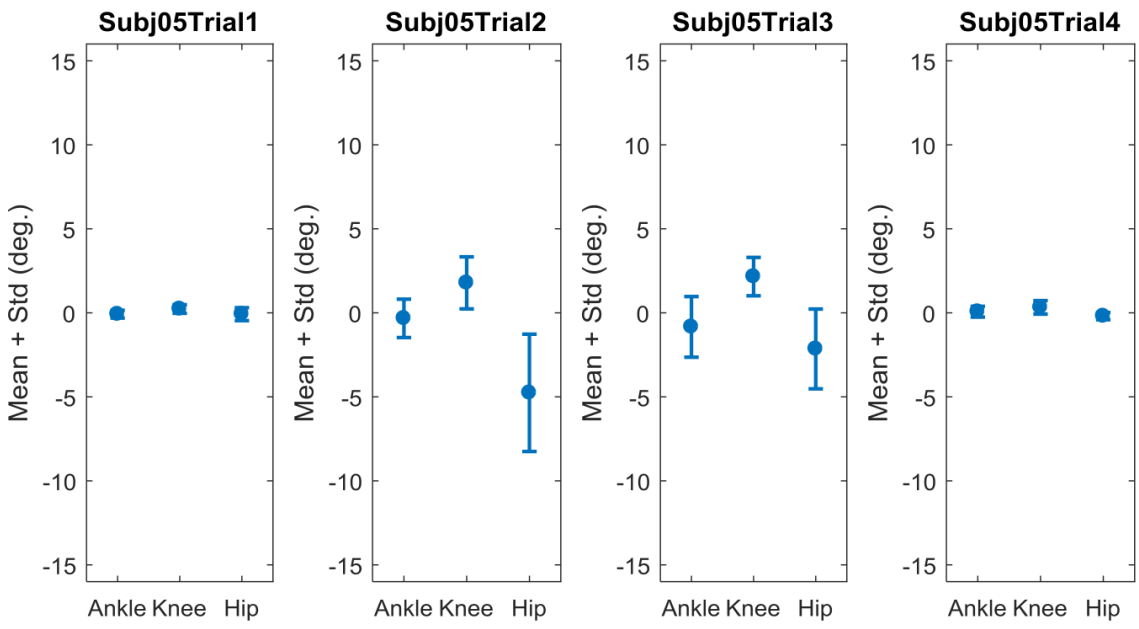


Figure 14: Joint angle analysis of subject 5. Analysis includes the mean and standard deviation of the ankle, knee, and hip joint motions.

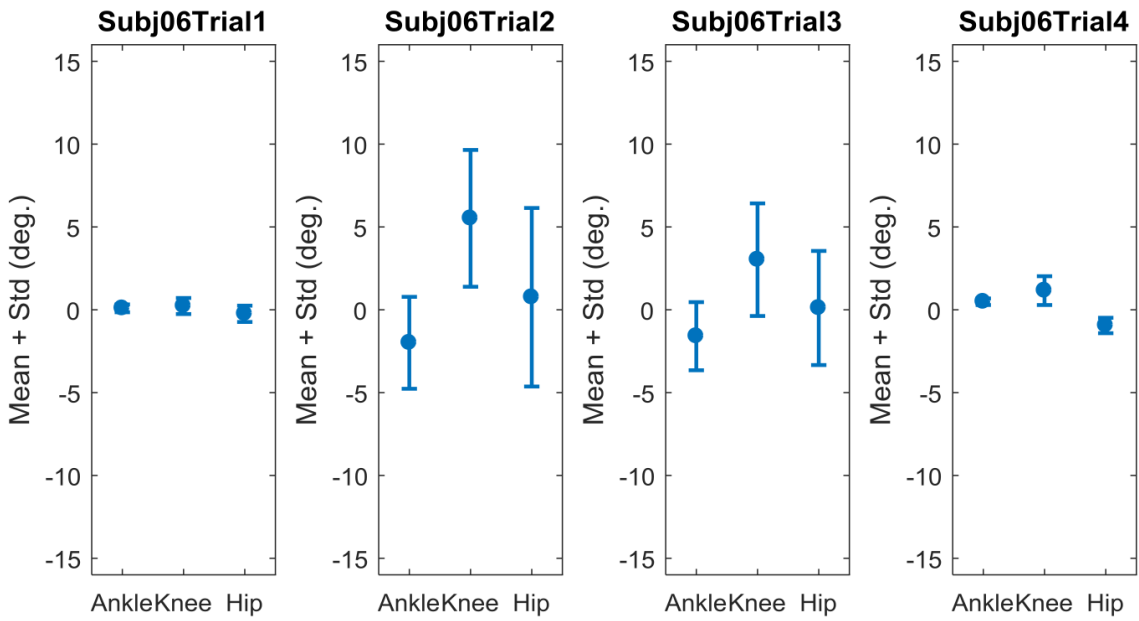


Figure 15: Joint angle analysis of subject 6. Analysis includes the mean and standard deviation of the ankle, knee, and hip joint motions.

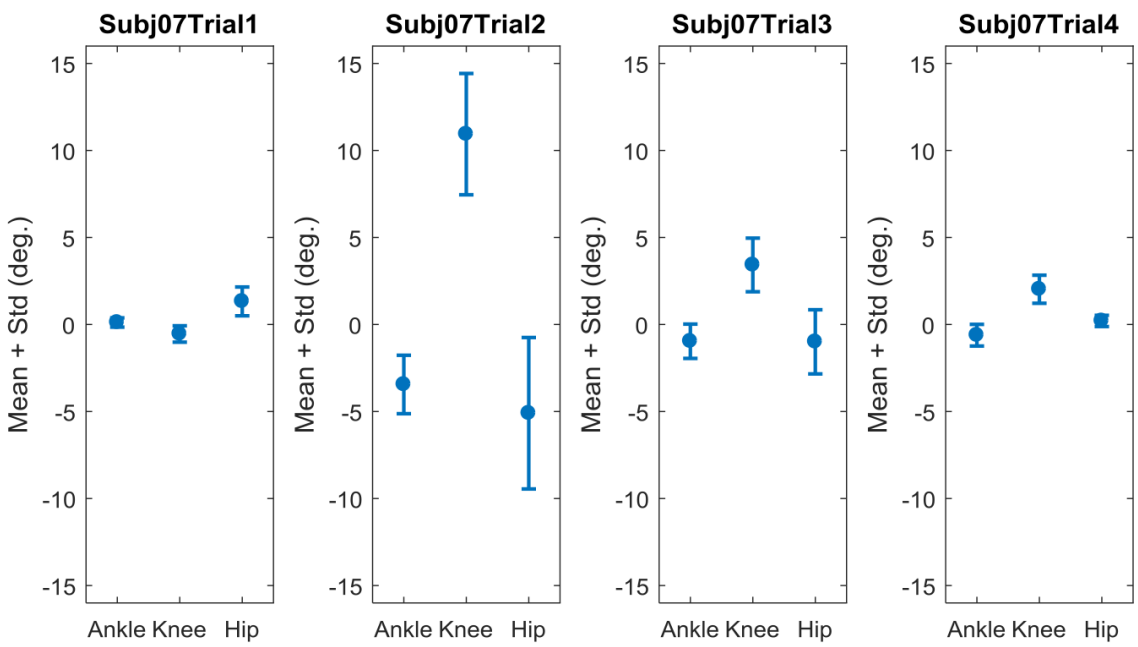


Figure 16: Joint angle analysis of subject 7. Analysis includes the mean and standard deviation of the ankle, knee, and hip joint motions.

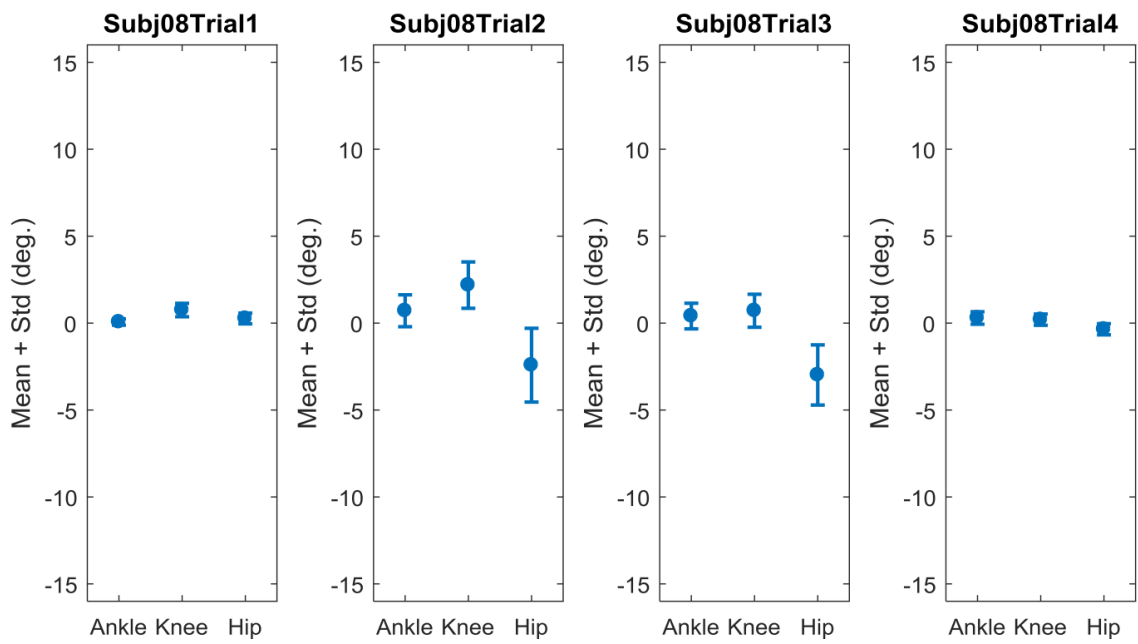


Figure 17: Joint angle analysis of subject 8. Analysis includes the mean and standard deviation of the ankle, knee, and hip joint motions.

### 3.4 Discussion

Based on our analysis, the data from the standing balance has sufficient quality for analysis. From the marker gap information, maximum period of missing data of all trials were less than 0.1 second (10 data frames) except the third trial of the second participant. The overall missing data percentage is less than 0.1% except for the third trial of the second participant. With 0.1 second data missing period, interpolation can help fill them up very well. Considering the first two participants were pilot studies (their data will not be used in the identification study), we consider the quality of the standing experiment data to be good.

As expected, the perturbation trials have larger motions than the quiet standing trials. This means that perturbation did cause participants to move their bodies while maintaining standing balance. The average knee angles are positive and average hip angles are negative for most participants. This means that they bent their knee and leaned their trunk forward in the standing balance experiment. This is typical reaction for most people in daily experience during standing balance. This standing balance experiment data can represent most people's reaction under perturbation. Thus the experiment data collected can be used to identify generalized feedback controller in human standing balance.

Perturbation trials do not affect the quiet standing balance for participants. The first and fourth trials of each participant are two quiet standing trials which were before and after perturbation trials. The range of joint motion in these two trials does not have a significant difference. This suggests that perturbation experience does not affect quiet standing balance. However, this have not be confirmed from qualitative study. We encourage some qualitative studies be done with the experiment data in future.

Participants have smaller joint motion range after the first perturbation experience. The repeated perturbation trial always has smaller motion range than the first perturbation trial

when comparing the motion range for each participant. Since the same perturbation signal was used in both perturbed trials, this means participants adapted to the perturbation and could keep balance using smaller body swing motions when experiencing the same perturbation.

### 3.5 Conclusion

In the standing balance experiment, over 160 minutes standing balance data of 8 participants were recorded. From the analysis, the collected standing balance data are in good quality. Joint motion are reasonable and satisfy our daily standing balance experience. The collected experiment data is suitable for identifying generalized feedback controller in standing balance task.

### 3.6 REFERENCES

- [1] Sukyung Park, Fay B Horak, and Arthur D Kuo. Postural feedback responses scale with biomechanical constraints in human standing. *Experimental brain research*, 154(4):417–427, 2004.
- [2] Torrence DJ Welch and Lena H Ting. A feedback model predicts muscle activity during human postural responses to support surface translations. *Journal of neurophysiology*, 2008.
- [3] Torrence DJ Welch and Lena H Ting. A feedback model explains the differential scaling of human postural responses to perturbation acceleration and velocity. *Journal of Neurophysiology*, 2009.
- [4] Tim Kiemel, Yuanfen Zhang, and John J Jeka. Identification of neural feedback for upright stance in humans: stabilization rather than sway minimization. *Journal of Neuroscience*, 31(42):15144–15153, 2011.

- [5] RJ Peterka. Sensorimotor integration in human postural control. *Journal of neurophysiology*, 88(3):1097–1118, 2002.
- [6] Herman Van Der Kooij and Erwin De Vlugt. Postural responses evoked by platform perturbations are dominated by continuous feedback. *Journal of neurophysiology*, 2007.
- [7] Herman Van Der Kooij and Robert J Peterka. Non-linear stimulus-response behavior of the human stance control system is predicted by optimization of a system with sensory and motor noise. *Journal of computational neuroscience*, 30(3):759–778, 2011.
- [8] Jason K Moore, Sandra K Hnat, and Antonie J van den Bogert. An elaborate data set on human gait and the effect of mechanical perturbations. *PeerJ*, 3:e918, 2015.
- [9] Peter Konrad. The abc of emg. *A practical introduction to kinesiological electromyography*, 1(2005):30–35, 2005.
- [10] David A Winter. *Biomechanics and motor control of human movement*. John Wiley & Sons, 2009.
- [11] Sandra K Hnat, Ben JH van Basten, and Antonie J van den Bogert. Compensation for inertial and gravity effects in a moving force platform. *Journal of Biomechanics*, 75: 96–101, 2018.
- [12] Sandra K Hnat and Antonie J van den Bogert. Inertial compensation for belt acceleration in an instrumented treadmill. *Journal of Biomechanics*, 47(15):3758–3761, 2014.

## CHAPTER IV

### IDENTIFICATION OF STABLE HUMAN POSTURAL CONTROL LAWS THROUGH STOCHASTIC TRAJECTORY OPTIMIZATION

#### **Conference Abstract:**

1. CONTROLLER IDENTIFICATION IN HUMAN STANDING BALANCE. Dynamic Walking 2018.

## ABSTRACT

*Background:* System identification can be used to obtain a model of the human postural control system from experimental data in which subjects are mechanically perturbed while standing. However, unstable controllers were sometimes found, which obviously do not explain human balance and cannot be applied in control of humanoid robots. Eigenvalue constraints can be used to avoid unstable controllers. However, this method is hard to apply to highly nonlinear systems and large identification datasets.

*New method:* To address these issues, we perform the system identification with a stochastic system model where process noise is modeled. The parameter identification is performed by simultaneous trajectory optimizations on multiple episodes that have different instances of the process noise.

*Results:* The stochastic and deterministic identification methods were tested on three types of controllers, including both linear and nonlinear controller architectures. Stochastic identification tracked the experimental data nearly as well as the deterministic identification, while avoiding the unstable controllers that were found with a deterministic system model.

*Comparison with Existing Method:* Comparing to eigenvalue constraints, stochastic identification has wider application potentials. Since linearization is not needed in the stochastic identification, it is applicable to highly nonlinear systems, and it can be applied on large data-sets.

*Conclusions:* Stochastic identification can be used to avoid unstable controllers in human postural control identification.

## 4.1 Introduction

Feedback control is a well accepted paradigm for human postural balance [1]. Identification of a feedback control system from human experiments has several important applications. In neuroscience, control system models are used to understand how humans maintain balance. In clinical applications, a quantitative description of the control system, e.g. as feedback gains and time delays, may have clinical applications. Finally, in humanoid robotics, a control system identified from human subjects can produce behavior that is more human-like than a control system designed from conventional control engineering principles.

System identification methods have been used, in both time and frequency domains, to identify feedback controllers from human experiments [2–4]. In the time domain, linear feedback controllers were identified on short experiments where ramp perturbations were applied to the standing surface. Results showed that controller gains were proportional to the amplitudes of ramp perturbations [3, 5], which suggests a nonlinear control system. In the frequency domain, controller architecture and sensory weights were identified on experimental data with random perturbations of long duration [2, 4].

However, one common issue of the identification work is that the best fit to the experiment was sometimes achieved with a controller that causes the closed loop system to be unstable. [3, 6]. While the best fit controller is always treated as the best identified controller, it is not useful since it can neither be applied to humanoid robots nor explain how humans control themselves. One possible reason of finding unstable controllers is that the process noise in both human system and experiment is not modeled. The identified controllers may take advantage of instability and sensitivity to initial conditions to achieve the best fit without falling.

To avoid instability, eigenvalue constraints have been used in the controller identification.

It enforces eigenvalues of the modeled closed loop system to be negative at a specific pose while identifying the controller parameters. This method was successful in avoiding unstable linear controllers in standing balance identification under ramp perturbations [3]. However, the application of this method is limited. For instance, it cannot work with highly nonlinear systems, since only a limited set of linearization points can be checked. For complex tasks such as walking, this could become impractical. In addition, it is hard to incorporate eigenvalue constraints into identifications with long experimental recordings, in which gradient-based optimization and collocation methods are needed. Long recordings, under continuous random perturbation, are needed to collect sufficient information to identifying more complex posture controllers. Direct collocation has been reported to be more efficient in such parameter identification problems [7, 8].

In this chapter, we hypothesize that a stochastic optimization, in which process noise is modeled, can help avoid finding unstable controllers in the standing balance identification problem. The stochastic optimization was applied on the identification of three types of controllers. Eigenvalue and forward simulations tests were done to examine the stability of the identified systems.

## 4.2 Methods

An indirect identification approach was used in this study [2–4, 6]. In the indirect approach, a model is built, which mathematically represents the closed loop system and an optimization method is used to fit experiment data by optimizing the model parameters. It has been reported that, in identifying the feedback controllers, the indirect approach can avoid the bias introduced by the direct approach which only uses the information of controller input and output [9]. In this paper, the mathematical model of the human standing balance system was treated as a closed-loop system which includes a body dynamics model and a feedback controller. The body dynamics model was simplified as a double-link pendulum,

since ankle and hip strategies are mostly used for standing balance [? ]. Three feedback controllers, as described below, were identified. The goal of the identification is to find the feedback controller parameters  $P$  which enable the closed-loop system generate the response that is closest to the human experimental data (Fig. 18).

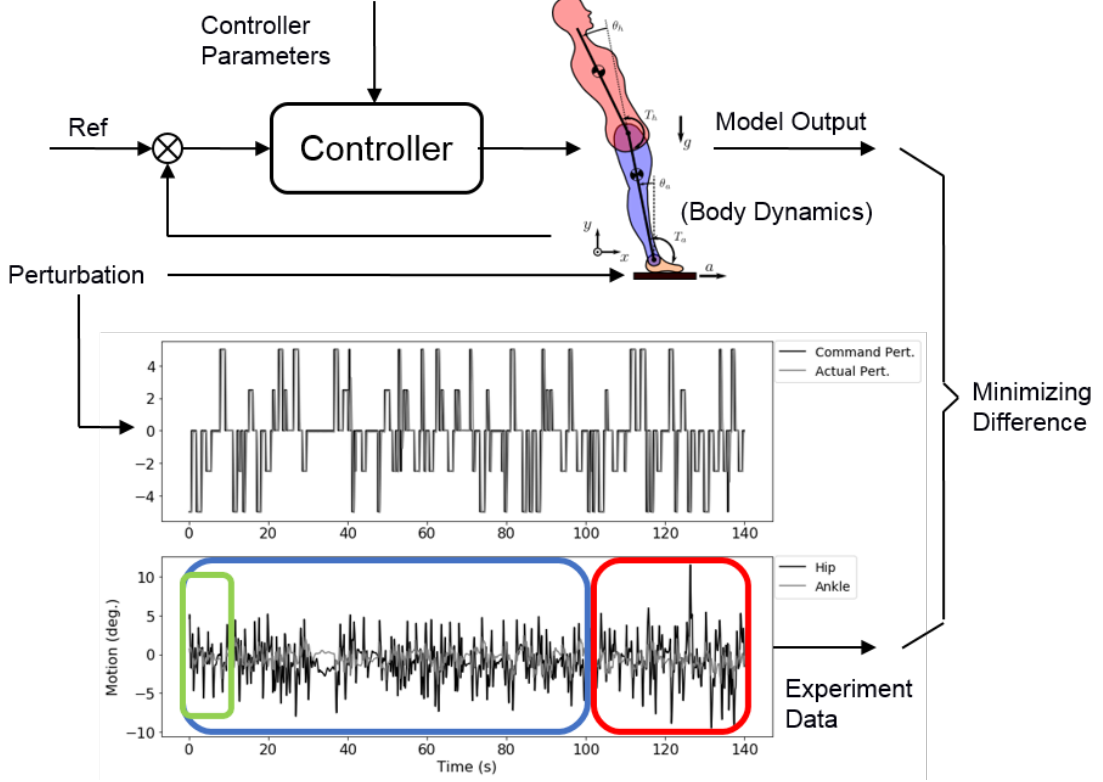


Figure 18: For identification of controller parameters, the same perturbation which was applied in the experiment was applied to the closed-loop system model. Controller parameters are optimized to fit the experimental data. The experimental data (140 seconds) was divided into 3 sections. The first 100 seconds (blue) were used to identify the linear controllers. The first 10 seconds (green) were used to identify the nonlinear controller. The last 40 seconds (red) were used to verify all identified controllers.

#### 4.2.1 Experiments

Experiments were performed on six participants (five male, one female, age 18-34 years) with approval from the Institutional Review Board of Cleveland State University with the study number IRB-FY2018-40. A R-Mill instrumented treadmill (Forcelink, Netherlands) was used to induce anterior-posterior (AP) perturbations of the standing platform through

its "sway" mechanism. Participants were asked to stand with their arms crossed in front of their chest and instructed to keep balance without taking a step. The perturbation signal was designed using random square pulses with five amplitudes ( $[-5, -2.5, 0, 2.5, 5]$  cm), and six pulse durations ( $[0.25, 0.5, 0.75, 1.0, 1.25, 1.5]$  seconds). Amplitudes and durations were randomly selected to generate a 140 second perturbation signal. Twenty-seven reflective markers were placed on each participant to record their reactions using a 10-camera motion capture system (Osprey, Motion Analysis Corp. Santa Rosa, CA). Hip and ankle joint motions were calculated from the recorded marker data, and the platform motion was recorded from encoders. The commanded perturbation signal, actual perturbation signal (standing platform motion) and balance reaction data (ankle and hip motion) of one participant can be found in Fig. 18. Data from one participant was used to show how the modeling of a stochastic environment affects the stability of identified controllers.

#### 4.2.2 Controller Structures

Three feedback controllers were identified on the data described in Section A. Two of them are linear: a proportional-derivative (PD) controller and a full-state proportional-derivative (FPD) controller. The other one is nonlinear: neural network (NN) controller. Formulas of these three controllers are shown below:

PD controller:

$$\begin{bmatrix} T_a \\ T_h \end{bmatrix} = \begin{bmatrix} K_{p_a} & 0 & K_{d_a} & 0 \\ 0 & K_{p_h} & 0 & K_{d_h} \end{bmatrix} \begin{bmatrix} \theta_a - \theta_a^r \\ \theta_h - \theta_h^r \\ \dot{\theta}_a \\ \dot{\theta}_h \end{bmatrix} \quad (4.1)$$

FPD controller:

$$\begin{bmatrix} T_a \\ T_h \end{bmatrix} = \begin{bmatrix} K_{p_{aa}} & K_{p_{ah}} & K_{d_{aa}} & K_{d_{ah}} \\ K_{p_{ha}} & K_{p_{hh}} & K_{d_{ha}} & K_{d_{hh}} \end{bmatrix} \begin{bmatrix} \theta_a - \theta_a^r \\ \theta_h - \theta_h^r \\ \dot{\theta}_a \\ \dot{\theta}_h \end{bmatrix} \quad (4.2)$$

where  $T_a$  and  $T_h$  are ankle and hip joint torques;  $\theta_a$  and  $\theta_h$  are ankle and hip joint angles;  $\theta_a^r$  and  $\theta_h^r$  are the reference joint angles for ankle and hip at quiet standing;  $\dot{\theta}_a$  and  $\dot{\theta}_h$  are ankle and hip joints angular velocities;  $K_p$  and  $K_d$  are proportional and derivative gains of feedback controllers.

For the nonlinear controller, a standard neural network architecture [? ] with 1 hidden layer and 4 hidden nodes was used. The inputs are the system state and a constant value node, and the outputs are joint torques. The smoothed leaky-ReLU function was used as activation function and is showing in Equation .4.3. The reason to smooth the activation function is make it continuously differentiable, which is essential to gradient-based optimization.

$$f(x) = x + 0.7\left(\frac{x - \sqrt{x^2 + 0.0001}}{2}\right) \quad (4.3)$$

The control parameters in the two types of linear controllers are the proportional-derivative gains  $K$  and reference joint angles  $\theta^r$ . The control parameters in neural network are the weights  $W_{ij}$  applied in between the input layer, the hidden layer, and output layer. The total number of controller parameters in the PD, FPD, and NN controllers are 6, 10 and 30, respectively.

#### 4.2.3 Controller Identification in Deterministic Environment

Deterministic environment, without modeling of process noise, has been used in most controller identification studies [3, 4, 6]. The deterministic standing balance controller identification problem was defined as a combined trajectory and parameter optimization problem:

Optimize trajectory  $x(t)$  and control parameters  $P$

$$\text{Minimize objective function } F = \int_0^T \|\theta_m(t) - \theta(t)\|^2 dt \quad (4.4)$$

Subject to: body dynamics:  $f(x(t), \dot{x}(t), P, a) = 0$

where  $x(t)$  is the state trajectory of the identified system, including ankle/hip joint angles  $\theta$  and angular velocities  $\dot{\theta}$ ;  $P$  represents the control parameters inside the feedback controller;  $T$  is the total time period of the measured experimental data;  $\theta_m$  is the measured joint angles;  $\theta$  is the optimized joint angles;  $a$  represents the acceleration of perturbation;

#### 4.2.4 Controller Identification in Stochastic Environment

In a stochastic environment, process noise is considered in the controller identification process. In controller identification with stochastic environment, the optimization is carried out over multiple episodes. Each episode simulates the motions with the same controller, and the same perturbation signal, but with a different process noise signal. The identifica-

tion problem for the stochastic environment is defined below:

Optimize trajectory  $\{x^1(t), \dots, x^M(t)\}$  and Controller Parameters  $P$

$$\text{Minimize objective function: } F = \sum_{s=1}^M \left( \int_0^T \|\theta_m(t) - \theta^s(t)\|^2 * dt \right)$$

Subject to: body dynamics: 
$$\left\{ \begin{array}{l} f_1(x(t), \dot{x}(t), P, a) + n_1(0, \sigma) = 0 \\ \dots \\ f_s(x(t), \dot{x}(t), P, a) + n_s(0, \sigma) = 0 \\ \dots \\ f_M(x(t), \dot{x}(t), P, a) + n_M(0, \sigma) = 0 \end{array} \right\} \quad (4.5)$$

where  $M$  is the total number of episodes;  $s$  is the  $s^{th}$  episode;  $x^s(t)$  is the state trajectory of human system model in  $s^{th}$  episode;  $n_s(0, \sigma)$  is random noise added to  $s^{th}$  episode.

The direct collocation method [10] was used in this paper. This transforms the trajectory optimization problem into nonlinear program (NLP) with a finite number of unknowns: the states  $x$  at  $N$  collocation nodes, and the controller parameters [8, 11]. The Midpoint Euler approximation was used to convert the body dynamics constraint into algebraic constraints:

$$f\left(\frac{x_{i+1} + x_i}{2}, \frac{x_{i+1} - x_i}{h}, P, a\right) = 0, \quad \text{for } i = 1, 2, \dots, N - 1. \quad (4.6)$$

The number of collocation nodes was 50 per second, and IPOPT was used to solve the NLP [1].

Four identification problems were solved for each controller structure. For each controller, a deterministic identification was performed first. For the linear controllers (PD, FPD), stochastic identifications with 2, 3, and 4 episodes were performed. For the nonlinear neural network controller, stochastic identification were performed with 6, 8, and 10 episodes. The

process noise was modeled as Gaussian random noise with amplitude of  $\pm 0.25 \text{ Nm}$ , added to the controller outputs (joint torques) at each time step. The process noise in each episode was randomly generated, and kept the same during the optimization process. For each identification problem, 10 optimizations with random initial guesses were performed. By selecting the best fit with experiment data among 10 optimizations, local optimum results can be largely prevented.

#### 4.2.5 Stability evaluation

Eigenvalues and forward simulations were used to evaluate the stability of the closed loop standing balance system with the identified controllers. In the eigenvalue test, the closed loop system dynamics were linearized to obtain eigenvalues at different operating points. These points covered the range of motion observed in the experiment. In the forward simulation tests, the identified controllers were used to perform 40 seconds simulations with all possible initial conditions inside the experiment data range. The perturbation (in red block) used in the forward simulation was different from the perturbation used in identifications. No process noise was used in these tests.

The distribution of four state variables (ankle angle, hip angle, ankle angular velocity, hip angular velocity) in the experimental data is shown in figure 2A. Ranges of these four state variables in degree (degree/s) are between [-3.87, -9.49, -16.53, -50.74] and [2.41, 11.50, 18.38, 65.00]. To check the stability of identified controllers in a standard way, eleven equidistant values were chosen within the range of each state variable, resulting in  $11 * 11 * 11 * 11 = 14641$  operating points where eigenvalues were calculated. The percentage of stable operating points (all eigenvalues negative) was calculated. Forward simulation tests used each of these operating points as an initial condition. A simulation was considered stable if the root mean square (RMS) between the forward simulations and the experiment data was within 3 times the standard deviation of experiment data. The percentage of stable simula-

tions was calculated for each identified controller. The eigenvalue and forward simulation tests were performed using the Ohio Super Computer System [12].

### 4.3 Results

Results of the identifications are summarized in Fig. 19. The percentage of stable eigenvalues and forward simulations (Fig. 2b) is always below 100%. One reason is that many of the checking points were outside of the range of actual state trajectories. Nevertheless, the effect of identification method on stability was clearly seen.

In the PD and NN controllers, results show that mostly stable controllers can be found by introducing a stochastic environment, while unstable controllers were found in the deterministic identifications. When the stochastic environment was introduced and the episode number increased to a specific number (3 episodes for PD controller type, 8 episodes for NN controller type), stable controllers were found, which resulted in high percentages of stable eigenvalues and stable forward simulations.

In the FPD control architecture, the deterministic identification already produced stability in about half of the tests. With the stochastic environment (2, 3, and 4 episodes), the percentage of stable eigenvalues and forward simulation remained high.

### 4.4 Discussion

Our results confirmed previous findings of unstable controllers when a deterministic model is used for identification of the human postural control system [3, 6]. The optimization is likely taking advantage of instability to improve the fit. In a deterministic unstable system, the final state can be made equal to the corresponding measurement, by extremely small changes in initial condition or controller parameters. We hypothesized that with a stochastic model, the optimization can no longer take advantage of instability to improve the fit

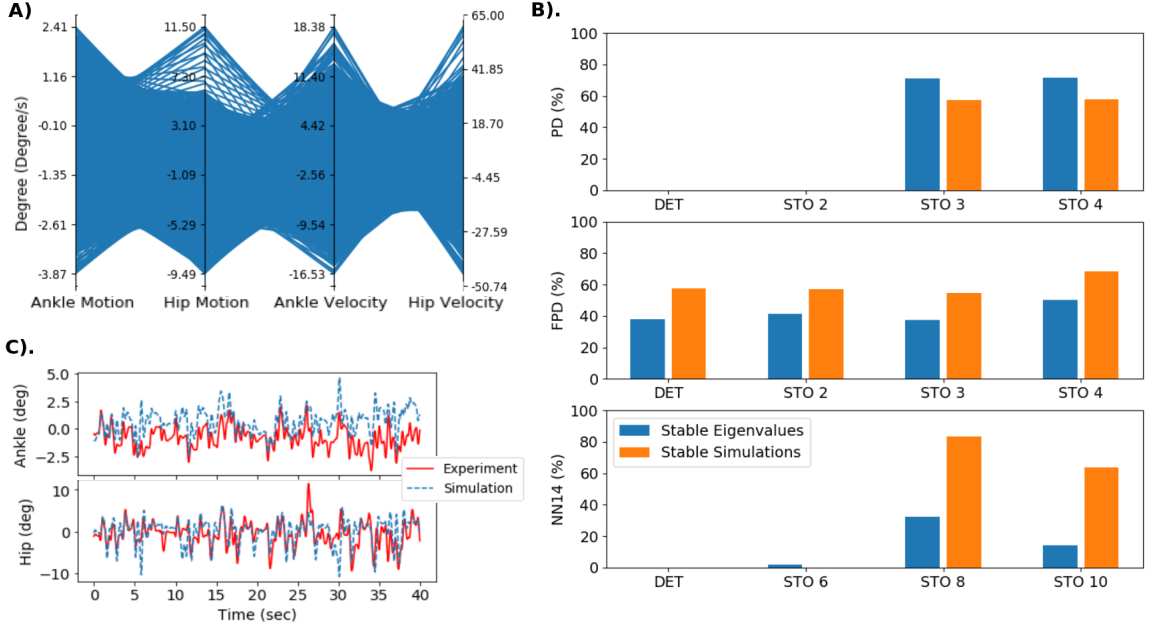


Figure 19: Eigenvalue and forward simulation test of identified best controllers among the whole state points. Subplot A is the range of each state variable from the human standing experiment data. subplot B is the percentages of stable eigenvalue and stable forward simulations of all 12 identified best controllers at all selected state points. "DET" means deterministic optimization. "STO i" means stochastic optimization with i episodes. Subplot C is one comparison between forward simulation and experiment data. RMS of this this forward simulation is about 1.3 STD of experiment data.

with the experiment. The stability tests using eigenvalue analysis and forward simulation tests supported our hypothesis. We also found that stochastic approach did not effect the stability very much when the deterministic approach already found a stable controller.

The eigenvalue analysis and forward simulation tests were mostly in agreement about the stability of the system, except in the NN controller. This is not surprising because linearization may not give a reliable evaluation of stability in a system with strong nonlinearities. This finding also suggests that the use of eigenvalues as constraints in the identification problem [3] is not likely to give useful results for nonlinear controllers. In contract, the stochastic trajectory optimization presented here is directly applicable to nonlinear systems without linearization.

Generally, more episodes were needed to find stable best controllers for more complex con-

trollers with more free parameters. In the case of our study, identification of a stable PD controller requires three episodes, while identification of a stable NN controller required eight episodes to get stable controllers. Because controller parameters (which are the same in each episode) and free initial conditions (which are different in each episode) can both be used to take advantage of instability, we suspect that the required number of episodes equals the number of control parameters divided by the number of system state variables.

The amplitude of Gaussian noise used in this paper was  $0.25 \text{ Nm}$ , applied to the joint torques of human balance system. This is approximately one percentage of the standard deviation of the joint torques in the standing balance experiment. An amplitude of  $0.5 \text{ Nm}$  was also tried, which had the same stability effect of  $0.25 \text{ Nm}$  but resulted in slightly larger control parameter differences between the identified stable controllers.

Recently, similar ideas of using a stochastic environment were also used in other studies to get realistic and stable results in robotic control. Mordatch increased the success rate of path planning in a biped robot by adding model uncertainty [13]. By adding model uncertainty and sensory noise, Peng largely increased the success rate in applying simulation environment trained policies to robot arms [14]. In model-based optimization research, simulation models are usually simplified to make research problems easier. However, the simplified model has a possibility of producing unrealistic results, since the optimization is not aware of the simplification and try to fit the simplified model to specific experiment data. By introducing a stochastic environment, optimization can no longer let the simplified model fit a specific data. Instead, simplified model will fit the general information of the data with noise, which can generate realistic results.

## 4.5 Conclusion

In this work, we showed that identification of human standing balance controllers by stochastic trajectory optimizations will produce controllers that are more robust than those obtained with a deterministic system model.

## Acknowledgement

The authors would like to thank the National Science Foundation (grant No. 1344954) and the Ohio Supercomputer Center.

## 4.6 REFERENCES

- [1] Arthur D Kuo. An optimal control model for analyzing human postural balance. *IEEE transactions on biomedical engineering*, 42(1):87–101, 1995.
- [2] RJ Peterka. Sensorimotor integration in human postural control. *Journal of neurophysiology*, 88(3):1097–1118, 2002.
- [3] Sukyung Park, Fay B Horak, and Arthur D Kuo. Postural feedback responses scale with biomechanical constraints in human standing. *Experimental brain research*, 154(4):417–427, 2004.
- [4] Herman Van Der Kooij and Erwin De Vlugt. Postural responses evoked by platform perturbations are dominated by continuous feedback. *Journal of neurophysiology*, 2007.
- [5] Torrence DJ Welch and Lena H Ting. A feedback model explains the differential scaling of human postural responses to perturbation acceleration and velocity. *Journal of Neurophysiology*, 2009.

- [6] Adam D Goodworth and Robert J Peterka. Identifying mechanisms of stance control: a single stimulus multiple output model-fit approach. *Journal of neuroscience methods*, 296:44–56, 2018.
- [7] Matthew Kelly. An introduction to trajectory optimization: how to do your own direct collocation. *SIAM Review*, 59(4):849–904, 2017.
- [8] Jason Keith Moore and Antonie J van den Bogert. opty: Software for trajectory optimization and parameter identification using direct collocation. *J. Open Source Software*, 3(21):300, 2018.
- [9] Herman van der Kooij, Edwin van Asseldonk, and Frans CT van der Helm. Comparison of different methods to identify and quantify balance control. *Journal of neuroscience methods*, 145(1-2):175–203, 2005.
- [10] Charles R Hargraves and Stephen W Paris. Direct trajectory optimization using nonlinear programming and collocation. *Journal of Guidance, Control, and Dynamics*, 10(4):338–342, 1987.
- [11] Jason. Moore and Antonie van den Begert. Human standing controller parameter identification with direct collocation. In *15th International Symposium on Computer Simulation in Biomechanics*, pages –. ISB, 2015.
- [12] Ohio Supercomputer Center. Ohio supercomputer center. <http://osc.edu/ark:/19495/f5s1ph73>, 1987.
- [13] Igor Mordatch, Kendall Lowrey, and Emanuel Todorov. Ensemble-cio: Full-body dynamic motion planning that transfers to physical humanoids. In *Intelligent Robots and Systems (IROS), 2015 IEEE/RSJ International Conference on*, pages 5307–5314. IEEE, 2015.

- [14] Xue Bin Peng, Marcin Andrychowicz, Wojciech Zaremba, and Pieter Abbeel. Sim-to-real transfer of robotic control with dynamics randomization. In *2018 IEEE International Conference on Robotics and Automation (ICRA)*, pages 1–8. IEEE, 2018.

#### IV.7 Appendix

The human body model in standing balance is simplified to a two-link pendulum as shown in 20. The standing plate is movable base and has a perturbation acceleration of  $a(t)$ . The format of dynamic equation of the human model is shown in Equation IV.7.

$$M(q) \cdot \ddot{q} + C(q, \dot{q}) \cdot \dot{q} + G(q) + A(q, a) = \tau \quad (\text{IV.7})$$

where  $q$  is the joint angles, including ankle and hip joints;  $a$  is the acceleration of standing plate;  $\tau$  is the joint torques;  $M(q)$  is the Mass matrix which includes the mass and inertia information of segments;  $C(q, \dot{q})$  is the Coriolis matrix;  $G(q)$  is the Gravity matrix which represent the potential energy changes;  $A(q, a)$  represents the force component caused by the acceleration of standing plate.

The feedback control in the standing balance is assumed to be state feedback control with the equation  $\tau = Con(P) \cdot [q, \dot{q}]$ , where  $P$  represents the control parameters. By putting the control law into the equation IV.7, close-loop dynamic model of human standing balance model is  $M(q) \cdot \ddot{q} + C(q, \dot{q}) \cdot \dot{q} + G(q) + A(q, a) - Con(P) \cdot [q, \dot{q}] = 0$ . The generalized close-loop dynamic equation of the human standing model is shown in Equation IV.8, where  $x = [q, \dot{q}]$  represents the system state.

$$f(x, \dot{x}, P, a) = 0 \quad (\text{IV.8})$$

## CHAPTER V

### IDENTIFICATION OF CONTROL LAWS IN HUMAN STANDING BALANCE

#### **Conference Abstract:**

1. STANDING BALANCE CONTROL PARAMETER IDENTIFICATION WITH DIRECT COLLOCATION. Dynamic Walking 2016.
2. CONTROLLER IDENTIFICATION IN HUMAN STANDING BALANCE. Dynamic Walking 2018.

## ABSTRACT

*Controller identification of standing balance is a well known research question. However, engineering applicable parametric controllers haven't been identified. In this paper, we identified stable standing balance controller from long period experiment data under random perturbations. Five controller types, from simple to complex, were identified in this paper. Eigenvalues were calculated of the identified controllers. Results shows that five out of six participants have similar eigenvalues, which means similar system reactions.*

### 5.1 Introduction

Feedback control, instead of preprogramed posture strategies, has been accepted to control posture in human standing balance task [1]. Although studies have been conducted trying to understand the feedback control system, controllers have not been got directly from human standing balance experiment data that could be applied on engineering devices, for instance, humanoid robots and P/O devices.

In optimal control aspect, studies have tried to design optimal controllers in the frame work of balance strategies in how human keep balance [1–3]. For example, in the framework of ankle & Hip strategies, optimal feedback controllers were designed using linear quadratic regulator (LQR) [4]. In simulation, these designed optimal controllers can keep human model (two-link pendulum) balance under external perturbations. However, their performances is different from how human reacts to perturbation.

CoM and Cop are the two important information when studies trying to explain the criteria that how human stay standing balance. It has been accepted that in order to keep standing balance, in general, CoP is suggested to stay inside the support area (area defined by the out curves of two feet) [5, 6]. However, how human keep Cop inside the support area is

still unclear with this research direction.

To understand how human use feedback control to keep standing balance, studies have been done to identify controllers from human standing balance experimental data [7–11]. In experiments, subjects were either perturbed with extra force, or the standing platform has a unexpected motion. The indirect identification approach is mostly used in these identification studies , since the open-loop identification will introduce bias [12].For instance, Park et al. identified stable full states PD controller parameters in different amplitudes of perturbations. It is concluded that the controller gains are changing along with the ramp perturbation amplitudes [7]. Welch et al. used ramp perturbation also to identify muscle activation [8, 13]. Kiemel et al. identified the non-parametric neural feedback of the standing balance under mechanical perturbation. The identified results suggested that human tends to keep stability rather than minimize sway [9]. Perterka and van der Kooji identified non-parametric motor-sensor control information from experiment data in frequency domain. They used continually perturbation and linear controller structures [10, 14, 15]. Goodworth et al. tested the identification method on simulation data in frequency domain, but have not reported results on human experiment data [11]. Although all these studies has been done, there is no engineering applicable controllers that has been extracted.

In this study, we proposed that there exists common general feedback controllers among healthy human to keep standing balance. Here, general means controller parameters do not change according to perturbation characters. In the chapter, We will identify the common control laws of healthy human standing balance. The identification will be done in time domain, which can be directly applied to engineering use. In order to identify this general controller, we applied long period continuous perturbation in experiment to collect how healthy human response to it. Linear and nonlinear control laws were identified in the chapter. Section 2 will describe the method used for identification. Experiment process

and data which used for identification were described in Chapter II. Section 3 shows identified results. Section 4 discusses the identified results. Conclusion and future work are mentioned in section 5.

## 5.2 Methods

In this section, identification approach, human body dynamics, controller types are described.

### 5.2.1 Indirect Approach

An indirect identification approach was used in this study to avoid the bias of direct identification [12]. In the indirect approach, a closed-loop system including human body dynamics, feedback controller were built to represent the human standing balance system. Since ankle and hip strategies are mainly used in keeping standing balance, human body dynamics was simplified to a double inverted pendulum model. Feedback controllers were used to control the motions of ankle and hip joint. Control parameters in the feedback controller were the targets of the identification. The indirect identification approach can be treated as an optimization problem, in which control parameters are optimized by minimizing the difference between the model output and the experiment data. The best control parameters are those who can make the close-loop model generate the same motion with experiment data under the same perturbation. The diagram of the indirect identification approach is shown in Figure 20.

More specifically, the optimization problem mentioned above is a trajectory optimization problem. To make it efficient, direct collocation method, other than shooting method, is used in this work. It has been shown that that direct collocation method is more efficient in trajectory optimization [16]. Here, direct collocation is used with 50 collocation nodes per second. Ipopt solver is used to solve optimization problems.

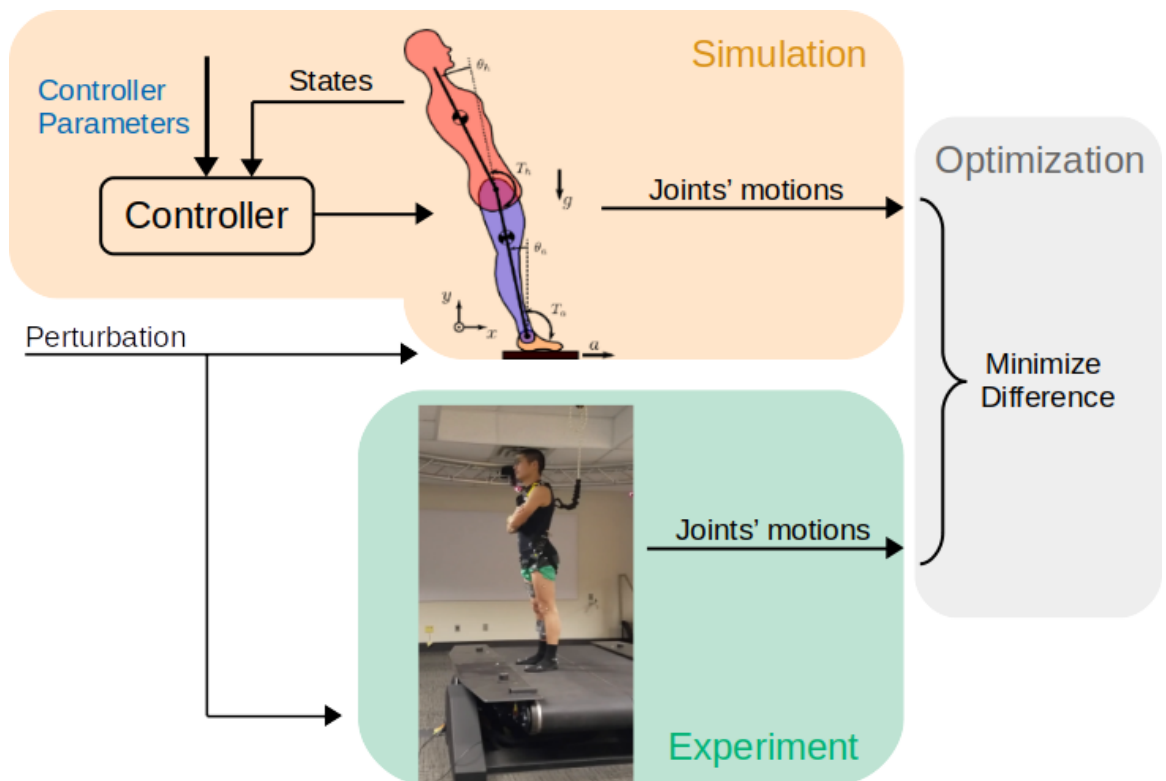


Figure 20: Structure of indirect identification approach in standing balance task. Identification can be treated as an optimization problem, in which control parameters are optimized by minimizing the difference between the model output and the experiment data

### 5.2.2 Human Body Dynamics

In the experiment, feet of participants were always rigidly attached with the ground. Therefore, human body dynamics is simplified to a double-link pendulum with foot combined with standing plate. The double-link pendulum is also a two dimensional model, since perturbation was only applied on sagittal plane. The segments lengths, mass, inertia were calculated based on participants' height and weight using the anthropometry table in Winter's book[17]. Dynamic equations of the double-link pendulum were generated using *Python Sympy* package[18].

### 5.2.3 Controller Structures

Five types of feedback controllers were used in this paper to identify control parameters on the experiment data mentioned in Chapter II. Two of them are linear: proportional-derivative (PD) controller and full-states proportional-derivative (FPD) controller. The other three are nonlinear: linear states combination with time delay (LSCTD) controller, neural network (NN) controller, and neural network with time delay (NNTD) controller. The formulas of these five controllers are shown below.

#### **PD controller:**

$$\begin{bmatrix} T_a(t) \\ T_h(t) \end{bmatrix} = \begin{bmatrix} K_{p_a} & 0 & K_{d_a} & 0 \\ 0 & K_{p_h} & 0 & K_{d_h} \end{bmatrix} \begin{bmatrix} \theta_a(t) - \theta_a^{ref} \\ \theta_h(t) - \theta_h^{ref} \\ \dot{\theta}_a(t) \\ \dot{\theta}_h(t) \end{bmatrix} \quad (5.1)$$

**FPD controller:**

$$\begin{bmatrix} T_a(t) \\ T_h(t) \end{bmatrix} = \begin{bmatrix} K_{p_{aa}} & K_{p_{ah}} & K_{d_{aa}} & K_{d_{ah}} \\ K_{p_{ha}} & K_{p_{hh}} & K_{d_{ha}} & K_{d_{hh}} \end{bmatrix} \begin{bmatrix} \theta_a(t) - \theta_a^{ref} \\ \theta_h(t) - \theta_h^{ref} \\ \dot{\theta}_a(t) \\ \dot{\theta}_h(t) \end{bmatrix} \quad (5.2)$$

**LSCTD Controller:**

$$\begin{bmatrix} T_a(t) \\ T_h(t) \end{bmatrix} = \sum_{m=0}^D \left( \begin{bmatrix} K_{p_{aa}}^m & K_{p_{ah}}^m & K_{d_{aa}}^m & K_{d_{ah}}^m \\ K_{p_{ha}}^m & K_{p_{hh}}^m & K_{d_{ha}}^m & K_{d_{hh}}^m \end{bmatrix} \begin{bmatrix} \theta_a(t - m * \delta t) - \theta_a^{ref} \\ \theta_h(t - m * \delta t) - \theta_h^{ref} \\ \dot{\theta}_a(t - m * \delta t) \\ \dot{\theta}_h(t - m * \delta t) \end{bmatrix} \right) \quad (5.3)$$

where  $T_a(t)$  is ankle joint torque at time point  $t$  and  $T_h(t)$  is hip joint torque at time point  $t$ ;  $\theta_a(t)$  and  $\theta_h(t)$  are ankle and hip joint angles at time point  $t$ ;  $\dot{\theta}_a(t)$  and  $\dot{\theta}_h(t)$  are ankle and hip joint angular velocities at time point  $t$ ;  $\theta_a(t - m * \delta t)$  and  $\theta_h(t - m * \delta t)$  are ankle and hip joint angles at  $m^{th}$  point prior to the current time point  $t$ ;  $\dot{\theta}_a(t - m * \delta t)$  and  $\dot{\theta}_h(t - m * \delta t)$  are ankle and hip joints angular velocities at  $m^{th}$  point prior to the current time point  $t$ ;  $K_p$  and  $K_d$  are proportional and derivative gains of feedback controllers multiplied with the state at time point  $t$ .  $K_p^m$  and  $K_d^m$  are proportional and derivative gains of feedback controllers multiplied with the state at  $m^{th}$  point prior to the current time point  $t$ .

**NN Controller:**

NN controller was defined as standard neural network with one hidden layer and four hidden nodes. It is nonlinear controller, since its activation function is a nonlinear function. The inputs of the NN controller are four states and outputs are two torques. Besides, one constant node (unit input) was added at both input and hidden layer. The activation function used in NN controller is smoothed leaky-ReLU function. The reason of smooth is to make

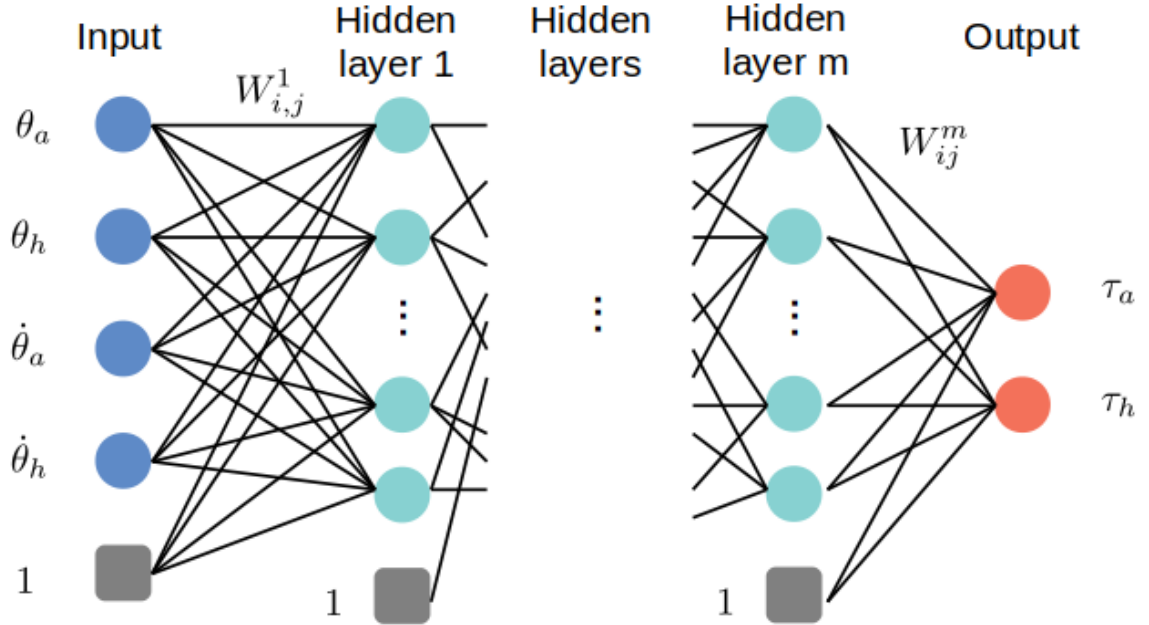


Figure 21: Structure of general neural network as controller. Control parameters are the weights between layers.

it differentiable at all points. The general structure of neural network is shown in Figure 21. The smoothed activation function is:

$$f(x) = x + 0.7 \left( \frac{x - \sqrt{x^2 + 0.0001}}{2} \right) \quad (5.4)$$

#### NNTD Controller:

NNTD controller used the same neural networking settings but with one hidden layer and eight hidden nodes. The difference is that the inputs of the NN controller are four current states and prior states (delay inputs). Outputs of NNTD controller are two torques.

The total number of optimizing parameters in PD, FPD, LSCTD, NN, and NNTD controllers are 6, 10, 34, 30, and 154, respectively.

#### **5.2.4 Avoid Unstable Controllers**

In chapter III, stochastic optimization was introduced to avoid identifying unstable controllers. In this identification work, we applied the stochastic optimization on PD and FPD controller identifications. Since complex controller types (with large control parameters) need more episodes in stochastic optimization. The computing power needed for LSCTD, NN, and NNTD are very high. Therefore, stochastic optimization was not applied on these three nonlinear controller types. Even though the identified controllers of these three controller types may not be stable, the fit between simulation model and experiment data can still reveal the ability of different controller types in explaining the human standing balance experiment data.

#### **5.2.5 Summary of the Identification**

Five controller structures were identified on six participants mentioned in Chapter II from participant 3 to participant 8. There are two perturbation trials of each participant. Here, we name the identification of one controller type on one perturbation data trial as one identification problem. In total, there are 60 (five controller types and twelve perturbation trials) identification problems in this standing balance controller identification task. In each identification problem of the first four controller types, ten optimizations were done with random initial guesses to avoid local optimum. For NNTD controller type, only one optimization was done for each identification problem, since it takes a long time to solve the optimization. Best identified controller was chosen has the best fit with experiment data inside ten optimizations.

### **5.3 Results**

Coefficient of determination ( $R^2$ ) of the best identified controllers in 60 identification problems are shown in Figure 22. For NNTD controller type, only several identification problems were succeed due to the difficulty of solving trajectory optimizations with such a

complex controller type. For other controller types, at least one optimization were successful in each identification problem.

One example of the fit between identified trajectories and experiment data (experiment trial 3 of participant 8) is shown in Figure 23 and 24. From simple to complex controller type, fit between simulation model and experiment data is getting better and better.

Since stochastic optimization help identified stable SPD and FPD controllers. The gains of identified controller and their eigenvalues can be studied to understand how healthy subjects control their standing balance under perturbation. Figure 25 and Figure 26 shows parameters and eigenvalues of identified PD controllers. Figure 27 and Figure 28 shows parameters and eigenvalues of identified FPD controllers. Gains in these figures are normalized by participants' body mass.

Gains of identified PD controllers have similar pattern among all participants except participant 7. Proportional gains are larger than derivative gains. Ankle proportional gains are larger than hip proportional gains. Reference angles of identified PD controllers are small, which agree with our expectation. However, the eigenvalues of them have a large variations. Eigenvalues of participant 4 and 7 are totally different from other participants. The rest four participants are not very close neither.

Gains of identified FPD controllers also have similar pattern among all participants except participant 7. The eigenvalues of them have a relative small variation than identified PD controllers. Five participants have close eigenvalues except participant 7.

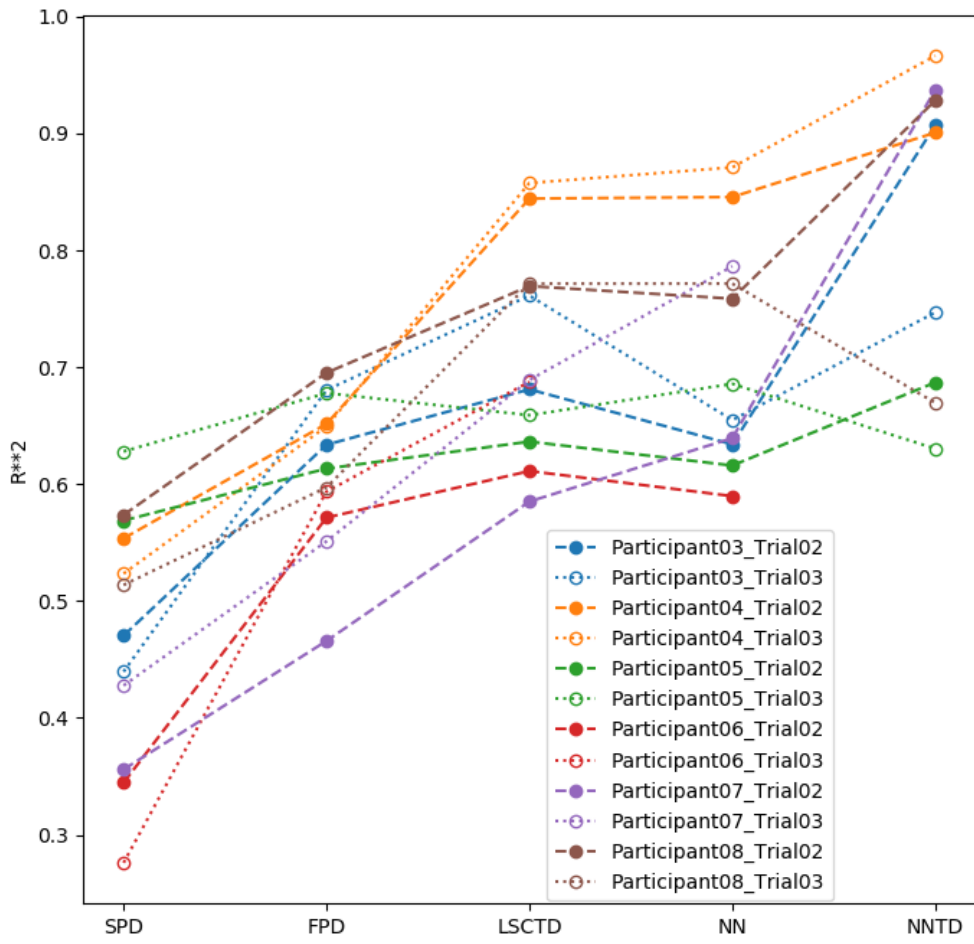


Figure 22:  $R^2$  between the best identified trajectories and experiment data. A higher value means a better fit.

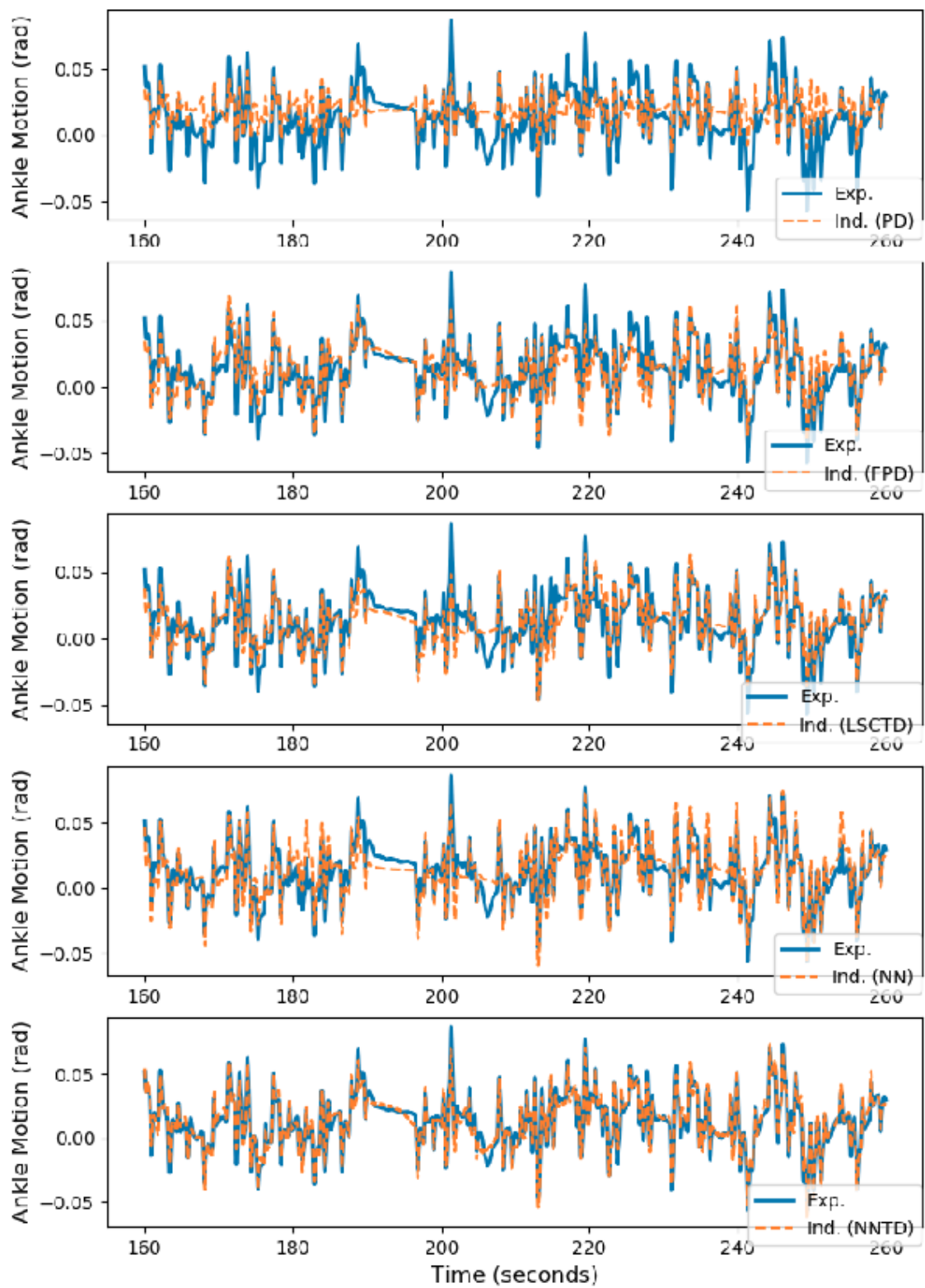


Figure 23: Ankle motion fit of participant 8 and trial 2. Fits get better with more complex controller types

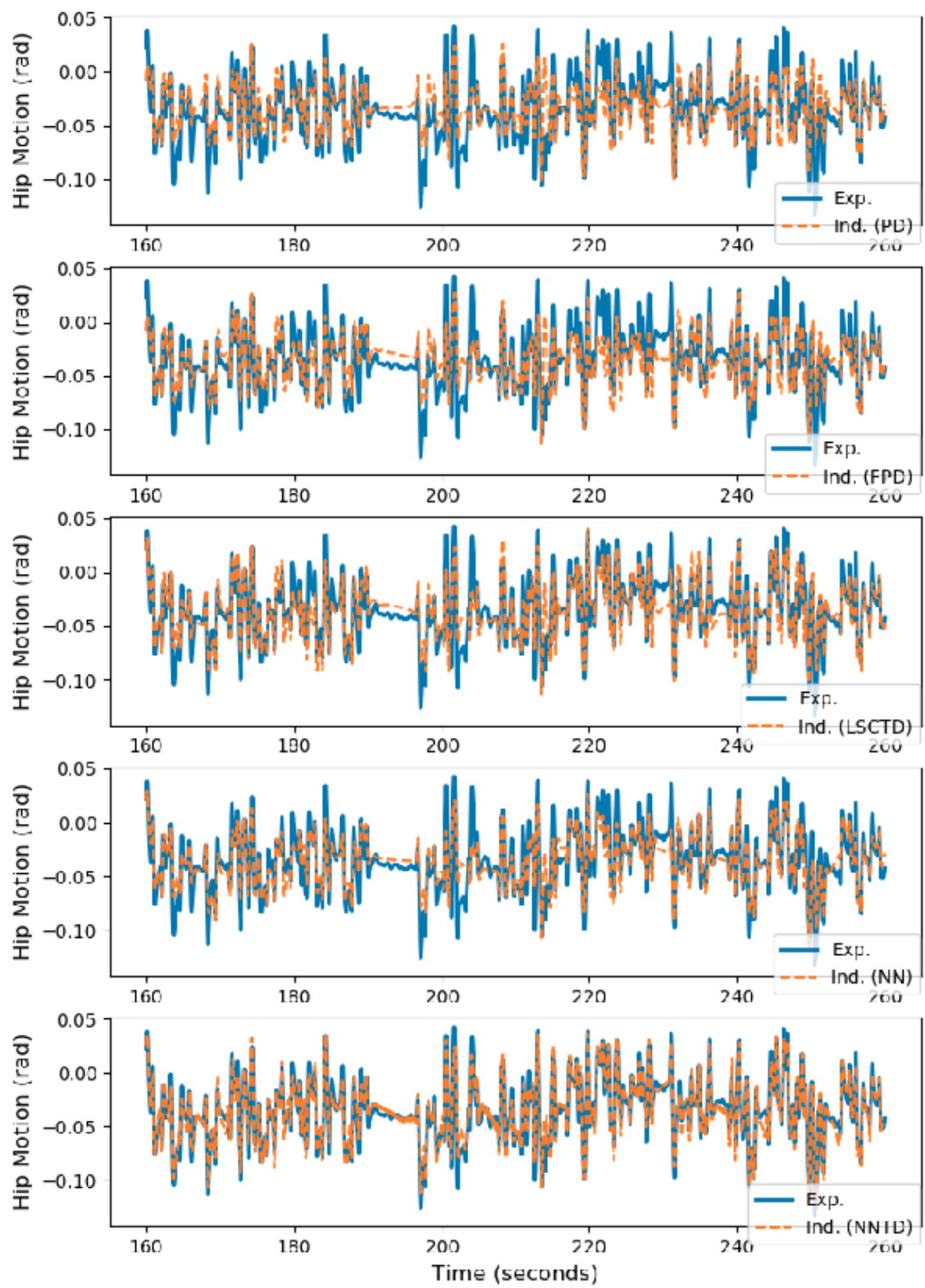


Figure 24: Hip motion fit of participant 8 and trial 2. Fits get better with more complex controller types

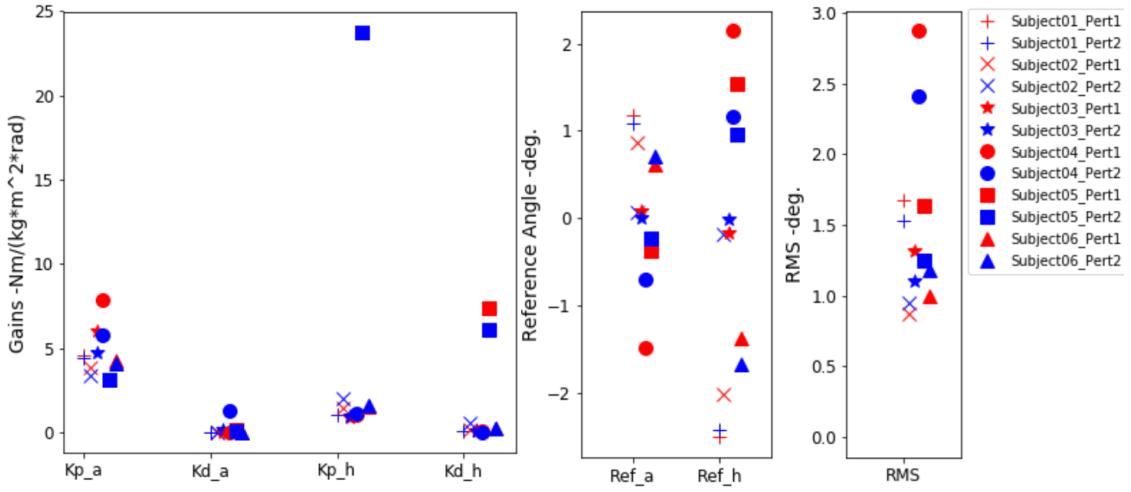


Figure 25: Gains of identified PD controllers of six participants. Five participants have similar gains except participant five.

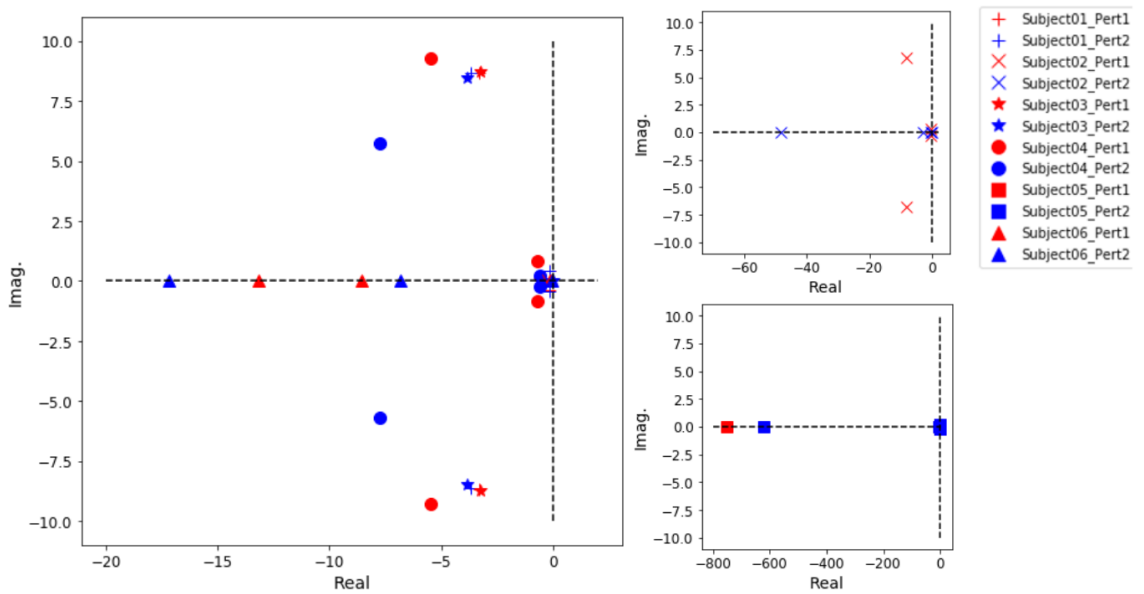


Figure 26: Eigenvalues of identified PD controllers of six participants. They have a large variations.

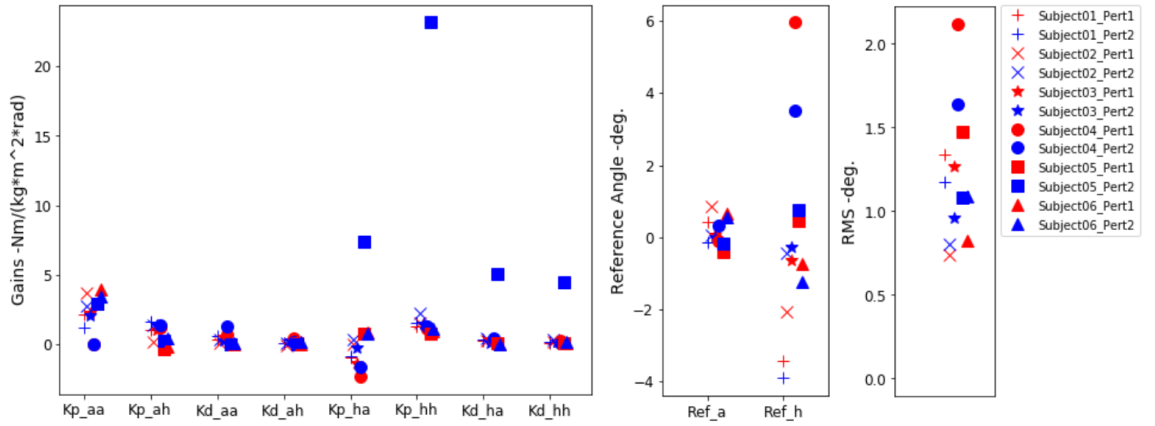


Figure 27: Gains of identified FPD controllers of six participants. Five participants have similar gains except participant five.

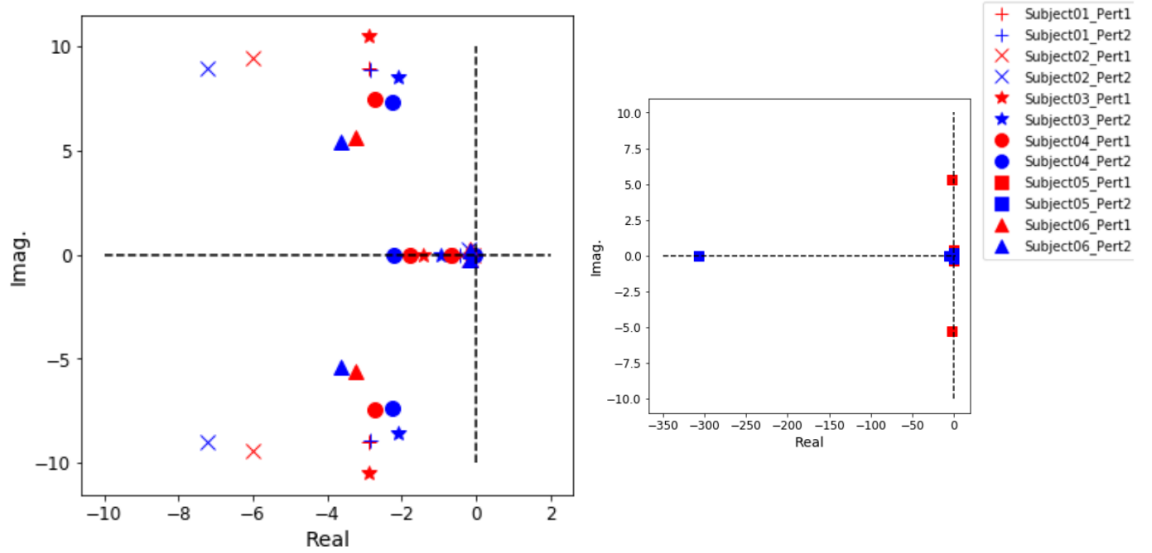


Figure 28: Eigenvalues of identified FPD controllers of six participants. They are closer to each other than identified PD controllers.

## 5.4 Discussion

The results suggested that a generalized time-invariant feedback controller can explain as long as 100 seconds experiment data under random square wave perturbation. In addition, more complex controller type results a higher fit between identified trajectories and experiment data in general. This is reasonable, since complex controller type has more control parameters which is more powerful in explaining the experiment data.

The mean  $R^2$  of FPD controller type of all identification problems is around 0.6. This is much lower than the  $R^2$  in Park's identification paper [7], in which short ramp perturbation was used. They identified FPD controller on 3 seconds experiment data. This suggested that FPD controller type is not complex enough to generalization and explain long duration balance data.

Identified PD controllers have similar control parameters. Proportional gains are larger than derivative gains, which is reasonable for PD controllers used in position control. Proportional gains of ankle are larger than hip, which means the ankle joint is stiffer than hip in standing balance. This results can be explained by the large torques at ankle joint and small motions during standing balance task. However, identified PD controllers have relatively large difference of system eigenvalues among participants.

Identified FPD controllers have similar control parameters. Proportional gains are larger than derivative gains, which is reasonable for PD controllers used in position control. Proportional gains of ankle are larger than hip, which means the ankle joint is stiffer than hip in standing balance. This results can be explained by the large torques at ankle joint and small motions during standing balance task. Self-state feedback gains are larger than cross-state feedback gains. This means that self-states information are usually used to keep standing balance under perturbation. Identified FPD controllers also have relatively small difference

of system eigenvalues among participants.

## 5.5 Conclusion

In this chapters, we identified five types of controllers from 100 seconds period standing balance experiment data. Stable controllers were able to identified for two linear controllers: PD and FPD. Even though stability was not able to guaranteed for the resting three types controllers, their identified results shows that complex controllers can generate motion trajectories which have a high fit with experiment. Identified FPD controllers have a relative smaller difference of eigenvalues among participants.

## 5.6 REFERENCES

- [1] Arthur D Kuo. An optimal control model for analyzing human postural balance. *IEEE transactions on biomedical engineering*, 42(1):87–101, 1995.
- [2] AV Alexandrov, AA Frolov, FB Horak, P Carlson-Kuhta, and S Park. Biomechanical analysis of strategies of equilibrium control during human upright standing. *Russian J Biomech*, 8(3):28–42, 2004.
- [3] Chenggang Liu and Christopher G Atkeson. Standing balance control using a trajectory library. In *2009 IEEE/RSJ International Conference on Intelligent Robots and Systems*, pages 3031–3036. Citeseer, 2009.
- [4] Benjamin Stephens. Humanoid push recovery. In *Humanoid Robots, 2007 7th IEEE-RAS International Conference on*, pages 589–595. IEEE, 2007.
- [5] David A Winter. Human balance and posture control during standing and walking. *Gait & posture*, 3(4):193–214, 1995.
- [6] Shirley Rietdyk, AE Patla, DA Winter, MG Ishac, and CE Little. Balance recov-

- ery from medio-lateral perturbations of the upper body during standing. *Journal of biomechanics*, 32(11):1149–1158, 1999.
- [7] Sukyung Park, Fay B Horak, and Arthur D Kuo. Postural feedback responses scale with biomechanical constraints in human standing. *Experimental brain research*, 154(4):417–427, 2004.
- [8] Torrence DJ Welch and Lena H Ting. A feedback model predicts muscle activity during human postural responses to support surface translations. *Journal of neurophysiology*, 2008.
- [9] Tim Kiemel, Yuanfen Zhang, and John J Jeka. Identification of neural feedback for upright stance in humans: stabilization rather than sway minimization. *Journal of Neuroscience*, 31(42):15144–15153, 2011.
- [10] RJ Peterka. Sensorimotor integration in human postural control. *Journal of neurophysiology*, 88(3):1097–1118, 2002.
- [11] Adam D Goodworth and Robert J Peterka. Identifying mechanisms of stance control: a single stimulus multiple output model-fit approach. *Journal of neuroscience methods*, 296:44–56, 2018.
- [12] Herman van der Kooij, Edwin van Asseldonk, and Frans CT van der Helm. Comparison of different methods to identify and quantify balance control. *Journal of neuroscience methods*, 145(1-2):175–203, 2005.
- [13] Torrence DJ Welch and Lena H Ting. A feedback model explains the differential scaling of human postural responses to perturbation acceleration and velocity. *Journal of Neurophysiology*, 2009.
- [14] Herman Van Der Kooij and Erwin De Vlugt. Postural responses evoked by platform

perturbations are dominated by continuous feedback. *Journal of neurophysiology*, 2007.

- [15] Herman Van Der Kooij and Robert J Peterka. Non-linear stimulus-response behavior of the human stance control system is predicted by optimization of a system with sensory and motor noise. *Journal of computational neuroscience*, 30(3):759–778, 2011.
- [16] Oskar Von Stryk and Roland Bulirsch. Direct and indirect methods for trajectory optimization. *Annals of operations research*, 37(1):357–373, 1992.
- [17] David A Winter. *Biomechanics and motor control of human movement*. John Wiley & Sons, 2009.
- [18] General information of atlas. <https://www.sympy.org/en/index.html>. Accessed: 2019-02-13.

PART II.

CONTROL OF WALKING

## CHAPTER VI

### IDENTIFICATION OF THE STEP STRATEGY IN HUMAN WALKING

#### **Conference Abstract:**

1. IDENTIFICATION OF SWING LEG FEEDBACK CONTROL IN HUMAN WALKING. Midwest ASB Conference, 2019.

## ABSTRACT

*Step strategy is essential for human walking balance. It controls the swing leg stepping to the desired foot placement, which is commonly accepted has the feedback control format. Even though some control algorithms of step strategy are able to achieve stable walking for the humanoid robots(e.g. the capture theory), the walking motion is not as natural as humans'. In addition, step strategy has not been directly extracted from human walking data, especially the perturbed walking data. In this work, we identified the step strategy on 27 trials of perturbed walking data (nine participants, three speeds each participant). Identified step strategies showed consistency results among all nine participants. In addition, the identified step strategy gains have similar values comparing to capture theory, which suggested that the capture theory is not a bad estimation of the human step strategy. However, one significant difference is that the identified step strategy control gains vary based on walking speed, while capture theory has constant gains for all walking speeds. This suggested that the feedback control of the step strategy is not a linear function of center of mass (CoM) position and velocity, but rather a nonlinear function.*

### 6.1 Introduction

Fall has been a main issue for the humanoid walking robots ever since they were first created. Step strategy is one of several strategies that can help solve the fall issue [1–4]. The concept of the step strategy is simple, which is to control the swing leg to take a step. In general, fall of the humanoid robots and human beings can always be prevented if the swing leg can step to the right location at the right timing. However, finding a useful control algorithm for the step strategy that can achieve stable walking is difficult, especially in the case of unpredictable environment. One of the most successful attempts is the capture theory [5], in which it predicts the desired foot location for the swing leg based on a linear inverted pendulum model (LIPM) [6] and the state feedback. Both simulations and hardware tests

have proved its usefulness in humanoid robots to maintain stable walking under some levels' unpredictable external perturbations [7]. Nonetheless, the algorithm for estimating the desired foot location inside the capture theory includes many assumptions. For example, the estimation of the desired foot location is based on the capture point, in which the LIPM will stop at the middle stance [5, 8]. While in healthy humans' walking, the CoM will keep a relatively constant speed. In addition, the swing leg dynamics and landing energy lost (impact) were not considered in the capture theory [9, 10]. These strong assumptions may limit its performance when resisting large external perturbations and may cause behavior that is not human-like. Studies have pointed out that humans do not step on the capture point or the extrapolated center of mass (XCoM), but behind and outward of them [11, 12]. Therefore, developing new control algorithms for the step strategy without above assumptions is worth well doing, even though the capture theory control algorithm can already achieve stable walking on humanoid robots.

Besides using model-based control approaches, such as the capture theory, one might also find step strategy algorithms by studying how humans control foot placement in walking. Studies have been done to directly extracting the step strategy from human motion data [13, 14]. Yet, the extracted step strategies are from the variation between normal walking and running gait cycles, which may not explain the step strategy under larger perturbations. In addition, since there is no plant involved in the process, it is not guaranteed that the extracted control algorithms will work for humanoid robots. Study has shown that this direct identification approach will introduce bias because of the lack of plant [15]. For close-loop systems, the direct identification of controller, which only used the control input and output, could result the inverse of plant dynamics, instead of the controller itself. One way to overcome the bias is to use indirect identification approach, in which a plant is involved in the close-loop system. In this paper, the indirect identification approach will be used.

There are two main components in the indirect identification of human walking. One component is a closed-loop simulation model of the human locomotion system, including a human body dynamic model and a state feedback locomotion controller. Another component is the experimental data which includes participants' reactions in the perturbed walking experiments. The indirect approach identifies parameters inside the locomotion controller by forcing the simulation model to generate the same reactions to the experimental data under the same perturbations. Thus, the identification can be considered as an optimization problem which optimize the control parameters by minimizing the difference between the outputs of simulation model and the experimental data. The best control parameters are those who can make the closed-loop model generate the closest motion with the experimental data. The diagram plot of the indirect approach for the walking step strategy identification is shown in Figure 29.

In this chapter, we identified humans' step strategy from perturbed walking data with a human body model. Perturbed walking data contains more balance information than normal walking data, which helps to extract more generalized algorithms for the step strategy. The human body model in-loop identification can guarantee that the identified step strategy algorithms can be applied to humanoid robots. The control structure identified in this paper is the same as existing algorithm in capture theory and XCoM, but we will identify the control gains from human data, rather than using the LIPM. This means that the identified results are highly engineering applicable. Furthermore, since the identified step strategy is directly from human walking data, it is more likely to generate human-like behavior than the manually designed or model-based step strategies.

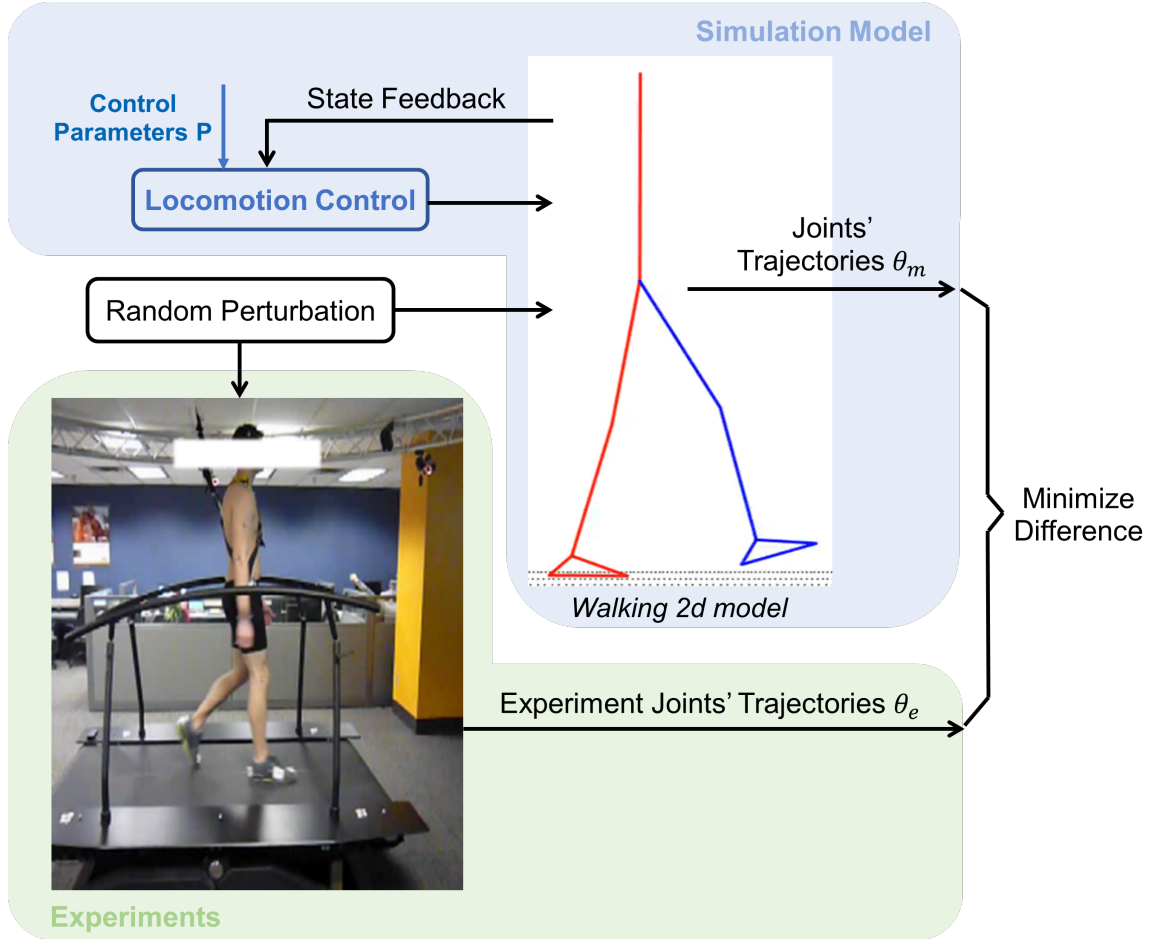


Figure 29: Plot diagram of the indirect identification approach in walking step strategy identification. There are two components in the identification: One is the simulation model which includes the human body dynamics and the locomotion control (the step strategy algorithm). Another component is the experimental data which includes participants' reaction during perturbed walking experiment. The overall goal of the indirect approach is to minimize the difference between the outputs of the simulation model and experimental data by optimizing the control parameters  $P$ .

## 6.2 Methods

In this method section, experimental data, indirect identification approach, step strategy control structure, and solution method are discussed in detail.

### 6.2.1 Experimental Data

The experimental data used in this study is from a human walking experiment conducted by Moore et al. [16]. In the experiment, participants' reactions were recorded while they

walked on a treadmill with random speed perturbations. Each subject was tested under three walking speeds: 0.8m/s, 1.2m/s, and 1.6m/s. The random speed perturbation was applied since it can trigger the human control system in large variety situations resulting more control information into the recorded motion data. This means that less experimental data is needed in the identification and more general walking controller can be found.

In the experiment, the motion capture system (Motion Analysis) and 47 markers were used to track participants' motion. An instrumented treadmill (Motekforce) was used to apply three walking speeds and random speed perturbations, as well as to record the ground reaction forces. From the recorded markers' data, participants' joint motion was calculated using the inverse kinematics with the Human Body Model (HBM) [17].

We selected nine participants whose data is in high quality (less marker missing) from the whole experimental dataset. For the controller identification, ten seconds perturbed walking data was selected in the middle of perturbation period of each experimental trial. Participants' characteristics are shown in Table V.

Table V: Information about the selected nine participants. There are four females and five males. They are all young adults with the average age of 24. There are two male participants with over-weighted BMI and one male participant in Obesity. All other participants are in normal weight category.

Id	Gender	Age (yr)	Height (m)	Mass (kg)	Original Id
1	female	29	1.72	$64.5 \pm 0.8$	7
2	female	32	1.62	$54 \pm 2$	3
3	female	21	1.70	$58 \pm 2$	13
4	female	28	1.69	$56.2 \pm 0.6$	16
1	male	20	1.57	$74.9 \pm 0.9$	8
2	male	20	1.69	$67 \pm 2$	9
3	male	23	1.73	$71.2 \pm 0.9$	5
4	male	26	1.77	$86.8 \pm 0.6$	6
5	male	19	1.77	$92 \pm 0.2$	10

### 6.2.2 Human Body Dynamic Model

The human body dynamic model used in this step strategy controller identification is a two dimensional seven-link gait model [18, 19], as shown in Figure 29. It contains an upper body and two legs. Each leg consists of a thigh, a shank, and a foot. Since the arm motion does not have a strong effect on the step strategy (step length) [20], it was not modeled here. The whole upper body was modeled as a single segment. The model has 9 degree of freedom and 6 active controlled joints. Part of the model parameters such as mass properties and CoM positions were calculated based on Winter's book [21], whereas other model parameters such as segment lengths were calculated based on the recorded maker data. The contact property between the human body model and ground was modeled as a nonlinear spring-damper system in the vertical direction. In the horizontal direction, a coulomb friction model that smoothed by a logistic function was included. The human body model is a torque driven model without muscles.

The effect of speed perturbation in this gait model is modeled in ground speed changes. The first order dynamic equation of this gait model in robotics format can be written as

$$\begin{bmatrix} \dot{q} - v \\ M \cdot \dot{v} + C \cdot v + G + f_{contact} - \tau \end{bmatrix} = 0 \quad (6.1)$$

where,  $q = [x, y, \theta_{trunk}, \theta_{Lhip}, \theta_{Lknee}, \theta_{Lankle}, \theta_{Rhip}, \theta_{Rknee}, \theta_{Rankle}]^T$  represents system motions including pelvis motion and joint angles;

$v = [v_x, v_y, \omega_{trunk}, \omega_{Lhip}, \omega_{Lknee}, \omega_{Lankle}, \omega_{Rhip}, \omega_{Rknee}, \omega_{Rankle}]^T$  represents the derivative of system motions including pelvis velocity and joint angular velocities;  $M$  represents the mass matrix of the human body dynamics and is function of  $q$ ;  $C$  represents the Coriolis matrix and is function of  $q$  and  $v$ ;  $G$  represents the gravity matrix and is function of  $q$ ;  $f_{contact}$  represents the ground contact force and is a function of joint angles  $q$ , joint angular velocity  $\dot{q}$ , and belt speed  $V_{belt}$ ;  $\tau$  represents joint torques in the human body dynamics.

Combine with step strategy state feedback control, the mathematics equation of the close-loop walking model can be written as  $f(x, \dot{x}, P, V_{belt}) = 0$ , in which  $x = [q, v]^T$  represents system states, including joint angles and angular velocities;  $P$  represents control parameters.

### 6.2.3 Human Walking Control System

The locomotion control system used in this paper is similar to the control architecture of M2V2 robot [7] comprised with two components: the stance leg control and the swing leg control (Figure 30). In this identification work, the step strategy (swing leg control) is the most of our concern. Therefore, open loop torques are used to control the motion of stance leg, and a feedback loop control system was used to control the motion of swing leg. In the swing leg, the ankle joint is also controlled by open loop torques because of the following two reasons. Firstly, the ankle motion does not have a significant effect on foot placement. Secondly, the swing leg control structure only supports in solving two independent joint angles: the hip and knee joints. The open-loop torque control will let these controlled joints just follow the experimental data without feedback. The focus of this paper is to identify control parameters inside the swing leg control loop. The close-loop swing leg control system consisted of four items: foot location estimator, swing path generator, inverse kinematics, and local tracking controller.

- **Foot Placement Controller**

The function of foot placement controller is to estimate a proper foot placement for next step. To make the controller identification easier and applicable to humanoid robots, we used the same feedback structure as described in the capture theory: use the CoM relative position and velocity as the feedback variables. In the capture theory, foot placement is

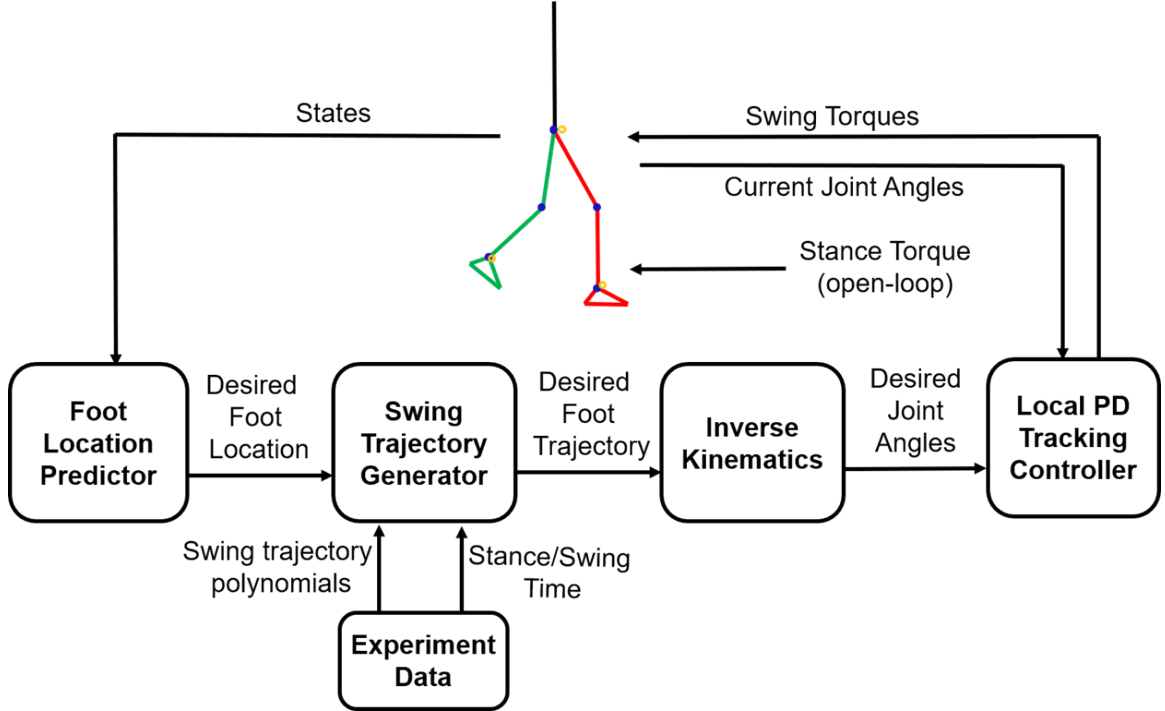


Figure 30: Structure of the locomotion control system for the step strategy identification. The stance leg and the ankle joint in swing leg are controlled by open loop torques. The hip and knee joints of swing leg are controlled by the state feedback control loop. The purpose of open-loop torque control is just to let these controlled joints following the experimental data. The focus of this paper is to identify control parameters inside the swing leg control loop.

controlled by the Equation 6.2 [8].

$$r_{ic} = r + \frac{\dot{r}}{\omega_0} \quad (6.2)$$

$$r_{ic}(\Delta t) = r_{ic}(0) \cdot e^{\omega_0 \cdot \Delta t}$$

where,  $r_{ic}$  is the instantaneous capture point based on the state feedback;  $r$  is the CoM position projected to the ground;  $\dot{r}$  is the horizontal velocity of CoM position;  $\omega_0$  is the reciprocal of the time constant of the LIPM model;  $r_{ic}(\Delta t)$  is the capture point at the coming  $\Delta t$  time point;  $r_{ic}(0)$  is the current instantaneous capture point.

To avoid the strong hypotheses in the capture theory, the original equation to calculate the instantaneous capture point will be changed to Equation 6.3. Instead of using the gain

value “1” in front of the CoM relative position and velocity, we identify these two gains from human walking data. In this study, the identification of the foot location estimator is only in the sagittal plane. In addition, since the CoM is close to the pelvis position, here we use pelvis position and velocity as the feedback state, shown in Equation 6.3.

$$x_{ifl} = P_1 \cdot x_p + P_2 \cdot \frac{\dot{x}_p}{\omega_0} \quad (6.3)$$

$$x_{ifl}(\Delta t) = x_{ifl}(0) \cdot e^{\omega_0 \cdot \Delta t}$$

where,  $x_{ifl}$  is the instantaneous desire foot location in sagittal plane based on the state feedback;  $x_p$  is the relative pelvis position to stance leg ankle position in sagittal plane;  $\dot{x}_p$  is the velocity of pelvis in sagittal plane;  $P_1$  and  $P_2$  are the two gains applied on the two feedback signals;  $\omega_0$  is the reciprocal of the time constant of a pendulum with the leg length of human;  $x_{ifl}(\Delta t)$  is the desired foot location at the coming  $\Delta t$  time point;  $x_{ifl}(0)$  is the current instantaneous desired foot location.

### • Swing Path Generator

The swing path generator calculates the swing trajectory of the swing ankle joint. It is a function of the starting swing position, desired foot location, and total swing time. Considering that the overall shape of the swing paths is consistent, the normalized polynomial function is used to describe it. The swing path function also decomposed into  $x$  and  $y$  directions to make each of the function simpler than describing together. One example of the swing path from over 500 gait cycles is showing in Figure 31. Both  $x$  and  $y$  direction polynomial functions have the same format as showing in Equation 6.4.

$$f(P_{sta}, P_{des}, T, t) = \sum_{n=1}^N A_n * (P_{des} - P_{sta}) * \left(\frac{t}{T}\right)^n \quad (6.4)$$

where,  $P_{sta}$  is the swing foot location at the starting swing time;  $P_{des}$  is the estimated foot

location at the ending swing time;  $T$  is the total swing time;  $t$  is the current swing time point;  $N$  is the total order of the polynomial function;  $A_n$  is the coefficient of the  $n^{th}$  order polynomial term.

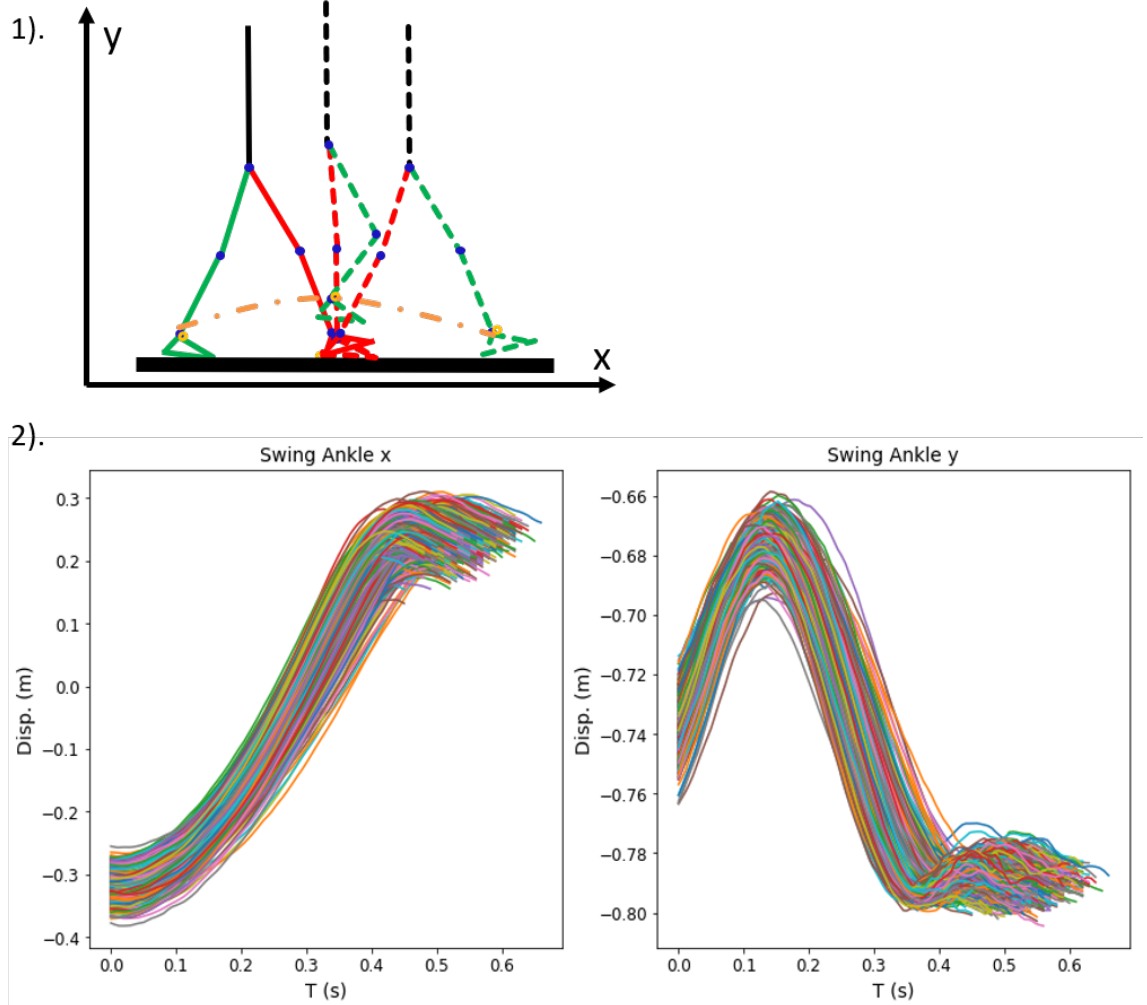


Figure 31: Swing trajectories from the experimental data. Subplot 1) shows the swing trajectory in the swing phase. It starts at the swing starting position and finishing at the touch down point. Subplot 2) shows the swing trajectory shape in the  $x$  and  $y$  directions over 500 gait cycles. The swing path of the ankle joint is relative to the pelvis position.

The coefficients  $A_n$  of the polynomial function are optimized over 500 experimental gait cycles. Different orders of the polynomial functions, from first and sixth, are optimized to find the number of orders that holds the best fit (Figure 32). Based on the fitting results, fifth order polynomials are selected for both  $x$  and  $y$  directions of the swing path.

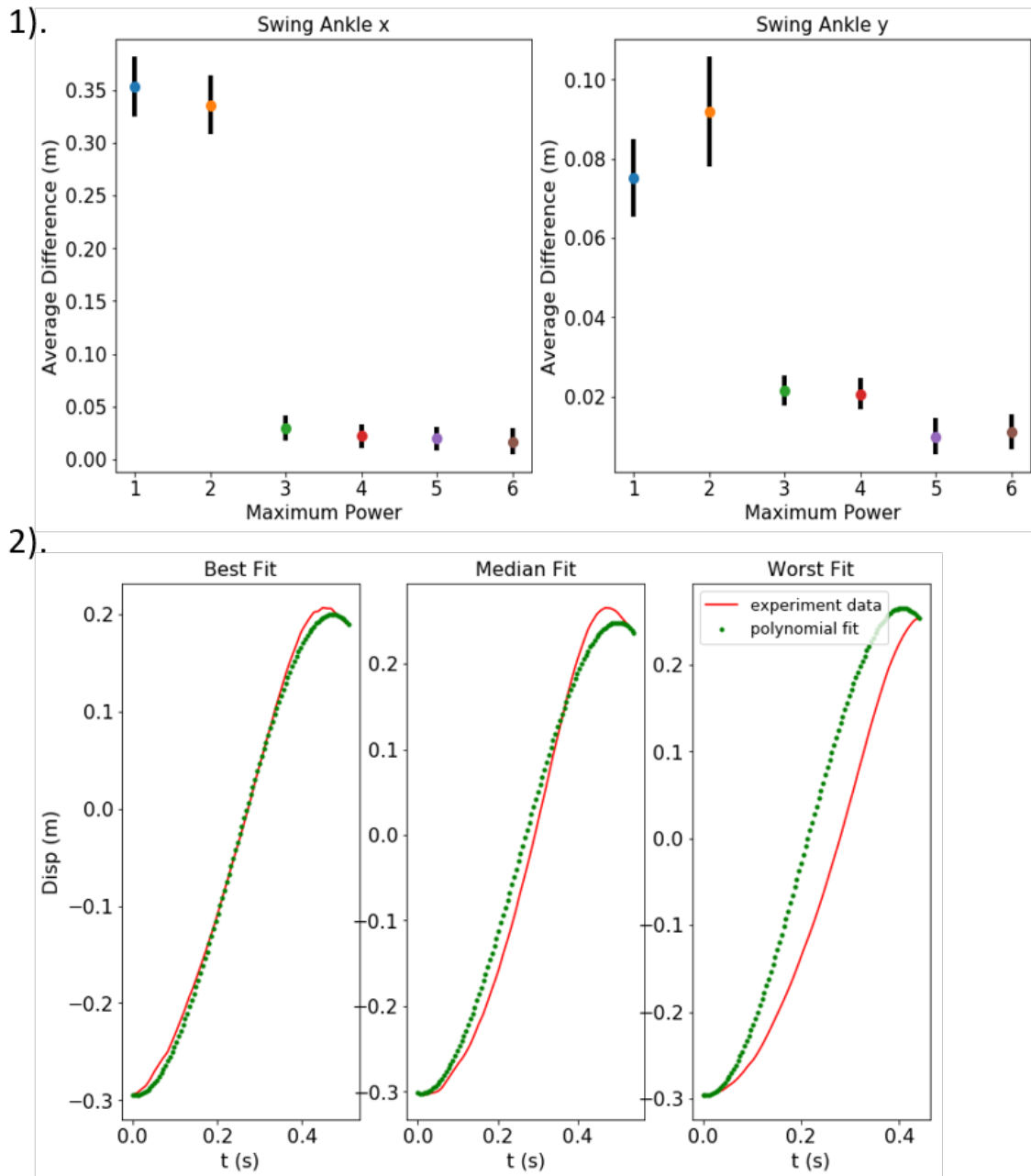


Figure 32: Fits between the optimized polynomial functions and the experimental swing paths. Subplot 1) shows the means and standard deviation of the difference between the polynomial functions and experimental data. Fit get better with the increase of the degree of polynomial functions. Subplot 2) shows one example of the fit for one optimized polynomial function. In which, the best, median, and worst fits in over 500 experimental swing trajectories are shown.

- **Inverse Kinematics**

The inverse kinematics module resolves the joint angles of the swing leg to match with the swing foot position at each time frame. Based on the geometry of the leg, the kinematic function between joint angles and foot position can be described in Equation 6.5.

$$\begin{aligned} P_x &= l_{thigh} * \sin(\theta_h) + l_{shank} * \sin(\theta_h + \theta_k) \\ P_y &= -l_{thigh} * \cos(\theta_h) - l_{shank} * \cos(\theta_h + \theta_k) \end{aligned} \quad (6.5)$$

where,  $P_x$  is the foot position in x direction;  $P_y$  is the foot position in y direction;  $l_{thigh}$  is the length of thigh;  $l_{shank}$  is the length of shank;  $\theta_h$  is the hip joint angle;  $\theta_k$  is the knee joint angle.

Through this kinematic equation, hip and knee joint angles can be calculated from the foot position. In our approach, the joint angles, instead of the swing trajectories, are directly optimized. It is important to transfer the swing trajectories or desired foot location to the joint angles.

- **Local Tracking Controller**

The local tracking controller controls the hip and knee joints in the swing leg to track the calculated joint angles from the inverse kinematics module (See section 2.4.2). The proportional-derivative (PD) control format was used in this paper to track the joint motions (Equation 6.6). The PD control parameters are also optimized in the identification process.

$$\begin{aligned} \tau_h &= Kp_h * (\theta_h^{ref} - \theta_h) + Kd_h * (\dot{\theta}_h^{ref} - \dot{\theta}_h) \\ \tau_k &= Kp_k * (\theta_k^{ref} - \theta_k) + Kd_k * (\dot{\theta}_k^{ref} - \dot{\theta}_k) \end{aligned} \quad (6.6)$$

where,  $\tau_h$  and  $\tau_k$  are the joint torques calculated from tracking controllers;  $Kp_h$  and  $Kd_h$

are the proportional and derivative feedback control gains for hip joint;  $Kp_k$  and  $Kd_k$  are the proportional and derivative feedback control gains for knee joint;  $\theta_h^{ref}$  and  $\dot{\theta}_h^{ref}$  are the reference joint angle and angular velocity of hip joint;  $\theta_h$  and  $\dot{\theta}_h$  are the feedback joint angle and angular velocity of hip joint;  $\theta_k^{ref}$  and  $\dot{\theta}_k^{ref}$  are the reference joint angle and angular velocity of knee joint;  $\theta_k$  and  $\dot{\theta}_k$  are the feedback joint angle and angular velocity of knee joint.

#### 6.2.4 Identification Problem Define

As mentioned in the introduction section, the indirect identification approach used in this study can be considered as an optimization problem. In the step strategy identification, optimization is defined to minimize the difference of joint trajectories between the simulation model and the experimental data. We choose joint trajectories instead of foot landing location because the joint trajectory is a continues variable which contains continues information of how the human closed-loop system responds to external perturbation. The optimization problem introduced by the indirect approach is also a trajectory optimization problem, since the joint trajectories are optimized simultaneously while optimizing the control parameters. The definition of the human walking step strategy identification in the trajectory optimization format is shown in Equation 6.7. There are no path constraints and boundary constraints inside this controller identification, the only goal is to fit the experimental data.

Optimize state trajectories  $x(t)$  and control parameters  $P$

$$\text{Minimize the objective function } F = \int_0^T \|\theta_m(t) - \theta(t)\|^2 dt$$

Subject to: human system dynamics:  $f(x(t), \dot{x}(t), P, V_{belt}) = 0$  (6.7)

bounds on state:  $x_{low} \leq x(t) \leq x_{upp}$

bounds on control parameters:  $P_{low} \leq P \leq P_{upp}$

where  $x(t) = [q(t), v(t)]^T$  is the state of human body model. Detail of  $q$  and  $v$  are described in section 6.2.2;  $P = [P_1, P_2, Kp_h, Kd_h, Kp_k, Kd_k, \tau_{open}]$  represents the control parameters inside the locomotion controller. Open-loop joint torques  $\tau_{open}$  are also inside parameter  $P$ ;  $T$  is the time length of the identified experimental data;  $V_{belt}$  is the velocity of the belt speed including random perturbations in walking experiment;  $x_{low}$  and  $x_{high}$  are the lower and upper bounds of the human system states;  $P_{low}$  and  $P_{high}$  are the lower and upper bounds of the control parameters.

### 6.2.5 Solution Method

The direct collocation method [22] was used in this paper. This transforms the trajectory optimization problem into nonlinear program (NLP) with a finite number of unknowns: the states  $x$  at  $N$  collocation nodes, and the controller parameters  $P$ . The Backward Euler approximation was used to convert the body dynamics constraint into algebraic constraints:

$$f(x_{i+1}, \frac{x_{i+1} - x_i}{h}, P, V_{belt,i+1}) = 0, \text{ for } i = 1, 2, \dots, N - 1.$$

The number of collocation nodes was 50 per second, and IPOPT was used to solve the NLP [23]. Detail of these solution methods can be found in chapter 2.

The local optimum was eliminated by selecting the best result from ten optimizations in one identification problem. An identification problem is defined as the step strategy identification on one experiment trial of a participant. In total, there are 27 identification problems (9 participants, 3 speed trials for each participant). Ten seconds experimental data, which contains about 8 to 10 gait cycles was studied in each identification problem. Ten optimizations were performed with random initial guesses were implemented in each identification problem to help prevent the local optimum results. The best identified results are those whose optimized joint trajectories had the best fit with experimental data. Overall, 270 optimizations were conducted in this study. They took about 500 computing hours in an

Intel i5-8300H CPU.

### 6.3 Results

The purpose of the study is to identify the control parameters inside the swing leg step strategy feedback control loop. Twenty-five out of twenty-seven identification problems were identified successfully. Table VI shows the coefficients of determination ( $R^2$ ) (highest among ten optimizations in one identification problem) between the identified joint trajectories and the experimental data for all the 27 trials. Two 'N/A' values in the table indicate unsuccessful identifications, in which no solutions were found from optimizations. Except these two, all other identification problems have very high  $R^2$  values, which indicates that the close loop simulation model was able to reproduce the experimental data with the identified step strategies. One example of the fit between identified trajectories and experimental data is shown in Figure 33. Beside the good fitting, another interesting aspect is that the simulation model with the identified step strategy can reproduce almost every large and small variations among gait cycles.

Table VI: Coefficient of determination ( $R^2$ ) between identified trajectories and experiment data. 'M' means male subjects; 'F' means female subjects. 'N/A' means the identification problem was not successful.

Speed	M1	M2	M3	M4	M5	F1	F2	F3	F4
0.8 m/s	0.990	0.982	0.991	0.973	0.964	0.991	0.988	0.983	0.992
1.2 m/s	0.989	0.977	0.991	0.981	0.983	0.992	0.993	0.989	N/A
1.6 m/s	0.979	0.974	0.989	0.983	0.982	0.988	0.988	N/A	0.986

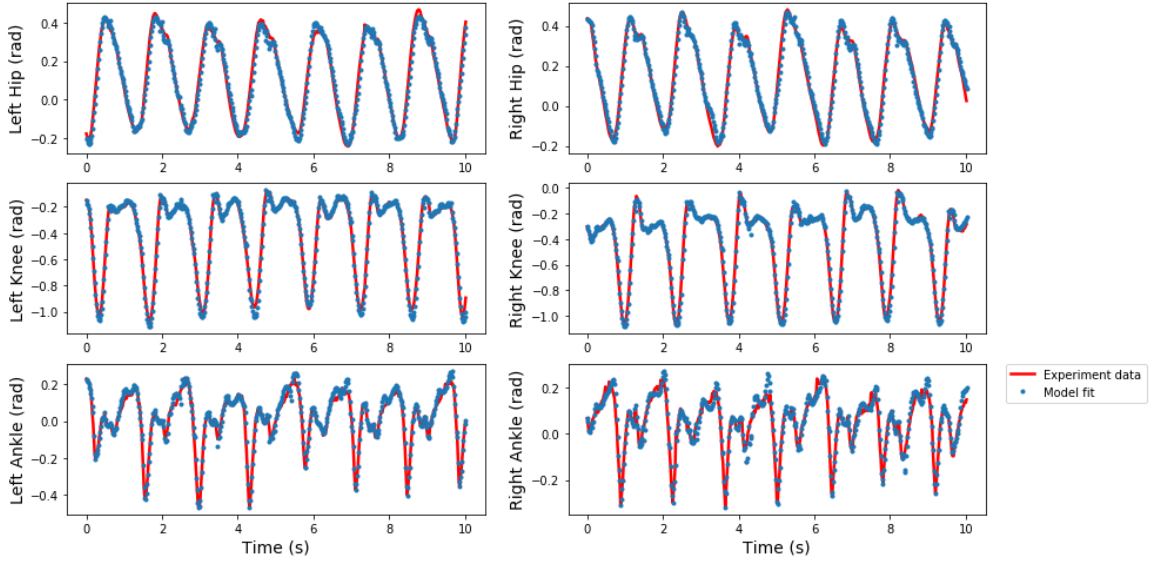


Figure 33: The identified joint trajectories of male subject 5 at speed 1.6m/s. The red solid line is the experimental trajectories, and the blue dash line is the identified trajectories.

To increase the confidence that the identified step strategies are the global optima, how many times the similar best results appeared in each identification problem (ten optimizations) were checked. The similar best results were defined within 5% variation when comparing the root-mean-square (RMS) of the difference between the identified trajectories and the experimental data. Table VII shows the numbers of similar best results that were found in each identification problem (ten optimizations). In most identification problems, the similar best results were found more than once, which suggests that the identified step strategies are the global optima. The standard deviation of the control gains in the corresponding best similar results are shown in Table VIII and IX. In general, these standard deviations are less than 5%, which suggests that the identified step strategies among the similar best fits are similar. This, in another aspect, suggests that the identified step strategies are global optima.

Table VII: The number of similar best results in each identification problem. In the majority of the identification problems, similar best results were found more than once. Only six identification problems found one best result. There are two identification problems which were not successful in finding feasible results.

Speed	M1	M2	M3	M4	M5	F1	F2	F3	F4
0.8 m/s	7	5	5	1	1	4	2	2	1
1.2 m/s	4	2	3	9	3	4	8	2	0
1.6 m/s	7	2	1	8	2	2	1	0	1

Table VIII: The standard deviation of the similar best results as a percentage of the averaged pelvis position gains. For the identification problems which have no solution, or only one best result, there is no standard deviation and 'N/A' was wrote.

Speed	M1	M2	M3	M4	M5	F1	F2	F3	F4
0.8 m/s	2.34%	2.44%	3.56%	N/A	N/A	5.34%	4.21%	2.47%	N/A
1.2 m/s	0.69%	0.45%	3.80%	2.56%	1.17%	3.39%	1.66%	1.58%	N/A
1.6 m/s	1.73%	1.82%	N/A	1.53%	0.16%	0.43%	N/A	N/A	N/A

Table IX: The standard deviation of the similar best results as a percentage of the averaged pelvis velocity gains. For the identification problems which have no solution, or only one best result, there is no standard deviation and 'N/A' was wrote.

Speed	M1	M2	M3	M4	M5	F1	F2	F3	F4
0.8 m/s	0.69%	0.71%	0.67%	N/A	N/A	0.14%	0.13%	0.49%	N/A
1.2 m/s	0.45%	0.54%	1.93%	1.97%	1.68%	0.30%	1.62%	1.81%	N/A
1.6 m/s	0.60%	0.34%	N/A	1.29%	0.30%	0.65%	N/A	N/A	N/A

Identified control gains in the step strategy are shown in Figure 34. There are two gains in the step strategy as motioned in the section 6.2.3: position gain and velocity gain. These two gains are dimensionless which were normalized by the subjects' height and gravity. In general, the identified gains are close to what the capture theory suggested (grey lines). Another clear trend from the plot is that the identified gains are changing along with different walking speeds. The position gains increase with the increasing of walking speed. While, the velocity gains decrease with the increasing of walking speed. This reveals that the step strategy feedback control in these participants is most likely a nonlinear function of the pelvis position and velocity, instead of the linear function which suggested by the

capture theory.

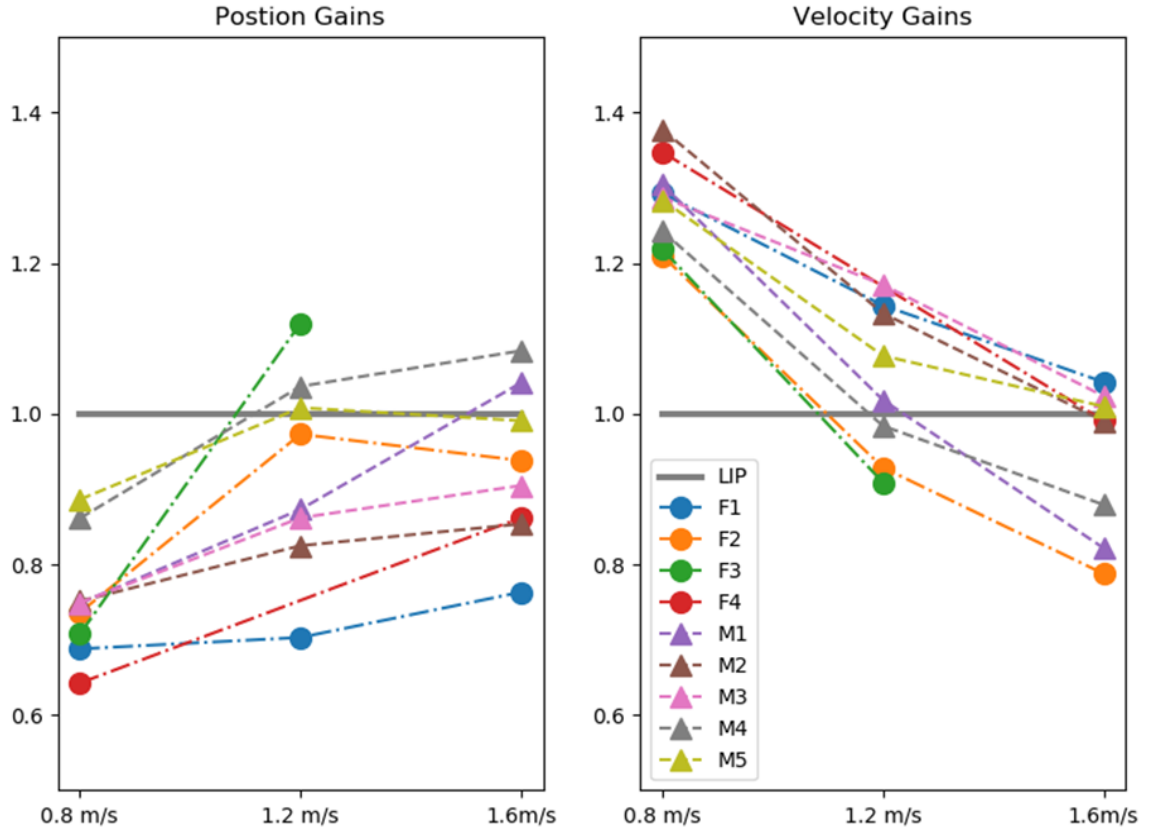


Figure 34: The identified step strategy gains in the foot location estimator component. The averaged similar best pelvis position and the velocity gains are showing in the subplot left and right, respectively. Female subjects are marked with solid circle and male subjects are marked with solid triangles. Identified gains in one participant are connected with dash lines.

A phase plot of one swing period is showing in Figure 35. The green dash line is the swing path generated by the identified step strategy algorithm. The two green points at the beginning and ending of the green dash line are the starting and ending swing points. It is apparent that the swing leg follows the generated swing path very well. One significant point is that the desired foot location calculated by the identified step strategy is not a fixed point on the ground in the swing period but keep changing based on the participant's motion. For instance, at  $t = 0.24$  second swing time, there is a large change of the desired foot location due to the sudden perturbation of the belt speed.

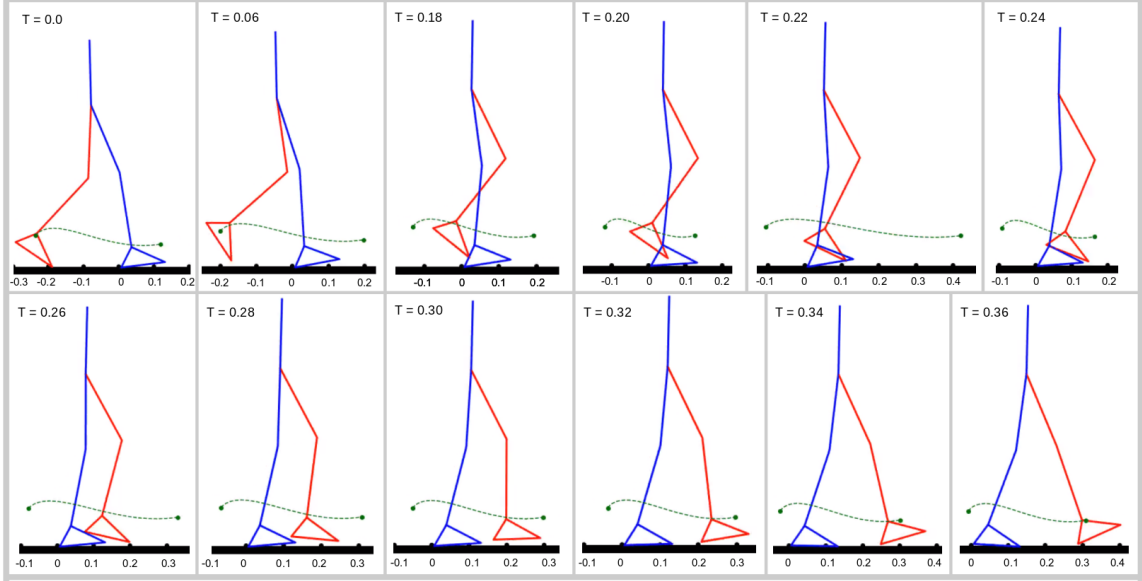


Figure 35: Stick plots of one swing phase. The red leg is the swing leg, and the blue leg is the stance leg. The green dash line is the swing path based on the identified step strategy algorithm. The beginning and ending two green points are the start swing and end swing points.

## 6.4 Discussion

By using the indirect identification approach, we identified the step strategies from the perturbed walking data. The identified control gains inside the step strategy suggest that the capture theory is not a bad estimation of how human take steps. However, the identified results also reveal that the feedback loop of human step strategy is more likely to be a nonlinear function, instead of the linear function which is suggested by the capture theory.

The identification step strategies can be easily applied to humanoid robots, since the identified feedback control structure is very close to the control structure which is mostly used for bipedal robots. It is also possible to only change two feedback gains for the humanoid robots who are using the capture theory to apply the identified step strategies. We believe that the identified step strategies can perform better balance ability and generate more human-like balance motion since they are directly come from the human motion and human's balance ability has kept improving in the million years' evolution.

However, the findings of the current study do not support one previous human step strategy extraction research [13]. The biggest difference is that they got phase dependency step strategy control gains, while our results show that one constant set of step strategy control gains can already reproduce the step changes in the perturbed walking data. One possible reason is that they studied the relationship between the walking status of specific phase and the foot landing position directly, which ignored the changes that happened after the studied phase. Another possible reason is that the variation among the normal gait cycles is very small comparing to the perturbed walking data.

The indirect identification approach guarantees that the identified step strategies are engineering applicable. This is because the human body dynamic model (2d gait model) was included in the identification (optimization) work. In optimizations (Section 2), the 2d gait model served as constraints which forced the identified step strategies having the capability to control the gait model achieving stable and desired motion. This is equivalent to the forward simulation test on a human dynamic model, which is another important reason why we chose the indirect identification approach instead of the direct identification approach.

Reproducing the joint motion is better than just studying the foot landing position. Foot landing position only happens once in one gait cycle which is accumulated results of all the previous changes or perturbation in the swing period (some changes in the previous stance period also contributes). It is impossible to redirect the final foot position information to multiple individual contributors. In contrast, the joint motion is continuous information which includes all the adjustments of the desired foot location. Analysis in Section 6.2.3 shows that the shape of the swing phase is relatively consistent though the step lengths and swing time lengths are different. Therefore, changes in the desired foot location will directly affect the swing leg joint motion.

Ten seconds experimental data is sufficient to identify the two feedback gains in the step strategy. Since joint motion is the reproducing target in this research, ten seconds perturbed walking data contains enough information for identifying the two feedback gains. We also identified the step strategy on another ten- and twenty-seconds perturbed walking data, which did not show significant differences with the results on the ten seconds data (Figure 36). One-way ANOVA tests showed that there is no significant difference ( $P > 0.05$ ) between the three periods. Tests on the gains of different speeds showed that there is significant difference ( $P = 0.015 < 0.05$  for position gain,  $P = 0.00878 < 0.05$  for velocity gains) between three speeds.

The time of swing period is not an optimization parameter in the step strategy. We predefined the stance and swing period time for each gait cycle based on the experimental data. One reason of doing this is because the sparse structure of the Jacobin will change when the number of direct collocation nodes for the stance and the swing phase changed. Using the sparse structure to more efficiently store the Jacobin matrix is essential for the long period trajectory optimization. In addition, adding the swing period time as optimizing parameter will make the optimization slower and harder to solve. On the other hand, since the goal of the identification is to reproduce the joint motions, fixing the swing period will automatically guarantee that the swing period is the same as experimental data once a solution is found.

Pelvis position and velocity are used in this study to represent the CoM position and velocity. One reason is because the pelvis position and velocity are easier to get from the gait model that we used. In addition, the CoM position is very close to the pelvis while walking. Besides, only the horizontal position and velocity of the CoM are used for feedback and the trunk rotation is small in walking. Therefore, horizontal position and velocity of the CoM

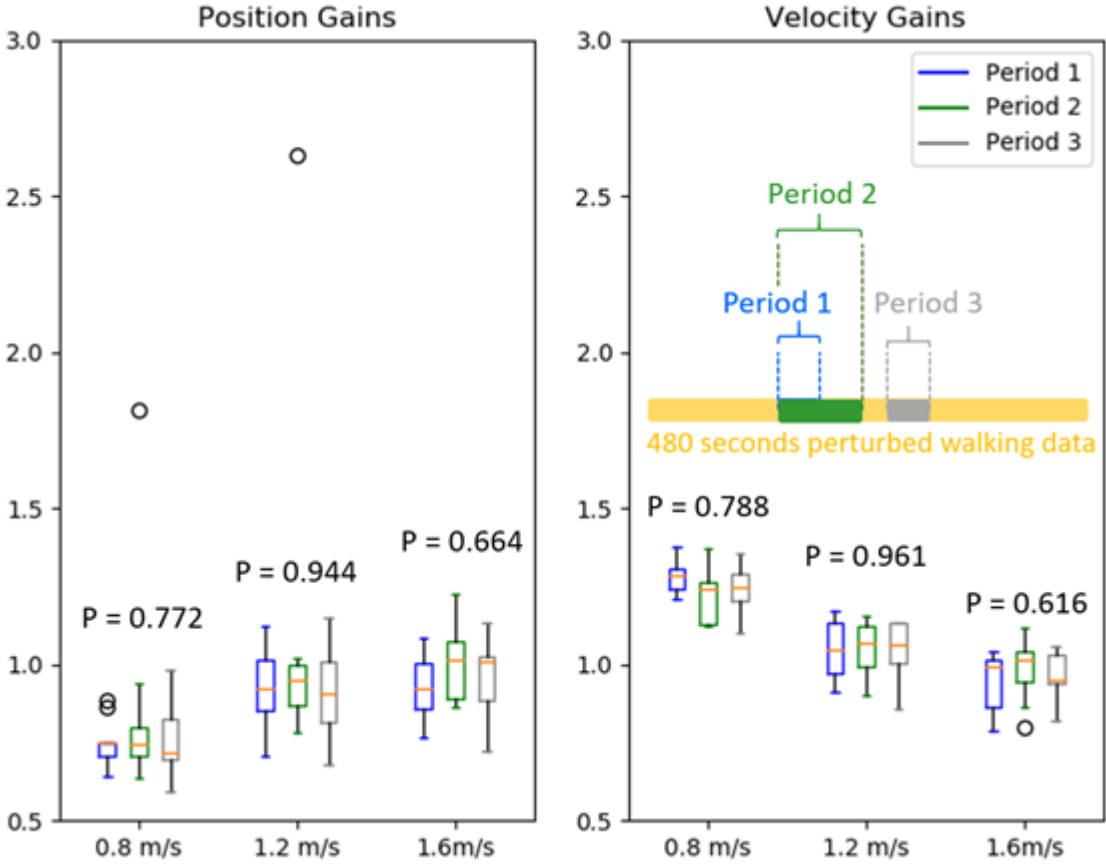


Figure 36: Comparison of the identified control gains among three periods of experimental data. In which, period 1 is the 10 seconds experimental data mentioned in the Result section; period 2 is the 20 seconds experimental data which includes the period 1 data; period 3 is another 10 seconds experimental data away from the period 1 and 2. One-way ANOVA tests show that there is no significant difference of the identified control gains ( $P > 0.05$ ) among the three data periods. Two-way ANOVA tests indicate that there is significant difference of the identified control gains ( $P = 0.015 < 0.05$  for position gain,  $P = 0.00878 < 0.05$  for velocity gains) among the three speeds.

are close enough to the pelvis, and it is acceptable to use the pelvis motion to represent the CoM motion.

The gains in local tracking controllers for the hip and knee joints were also optimized in the step strategy identifications. However, the results of them are not the main concerns in this study. In practice, these local tracking gains are designed based on the body dynamics. In humanoid robots, local tracking controller is usually designed based on the specific structure of the robot hardware and our identified gains cannot provide a good reference.

In addition, PD control structure is not the only structure that can achieve the local joint tracking. However, it is better to optimize these gains in our identification work other than pre-select the values, since manually setting the local tracking gains will limit the tracking ability and may affect the identified step strategy.

## 6.5 Conclusion

In this study, step strategies were successfully identified from walking experiment data, and results revealed that the feedback loop of the step strategy is a nonlinear function of the CoM position and velocity, instead of the linear function which suggested by the capture theory. Since the identified step strategy control gains are directly from human motion data, they may provide better and more human-like balance ability than the capture theory which has been claimed conservative. The identification framework used in this paper can also be used to identify feedback controllers in other human motions, for instance running.

## 6.6 REFERENCES

- [1] Miles A Townsend. Biped gait stabilization via foot placement. *Journal of biomechanics*, 18(1):21–38, 1985.
- [2] James J Kuffner, Satoshi Kagami, Koichi Nishiwaki, Masayuki Inaba, and Hirochika Inoue. Dynamically-stable motion planning for humanoid robots. *Autonomous Robots*, 12(1):105–118, 2002.
- [3] Tomomichi Sugihara and Yoshihiko Nakamura. Whole-body cooperative balancing of humanoid robot using cog jacobian. In *IEEE/RSJ international conference on intelligent robots and systems*, volume 3, pages 2575–2580. IEEE, 2002.
- [4] Benjamin Stephens. Humanoid push recovery. In *Humanoid Robots, 2007 7th IEEE-RAS International Conference on*, pages 589–595. IEEE, 2007.

- [5] Jerry Pratt, John Carff, Sergey Drakunov, and Ambarish Goswami. Capture point: A step toward humanoid push recovery. In *Humanoid Robots, 2006 6th IEEE-RAS International Conference on*, pages 200–207. IEEE, 2006.
- [6] Shuuji Kajita, Fumio Kanehiro, Kenji Kaneko, Kazuhito Yokoi, and Hirohisa Hirukawa. The 3d linear inverted pendulum mode: A simple modeling for a biped walking pattern generation. In *Proceedings 2001 IEEE/RSJ International Conference on Intelligent Robots and Systems. Expanding the Societal Role of Robotics in the the Next Millennium (Cat. No. 01CH37180)*, volume 1, pages 239–246. IEEE, 2001.
- [7] Jerry Pratt, Twan Koolen, Tomas De Boer, John Rebula, Sebastien Cotton, John Carff, Matthew Johnson, and Peter Neuhaus. Capturability-based analysis and control of legged locomotion, part 2: Application to m2v2, a lower-body humanoid. *The International Journal of Robotics Research*, 31(10):1117–1133, 2012.
- [8] Twan Koolen, Tomas De Boer, John Rebula, Ambarish Goswami, and Jerry Pratt. Capturability-based analysis and control of legged locomotion, part 1: Theory and application to three simple gait models. *The International Journal of Robotics Research*, 31(9):1094–1113, 2012.
- [9] Lei Zhang and Chenglong Fu. Predicting foot placement for balance through a simple model with swing leg dynamics. *Journal of biomechanics*, 77:155–162, 2018.
- [10] Arthur D Kuo, J Maxwell Donelan, and Andy Ruina. Energetic consequences of walking like an inverted pendulum: step-to-step transitions. *Exercise and sport sciences reviews*, 33(2):88–97, 2005.
- [11] AL Hof, MGJ Gazendam, and WE Sinke. The condition for dynamic stability. *Journal of biomechanics*, 38(1):1–8, 2005.
- [12] At L Hof. The ‘extrapolated center of mass’ concept suggests a simple control of balance in walking. *Human movement science*, 27(1):112–125, 2008.

- [13] Yang Wang and Manoj Srinivasan. Stepping in the direction of the fall: the next foot placement can be predicted from current upper body state in steady-state walking. *Biology letters*, 10(9):20140405, 2014.
- [14] Nidhi Seethapathi and Manoj Srinivasan. Step-to-step variations in human running reveal how humans run without falling. *eLife*, 8:e38371, 2019.
- [15] Herman van der Kooij, Edwin van Asseldonk, and Frans CT van der Helm. Comparison of different methods to identify and quantify balance control. *Journal of neuroscience methods*, 145(1-2):175–203, 2005.
- [16] Jason K Moore, Sandra K Hnat, and Antonie J van den Bogert. An elaborate data set on human gait and the effect of mechanical perturbations. *PeerJ*, 3:e918, 2015.
- [17] Antonie J Van den Bogert, Thomas Geijtenbeek, Oshri Even-Zohar, Frans Steenbrink, and Elizabeth C Hardin. A real-time system for biomechanical analysis of human movement and muscle function. *Medical & biological engineering & computing*, 51(10):1069–1077, 2013.
- [18] Marko Ackermann and Antonie J Van den Bogert. Optimality principles for model-based prediction of human gait. *Journal of biomechanics*, 43(6):1055–1060, 2010.
- [19] Hartmut Geyer and Hugh Herr. A muscle-reflex model that encodes principles of legged mechanics produces human walking dynamics and muscle activities. *IEEE Transactions on neural systems and rehabilitation engineering*, 18(3):263–273, 2010.
- [20] Kuangyou B Cheng, Yi-Chang Huang, and Shih-Yu Kuo. Effect of arm swing on single-step balance recovery. *Human movement science*, 38:173–184, 2014.
- [21] David A Winter. *Biomechanics and motor control of human movement*. John Wiley & Sons, 2009.

- [22] Charles R Hargraves and Stephen W Paris. Direct trajectory optimization using nonlinear programming and collocation. *Journal of Guidance, Control, and Dynamics*, 10(4):338–342, 1987.
- [23] Andreas Wächter and Lorenz T. Biegler. On the implementation of an interior-point filter line-search algorithm for large-scale nonlinear programming. *Mathematical Programming*, 106(1):25–57, Mar 2006. ISSN 1436-4646. doi: 10.1007/s10107-004-0559-y. URL <https://doi.org/10.1007/s10107-004-0559-y>.

## PART III.

# SUMMARY AND PROPOSED WORK

## CHAPTER VII

### SUMMARY AND PROPOSED WORK

#### **7.1 Completed Work**

There are three aims in this dissertation study. So far: Aim 1 was completed; aim 2 is 75% completed; and we started aim 3 in May.

##### **Aim 1: *identify control laws in human standing balance***

- **Chapter II: Standing balance experiment with long duration random perturbation.** In the standing balance experiment, over 160 minutes reaction data of 8 participants under random perturbation were recorded. The recorded information includes motion capture marker data, ground reaction force data, and ten Electromyography (EMG) sensors' data. The motion capture marker data was used to calculate subjects' body motion, for instance the joint angles. Ground reaction force data was used to calculate joint torques through inverse dynamics. EMG data represents the muscle activations in one side of standing legs. From the analysis in this chapter, we concluded that the collected standing balance data is in good quality. Thus, it is suitable for identifying generalized feedback controller in standing balance task.
- **Chapter III: Identification of stable human posture control laws through stochastic trajectory optimization.** In this chapter, we showed that identifying human

standing balance controllers with stochastic trajectory optimization can help prevent finding unstable controllers. In addition, when stable controllers were identified from experimental data in deterministic identifications, there is a rare change of the identification results by introducing stochastic identifications. Having the advantage that linearization is not needed, stochastic trajectory optimization can be applied to controller identifications in strong nonlinear systems. This technique was used in next chapter to identify stable feedback controllers in human standing balance task.

*Potential Publication:* Identification of stable human posture control laws through stochastic trajectory optimization. *Journal of Neuroscience Method, Under Review.*

- **Chapter IV: Identification of posture control laws in human standing balance.**

In this chapter, we identified five types of feedback controllers for each of six subjects' one hundred seconds experimental data. Two linear types of controllers were identified: proportional derivative (PD) controller and full-state proportional derivative (FPD) controller. Stability of these two linear control types was able to guaranteed by using stochastic identification techniques mentioned in previous chapter. Eigenvalue analysis showed that the identified PD/FPD controllers have a relative smaller difference of eigenvalues among participants. Three nonlinear controllers were identified: linear state combination with time delay (LSCTD) controller, neural network (NN) controller, and neural network with time delay (NNTD) controller. Even though stability was unable to guaranteed for these three nonlinear controllers, identified results showed that controller with non-linearity and time delay can explain the experiment data the best.

*Potential Publication:* Identification of posture control laws in human standing balance. *Journal of Biomechanical Engineering, Drafting.*

**Aim 2:** *identify step strategy control laws in human walking.*

- **Chapter V: Identification step strategy control laws from human walking experiment data.** In this chapter, step strategy control laws were successfully identified from walking experiment data. Identified control gains of 9 subjects have similar values with gains suggested by the capture theory. However, the identified controller gains are changing along with walking speed, while capture theory suggested constant gains for all walking speeds. The changing gains along with walking speed suggested that the step strategy that human used is more likely to be a nonlinear feedback control, instead of the linear feedback control which are commonly used currently.

*Potential Publication:* Identification swing leg control laws from human walking experiment data.

*Journal of Biomechanics, Drafted.*

## 7.2 Future Work

Future work includes the second part of the proposed work in aim 2 and all parts of proposed work in aim 3.

**Aim 2:** *identify step strategy control laws in human walking.*

- **Chapter VI: Testing identified step strategy control laws and capture theory in forward simulations.** In this chapter, we will run forward simulation of walking with both the identified step strategy control laws and the capture theory. Here, the purpose is to test and compare the walking performance between identified control laws and the capture theory.

In forward simulations, we will use the same 7-links human body dynamic model which is used in the controller identification. Stance leg will be controlled by open-torques plus PD controllers to track the experimental data. Swing leg will be con-

trolled using the identified step strategies or the capture theory. Capture theory has been widely used in many humanoid robots and has helped them achieved stable walking motion[1–3]. Identified step strategy control laws have the same function and control structure as the capture theory, which is to estimate the next foot location. The success of the capture theory suggested that forward simulation with identified step strategies will result stable walking motion also. In addition, we expect that the forward simulation of identified step strategies will generate behaviors which is more human-like than the capture theory. The reason is that the identified step strategies are directly from human walking data, while the capture theory was resulted from model based analysis.

**Aim 3:** *identify impedance control parameters in human walking.*

- **Chapter VII: Identification of impedance control parameters from human walking experimental data.** In this chapter, we will identify joint impedance properties from human walking data. Here, the purpose is to provide good references for the impedance control of prosthetic or orthotic (P/O) devices.

Impedance control is defined in the following equation, which has virtual spring-damper property when reaching the target position.

$$T = K_p * (\theta_{tar} - \theta) + K_d * (0 - \dot{\theta})$$

where  $T$  is the torque generated by the impedance controller;  $K_p$ ,  $K_d$ , and  $\theta_{tar}$  are three impedance control parameters: proportional gains, derivative gains, and target joint position;  $\theta$  and  $\dot{\theta}$  are the current joint position and joint velocity.

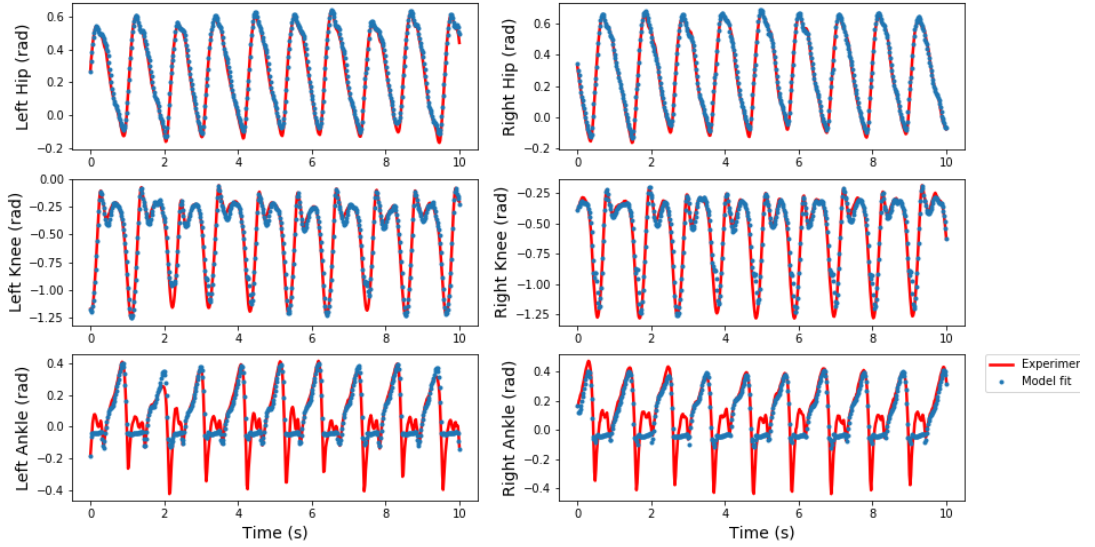


Figure 37: Fit between identified trajectory with impedance parameters and experiment data of Subject 1.

A pilot study have been done to identify ankle joint impedance parameters from 10 seconds walking data. In the pilot study, two sets impedance parameters were identified from two trials walking data of two subjects. For one data trial, only one set impedance parameters ( $K_p$ ,  $K_d$ ,  $\theta_{tar}$ ) is used to control ankle joint among entire gait cycles including both stance and swing phases. The identified impedance parameters are shown in Table X. Fits between identified trajectories and experiment data are shown in Figure 37.

Table X: Identified impedance parameters of the pilot study

Subject ID	Speed (m/s)	$K_p$ (Nm/rad/kg)	$K_d$ (Nm * s/rad/kg)	$\theta_{tar}$ (degree)
1	1.2	3.40	1e-9	-5.11
2	1.6	3.78	1e-8	-2.29

The identified ankle joint impedance parameters showing above are as expected. Zero damping is the best choice in the identified control structure, in which ankle joint needs negative damping (positive power) to lift up the toe in swing phase, while damping parameter is bounded to be positive only. The identified stiffness param-

eters are within the normal range that has been reported in several previous studies [4–6]. The identified trajectory also satisfies our expectation. Ankle joint has a good fit with experiment data in the stance phase and bad fit in swing phase. This is because that ankle joint trajectory is critical for balance at standing phase. In swing phase, ankle joint trajectory does not affect walking balance as long as the foot does not contact with ground. The trajectory fit also shows that the identified ankle stiffness parameter is mainly from the standing phase.

This pilot study proved that our approach is valid to identify impedance control parameters from walking data. For future work, we will expand the impedance identification work to knee and hip joints. Phase-dependent impedance control structures will be included also. Our current plan is to use the four phases structure which was used in Sup's research work. [7].

- **Chapter VIII: Testing identified impedance control parameters on hardware.** In this chapter, we will test the identified impedance parameters on Indego exoskeleton. The purpose here is to prove that the identified impedance control parameters are useful for P/O devices.

One way to test the identified impedance control parameters is to check whether the activation of leg muscles will be reduced when wearing the impedance controlled exoskeleton. We plan to use this method and expect a large reduction in muscle activation, since the identified impedance controllers can generate the most joints' torques which are needed in walking. The main function of human in loop is to keep walking balance, which needs only a small amount of effort. In the testing, we will use EMG sensors to record the activation of subjects' leg muscles with and without wearing

the impedance controlled exoskeleton. Impedance control has been used in several leg exoskeletons to assist patients who have muscle disorder and weakness to achieve walking motion[8–10]. With these succeed studies, we believe that our goal of testing the identified impedance controllers on Indego exoskeleton can be achieved.

The time-line and milestones for dissertation work is shown in Table XI.

Table XI: Time-line and Milestones

Semesters	2019 Fall					2020 Spring				
Months	08	09	10	11	12	01	02	03	04	05
Submit Step Strategy Paper										
Impedance Controller Identification										
Write/Submit Standing Paper										
Forward Simulation of Id. Controllers										
Write/Submit Impedance Id paper										
Applied Id. Con. on Hardware										
Write Dissertation										
Find A Job										
Defense										
Dissertation Credits	10					10				

### 7.3 REFERENCES

- [1] Jerry Pratt, Twan Koolen, Tomas De Boer, John Rebula, Sebastien Cotton, John Carff, Matthew Johnson, and Peter Neuhaus. Capturability-based analysis and control of legged locomotion, part 2: Application to m2v2, a lower-body humanoid. *The International Journal of Robotics Research*, 31(10):1117–1133, 2012.
- [2] Yoshiaki Sakagami, Ryujin Watanabe, Chiaki Aoyama, Shinichi Matsunaga, Nobuo Higaki, and Kikuo Fujimura. The intelligent asimo: System overview and integration. In *Intelligent Robots and Systems, 2002. IEEE/RSJ International Conference on*, volume 3, pages 2478–2483. IEEE, 2002.
- [3] Nicolaus A Radford, Philip Strawser, Kimberly Hambuchen, Joshua S Mehling, William K Verdeyen, Stuart Donnan, James Holley, Jairo Sanchez, Vienny Nguyen,

Lyndon Bridgwater, Reginald Berka, Robert Ambrose, Christopher Mcquin, John D Yamokoski, Stephen Hart, Raymond Guo, Adam Parsons, Brian Wightman, Paul Dinh, Barrett Ames, Charles Blakely, Courtney Edmonson, Brett Sommers, Rochelle Rea, Chad Tobler, Heather Bibby, Brice Howard, Lei Nui, Andrew Lee, Michael Conover, Lily Truong, Jacobs Engineering, David Chesney, Robert Platt, Gwendolyn Johnson, Chien-Liang Fok, Nicholas Paine, Luis Sentis, Eric Cousineau, Ryan Sinent, Jordan Lack, Matthew Powell, Benjamin Morris, and Aaron Ames. Valkyrie: NASA’s First Bipedal Humanoid Robot. Technical report.

- [4] Elliott J Rouse, Levi J Hargrove, Eric J Perreault, and Todd A Kuiken. Estimation of human ankle impedance during the stance phase of walking. *IEEE Transactions on Neural Systems and Rehabilitation Engineering*, 22(4):870–878, 2014.
- [5] Hyunglae Lee and Neville Hogan. Time-varying ankle mechanical impedance during human locomotion. *IEEE Transactions on Neural Systems and Rehabilitation Engineering*, 23(5):755–764, 2015.
- [6] Hyunglae Lee, Elliott J Rouse, and Hermano Igo Krebs. Summary of human ankle mechanical impedance during walking. *IEEE journal of translational engineering in health and medicine*, 4:1–7, 2016.
- [7] Frank Sup, Amit Bohara, and Michael Goldfarb. Design and control of a powered transfemoral prosthesis. *The International journal of robotics research*, 27(2):263–273, 2008.
- [8] Jan F Veneman, Rik Kruidhof, Edsko EG Hekman, Ralf Ekkelenkamp, Edwin HF Van Asseldonk, and Herman Van Der Kooij. Design and evaluation of the lopes exoskeleton robot for interactive gait rehabilitation. *IEEE Transactions on Neural Systems and Rehabilitation Engineering*, 15(3):379–386, 2007.

- [9] José L Pons. *Wearable robots: biomechatronic exoskeletons*. John Wiley & Sons, 2008.
- [10] Conor James Walsh, Ken Endo, and Hugh Herr. A quasi-passive leg exoskeleton for load-carrying augmentation. *International Journal of Humanoid Robotics*, 4(03):487–506, 2007.